UC Irvine

UC Irvine Electronic Theses and Dissertations

Title

The Role of Hydrophobicity in Biomacromolecular Interactions with Abiotic Affinity Agents

Permalink

https://escholarship.org/uc/item/71z022t1

Author

Chou, Beverly

Publication Date

2016

Peer reviewed|Thesis/dissertation

eScholarship.org Powered by the California Digital Library
University of California

UNIVERSITY OF CALIFORNIA,
IRVINE

The Role of Hydrophobicity in Biomacromolecular Interactions with Abiotic Affinity Agents

DISSERTATION

submitted in partial satisfaction of the requirements
for the degree of

DOCTOR OF PHILOSOPHY

in Chemistry

by

Beverly Chou

Dissertation Committee:
Professor Kenneth J. Shea, Chair
Professor Zhibin Guan
Assistant Professor Aaron P. Esser-Kahn

2016

Chapter 2 © 2016 American Chemical Society
All other materials © 2016 Beverly Chou

DEDICATION

To

My family, my friends, and my coworkers,
for their love and support

TABLE OF CONTENTS

	Page
LIST OF FIGURES	v
LIST OF TABLES	x
LIST OF SCHEMES	xii
ACKNOWLEDGMENTS	xiii
CURRICULUM VITAE	xiv
ABSTRACT OF THE DISSERTATION	xvi
CHAPTER 1: Polymer Hydrophobicity and Biomacromolecules. How hydrophobicity of synthetic affinity agents can affect intra and intermolecular interactions with themselves and with biomacromolecules.	1
A. Introduction	1
B. Hydrophobic Contributions to NP-Protein Interactions	2
C. Contribution of Hydrophobicity to Hydrogel Structure	6
D. Stability and Activity of Proteins after Adsorption	18
E. Conclusions	26
F. References	27
CHAPTER 2: Tuning Hydrophobicity in an Abiotic Affinity Reagent. Polymer hydrogel affinity reagents for molecules with lipid-like domains.	31
A. Introduction	31
B. Synthesis and Characterization of NiPAm based Co-Polymer Nanoparticles	34
C. Fluorescence Polarization Analysis of NP-LPS Interaction as a Function of the Hydrophobic Monomer.	36
D. NMR Investigations of NPs – Compositional Analysis	38
E. NMR Investigations of NPs – 1D and 2D NMR Spectra of NPs	40
F. Influence of Charged Monomers on NP-LPS Capacity.	44
G. Polymer Coated Agarose Beads – Evaluation of Clearance Effectiveness	45
H. Conclusions	49
I. Experimental Procedures	50
J. Supplementary Information	59
K. References	71

CHAPTER 3: Designing *N*-isopropylacrylamide Thermal Protectants for Immunoglobulin G. A Functional Synthetic Analog of HSP60. 76
A. Introduction 76
B. NP Synthesis and Characterization 80
C. Hydrophobic Contributions to IgG binding 82
D. Electrostatic Contributions to IgG-NP Binding 83
E. Optimization of NP-IgG Binding in Sodium Phosphate Buffer 84
F. The Hydrophobicity of Monomer Side Chains Affects NP Swelling and NP-IgG Binding 86
G. NMR Studies of Side Chain Solvation 87
H. Effect of pH on NP-IgG Capacity 90
I. Determining Structural Integrity of Bound-Released IgG using Circular Dichroism. 92
J. Determining Structural Integrity of Bound-Released IgG using SEC-HPLC 93
K. Size Change of the NP-IgG Complex 95
L. Hydrophobicity of NPs Above and Below LCST 97
M. VP-DSC Analysis of T_m of IgG 99
N. Conclusion 102
O. Materials and Methods 105
P. Supplementary Information 110
Q. References 114

CHAPTER 4: A Novel Cysteine Active End-Cap for Self Immolative Polymers 121
A. Introduction 121
B. End-cap Design 123
C. HPLC Analysis of Trigger Breakdown 124
D. HPLC Analysis of Tetramer Breakdown 125
E. Visual Decomposition of Tetramer Film 128
F. Conclusion 129
G. Supplementary Information 130
H. References 141

LIST OF FIGURES

Page

Figure 1.1. A. The chemical structures of functional monomers attached to cationic gold NPs. B. Binding constants (K_b) determined by ITC compared to the partition coefficients (log P_{oct}) of the functional monomers used. Adapted with permission from reference [6]. Copyright 2014 Royal Society of Chemistry. 4

Figure 1.2. ITC binding data for NP-HSA binding of 50:50 NiPAm/tBAm NPs of varying sizes. Particle concentration in the cell was 1 mg/mL, with protein concentration in the syringe at 40 μM. Adapted with permission from reference [7]. Copyright 2007 American Chemical Society. 6

Figure 1.3. Structure of NiPAm-BIS NPs above and below their temperature controlled transition (LCST). Adapted with permission from reference **[8].** Copyright 2004 American Chemical Society. 7

Figure 1.4. A. Shows the difference in organization of the monomer chains above and below LCST. B. Shows the r_g and r_h determined by SLS and DLS over a range of temperatures. C. Shows the r_g/r_h ratios calculated at various temperatures, as determined by the data found in B. Adapted with permission by reference [11]. Copyright 2012 American Institute of Physics. 8

Figure 1.5. Structure and suspected depolymerization scheme of NiPAm-DHEA NPs. Adapted with permission from reference [13]. Copyright 2011 American Chemical Society. 9

Figure 1.6. Scheme demonstrating the how the physical properties of microgels change upon cytochrome C loading. Adapted with permission from reference **[14].** Copyright 2011 American Chemical Society. 11

Figure 1.7. A. Schematic of the temperature responsiveness of NiPAm based NPs to protein targets. B. Schematic of the "catch-and-release" experiment of the selective capture of lysozyme from egg white. Adapted with permission from reference [16]. Copyright 2012 Wiley-VSH Verlag GmbH & Co. KGaA, Weinheim. 12

Figure 1.8. Micromanipulator-assisted light microscopy images showing a microgel, sucked onto the tip of a micropipet. The different time points show a titration of lysozyme into the microgel solution. Adapted with permission from reference [19]. Copyright 2009 American Chemical Society. 15

Figure 1.9. A. The mean r_H obtained by DLS and B. $<\Delta\%R_{NP}>$ determined by SPRM of the NPs (30 pM) in the presence of melittin (0 – 2.5 μM). C. The NP composition used for the SPRM experiment. D. A 58.5 μm x 58.5 μm Fourier filtered SPRM 3 s differential reflectivity image showing the adsorption of 2 NPs onto a C11-functionalized gold film. Adapted with permission from reference [9]. Copyright 2015 American Chemical Society. 17

Figure 1.10. Schematic showing conformation and orientation of binding of albumin and fibrinogen depending on surface curvature. Adapted with permission from reference [20]. Copyright 2006 American Chemical Society. 19

Figure 1.11. A. Chemical structure of polymer used. B. Formation of micellar structure of synthetic affinity agents in water. C. Schematic representation of polymer affinity agent interaction with ChT. Adapted with permission from reference [22]. Copyright 2005 American Chemical Society. 21

Figure 1.12. Scheme showing possible mechanisms of inhibition of fibrillation by NPs. Adapted with permission from reference [26]. Copyright 2008 American Chemical Society. 26

Figure 2.1 The inner core and lipid A portions of LPS. These are the portions being targeted by polymer hydrogel NPs. KDO: 3-Deoxy-D-manno-oct-2-ulosonic acid, Hep: Heptose. 33

Figure 2.2 DLS hydrodynamic size measurements taken of three NPs (♦ = **OAm10**, ▲ = **HAm10**, ■ = **BAm10**) at various temperatures from 15 – 50 °C to measure approximate LCST. 35

Figure 2.3 Fluorescence polarization study of NPs titrated into a solution of LPS (500 ng/mL) in 10 mM SPB at pH 6.8 at 25 °C. This figure shows the results of three NPs, each containing 10% of a *N*-alkylacrylamide monomer (♦ = **OAm10**, ■ = **HAm10**, ▲ = **BAm10**). A greater slope indicates higher LPS binding. 37

Figure 2.4 ^{1}H NMR's taken in $CDCl_3$ at 25 °C for NPs containing 10% *N*-alkylacrylamide, NiPAm, and BIS copolymers (1: **BAm10**, 2: **HAm10**, 3: **OAm10**). Peak A is a broad singlet at ~0.9 ppm representing the terminal methyl group in the hydrophobic monomers (BAm, HAm, OAm), and peak B is the broad singlet at ~4.1 ppm assigned to the methine proton of the isopropyl group in NiPAm. 39

Figure 2.5 The 400 MHz spectra of 1. **BAm10**, 2. **HAm10**, and 3. **OAm10** in 90:10 H_2O:D_2O. Peak A refers to the side chain methyl and peak B refers to the side chain methylene protons. 41

Figure 2.6 Truncated 2D NOESY spectrum showing the interaction between the terminal methyl group (0.9 ppm) of A. BAm, B. HAm, and C. OAm, and the methine (3.9 ppm) of NiPAm. The NP spectrums (A. **BAm10,** B. **HAm10**, C. **OAm10**) were acquired in 90:10 H_2O:D_2O with a 0.4 s mixing time. For full spectra, see Figure 2.S4. 42

Figure 2.7 Fluorescent polarization study of four NPs, with and without 5% APM (▲ = **BAm20APM5**, ♦ = **BAm30APM5**, ● = **BAm20**, ■ = **BAm30**), titrated into a solution of LPS (500 ng/mL) in 10 mM SPB at pH 6.8. 44

Figure 2.8 Fluorescence results from FITC-LPS solutions incubated in polymer coated agarose beads (n ≥ 3). PMB represents the commercially available polymyxin B column. 47

Figure 2.9 Monomers used for the synthesis of polymer NPs. NiPAm and BIS were used as the backbone and crosslinker of the synthetic polymers, respectively. 53

Figure 2.S1 Fluorescence data on BAm30 NP interaction with FITC-LPS. NPs (1 mg/mL) were incubated in a FITC-LPS solution (1 µg/mL) for 30 min at either 25 °C or 37 °C in SPB (10 mM, pH 7.0) with two controls (FITC-LPS only and NP only). The NPs were then pelleted (15,000 rpm, 45 min), and the supernatent was measured for presence of FITC-LPS (Ex: 495 nm, Em: 496 – 515 nm). The background fluoresence from the NP only solution was subtracted from the samples containing NPs. 63

Figure 2.S2 Fluorescence polarization study on NPs. NPs were titrated into a solution of 500 ng/mL FITC-LPS in 10 mM sodium phosphate buffer at pH 6.8. A: ■ = BAm10, ▲ = BAm20, ♦ = BAm39. B: ■ = OAm20APM5, ♦ = HAm10APM5, ▲ = BAm30APM5. C: ♦ = BAm20GUA5, ■ = BAm30GUA5, ▲ = BAm20, ● = BAm30. D: ♦ = BAm10APM5, ■ = BAm20APM5, ▲ = BAm30APM5. E: ♦ = Fluorescein, ■ = FITC-LPS. 64

Figure 2.S3 These represent the ^1H NMR's taken for most of the NPs in the library. The incorporation ratios are qualitatively deduced from observing the change in peaks A and B, with a change in feed ratio of the monomers. Peak A is a broad singlet around 0.9 ppm representing the terminal methyl group in the new hydrophobic monomers (BAm, HAm, OAm), and peak B is the broad singlet at ~4.1 ppm representing the methine of the isopropyl group in NiPAm. 66

Figure 2.S4 2D NOESY NMR of three NPs, A. tBAm10, B. BAm10, C. HAm10, D. OAm10, in 90:10 H_2O: D_2O. 68

Figure 3.1. Monomers used in this study. 79

Figure 3.2. Capture of FITC-IgG (20 μg/mL) using tBAm NPs (250 μg/mL) with 10% AAc in water at 37 °C after 30 min incubation. 83

Figure 3.3. Capture of FITC-IgG (20 μg/mL) using AAc NPs (250 μg/mL) with A. 40% tBAm or B. 10% OAm in water at 37 °C after 30 min incubation. 84

Figure 3.4. Capture of FITC-IgG (20 μg/mL) using NPs in SPB (35 mM, pH 5.5) at 37 °C after 30 min incubation. 86

Figure 3.5. ^{1}H-NMR of **HAm5AAc35**, **OAm5AAc35**, and **tBAm5AAc35** in A. deuterated methanol and B. H_2O/D_2O (90:10) with water suppression. Peak I (3.9 ppm) represents the methine of NiPAm, peak II (1.8 ppm) represents either the methylene peaks in OAm and HAm or the terminal methyl in tBAm, and peak III (0.9 ppm), represents the terminal methyl in OAm and HAm. 89

Figure 3.6. Release of the IgG from the NP-IgG complex (Figure 3.4) in PBS (35 mM, pH 7.3, 150 mM NaCl) solution at 25 °C after 30 min incubation. 91

Figure 3.7. CD analysis of recovered IgG after thermal stress. A control (IgG) sample shows the CD spectrum of native IgG without heating (IgG). All other samples are of IgG heated to 60 °C for 5 min with or without NPs. The NPs were first pelleted (SPB, pH 5.5), and unbound IgG was removed. The IgG bound to NPs were then released (PBS), the NPs were pelleted, and the released IgG was analyzed. 92

Figure 3.8. SEC-HPLC analysis of IgG after thermal stress. 94

Figure 3.9. DLS analysis of NP-IgG complex (NP 1 mg/mL) at various IgG concentrations (50 – 200 μg/mL) in SPB (35 mM, pH 5.6) at 37 °C. 96

Figure 3.10. VP-DSC trace of IgG (200 μg/mL) with addition of various NPs (1 mg/mL). Solutions were heated from 15 – 90 °C at 50 °C/h under ~25 psi. 100

Figure 3.S1. Data shows the percent of FITC-IgG (20 μg/mL) remaining in solution after addition of NPs (250 μg/mL) in SPB (35 mM, pH 5.5) at 37 °C with 30 min incubation. 111

Figure 3.S2. Change in hydrodynamic radius of different NPs from 15 to 50 °C. 112

Figure 3.S3. Pyrene fluorescence in three NP solutions (2 mg/mL, water). Pyrene was dissolved in EtOH to 2 μM and added into the NP solution (0.5% volume). Each solution was incubated at either 15 or 40 °C for 10 min before measurement. The solutions were excited at 335 nm. 113

Figure 4.1. Summary of SI polymer function. 121

Figure 4.2 HPLC data based on scheme 4.1. HPLC scans had 5 μL injections of the mixture at 0 – 70% ACN in water over 7 min. Molecule 1 (25 μg/mL) was mixed with L-cysteine (5 mg/mL) in HEPES buffer (20 mM, CTAB 1 mM, pH 7.4). Each data point is associated with the time of the HPLC injection with 30 s being the time of L-cysteine addition to molecule 1. 124

Figure 4.3. HPLC run data. A sample of tetramer 7 (0.5 mg/mL) in HEPES buffer (20 mM, CTAB 1 mM, pH 7.4) with addition of L-cysteine with A. detection at 254 nm, B. detection at 220 nm. 127

Figure 4.4. Visual observation of film decomposition. Films were made from a concentrated EtOAc solution of the tetramer 9. The films were incubated in A. DI water and B. in a HEPES buffer solution (20 mM, CTAB 1 mM, pH 7.4) containing L-cysteine. In both cases, the first panel shows the film, the second panel shows the films incubating in the respective solutions, and the third panel shows each film after a 5 min incubation, with the aqueous solutions lightly rinsed off with DI water. 128

LIST OF TABLES

Page

Table 2.1 A summary of NP compositions. All NPs contain 2 mol% BIS with the indicated amounts of functional monomer. The remainder was comprised of NiPAm (see Table S1 for complete data). Hydrodynamic diameters (Z-avg) were determined at 25 °C. 34

Table 2.2 Incorporation ratios of **BAm10**, **HAm10**, and **OAm10**. These values were obtained by integration of peaks A and B in Figure 2.4. The feed ratio in all cases were 10:88 hydrophobic monomer to NiPAm. 39

Table 2.3 Monomer Feed Ratio of Polymers Coated onto Agarose 46

Table 2.4 Raw Data from Elemental Analysis. 46

Table 2.S1 Details of which nanoparticles were synthesized, and their sizes, determined by dynamic light scattering (DLS) at 25 °C, diluted 1:10 in nanopure water. NP were synthesized using an AIBN initiator and CTAB surfactant. All monomer solutions were flushed with N_2 for 15 minutes prior to addition of initiator. All NPs were stirred for 3 h at 60 °C. Yields were determined by lyophilizing 5 - 10 mL of solution, and weighing the product to determine mass percentage. The polymer EC_{50}'s (pEC_{50}) was calculated using a four parameter logistic equation with a sigmoidal fit of anisotropy change in FP against log (NP concentration), with the polymers acting as the receptor, and the anisotropy change being the activity observed. The molecular weight of each NP was estimated to be 5000 kDa based off averages of previous molecular weight calculations. The raw data is shown in Figure 2.3, and 2.S2. ND = Not Determined, NC = No Change in anisotropy. 59

Table 2.S2 Lower critical solution temperature (LCST) study on DLS data showing trends in size of various NPs based on changing temperature. NPs were diluted with nanopure water in 1:10 dilution from stock solutions. The study was done using disposable cuvettes. Each sample was equilibrated for 10 minutes prior to each reading. The italicized values represent values with PDI's that were too high for the particles to be considered monodisperse. All values are determined by the Z-avg of the samples. 61

Table 3.1A. Summary of NP compositions used and their yields. For full table, see Table 3.S1. 80

Table 3.1B. Summary of NP analysis data obtained by DLS, MALS, and RI. 80

Table 3.2. Pyrene fluorescence in NP environment, above and below LCST. 99

Table 3.S1A. Summary of NP compositions and sizes, determined by DLS. 110

Table 3.S1B. Summary of density and LCSTs of NPs. 111

Table 3.S2. Titrations to determine AAc content in NP. 111

Table 3.S3. Denaturation temperatures and enthalpy if thermal denaturation of IgG in presence or absence of NPs from figure 3.4. 113

Table 4.S1. Summary of coupling reaction components. 132

LIST OF SCHEMES

Page

Scheme 2.1 Synthesis of NiPAm based co-polymer NPs. 53

Scheme 2.2 Functionalization of agarose beads. 55

Scheme 3.1. Inter and intra molecular crosslinking of hydrophobic side chains affect IgG binding. Increasing hydrophobicity of side chain is represented by an increasingly red color, with A. representing **tBAm5AAc35**, B. **HAm5AAc35**, and C. **OAm5AAc35**. 88

Scheme 3.2. Three different places IgG can bind to NPs. 97

Scheme 3.3. Size and hydrophobicity of NPs above and below LCST. 98

Scheme 4.1. Novel end-cap and scheme of the suspected mechanism for removal. 123

Scheme 4.2. Degradation scheme of end-capped tetramer 7. Removal of end-cap by L-cysteine proceeds as shown in scheme 4.1. The degradation then proceeds through decarboxylation to reveal the electron-rich amine, which then proceeds through a series of 1,6-eliminations and decarboxylations until the tetramer has completely degraded. 126

Scheme 4.S1. Synthesis of trigger. 130

Scheme 4.S2. Activation of 4-nitrobenzyl alcohol with phenylchloroformate. 131

Scheme 4.S3. Tetramer synthesis. 132

Scheme 4.S4. Bulk polymer synthesis. 135

ACKNOWLEDGMENTS

First, I would like to thank my boss for the last 5 years, Ken Shea. Thanks for being supportive of me, and believing in me, especially when I was feeling bad about myself, and defending me against people who you thought were disrespecting me. I appreciated how much you trusted me in my projects and my ideas and how much you encouraged me to try everything and gave me the freedom to work on projects that were unrelated to our subgroup. Also thanks to prior and former members of the Shea group, who provided guidance, entertainment, and support during the past 5 years. A special shout out to Rishad, my undergrad, who worked tirelessly to help me finish my last project, and who put up with my sometimes vague suggestions when I was uncertain of how to proceed.

Thanks to my committee members, Professors Zhibin Guan and Aaron Esser-Kahn for providing guidance and helpful suggestions on how to proceed on my projects when I got stuck. Thanks to Professor Szu-Wen Wang for helping provide guidance and helpful discussions on my project, and Dr. Peter Mirau, for helping figure out NMR analysis on my NPs.

I would like to thank my mom and dad for being supportive of me, both emotionally and financially and teaching me the life skills I would need to be successful. Without you being there for me and helping me every time I hit a bump in the road, I would not be where I am today. I'd also like to thank my sisters Daisy and Suzanne, for taking me out for fun and food, keeping me grounded when I got too proud of myself, and for being proud of your baby sister and encouraging me to join you in the rank of "doctorate".

I would like to thank my boyfriend Tom for taking me out to fun things and being aggressively supportive of me. You have taught me to fight for the things I deserve, and have often fought for those things for me, when I felt I didn't deserve them. I would also like to thank the Ford-Hutchinson family for being equally supportive of me, treating me out places, and making me feel like part of the family.

I would like to thank all of my friends, both at UCI and from before. Thanks to my best friend Kiana, who abandoned me for Chicago, but made up for it by talking to me almost every day, giving me a place to go for mini-vacations, and giving me advice, in between all the gossiping and venting. Thanks to Clarissa, my roomie for life, for going with me on food adventures, trying new places, giving me great food and fun advice, and providing a steady supply of yummy baked goods. Thanks to Domarin, my roomie in Irvine, for putting up with me for 4 years, having conversations about this and that, going shopping, hiking, getting coffee, and providing a fun home environment to come back to every day. Thanks to Bao, Camila, Gui, and Riann for being an awesome friend group, exploring new restaurants and random UCI events with me.

I would like to thank UCI facilities, especially Dr. Dima Fishman, Dr. Phil Dennison, Beniam Berhane, and the LFD for helping me figure out my experiments and get them working. Thanks to the MCP program, for providing a great opportunity for me and providing

support for my first two quarters at UCI. Thanks to the people in the UCI Chemistry department office for working out all my paperwork issues for me, and for being patient with me when I asked for extra clarification, or came panicked about something that I thought I forgot.

Finally, I would like to thank the American Chemical Society, Wiley-VSH Verlag GmbH & Co. KGaA, Weinheim, the American Institute of Physics, and the Royal Society of Chemistry for permission to include copyrighted figures as part of my thesis/dissertation. I also thank the American Chemical Society for permission to include Chapter 2 of my dissertation, which was originally published in Biomacromolecules. Financial support was provided by the University of California, Irvine, NSF Grant DMR-1308363, and the Beall Center.

CURRICULUM VITAE

Beverly Chou

***Education*.**

University of California, Irvine (UCI) (September 2011 – July 2016)
PhD in Chemistry.
Advisor: Dr. Kenneth J. Shea.
Research focuses:
1. Developing polymer hydrogel nanoparticles as abiotic protein affinity reagents for use as inexpensive alternatives for biomacromolecule purification and as artificial heat shock proteins.
2. Developing coatings and polishes that can be safely and easily removed by integration of self-immolative polyurethanes with a novel end cap.

University of California, San Diego (UCSD) (September 2007 – June 2011)
BS in Pharmacological Chemistry, minor in Economics.
Advisor: Dr. Tony Yaksh.
Research focus: Studying the use of adeno-associated virus serotype 5 as a siRNA delivery vesicles.

***Skills and training*.**

Small molecule and polymer synthesis.
Extensive experience in polymer and material characterization techniques including DLS, GPC, DSC, TGA, MALS, RI, NMR, MS, FTIR.
Evaluation of protein-polymer nanoparticle interactions using HPLC, ELISA, SDS-PAGE, UV-VIS, CD, Fluorescence Polarization, ITC.
Evaluation of polymer decomposition rates.
Polymer thin film preparation and analysis.
Organized the first annual University of California Symposium for Chemical Sciences (UCSCS), sponsored by the Royal Society of Chemistry (RSC).
Mentored undergraduate student researchers and several visiting scholars.
Planned experiments, and discussed research directions.
Revised papers and presentations.

Teaching Assistant for undergraduate discussion and laboratory sections.
Helped develop laboratory experiments and assisted other teaching assistants with problems while serving as Head TA.
Prepared discussion materials, and assisted in preparing exams.
Organized grading teams for exams for large undergraduate lectures.

Created and maintained the Shea group website.
Organized locations and times and procured appropriate materials for weekly group meeting.

Publications and Patents.

Xu, Q., Chou, B., Fitzsimmons, B., Miyanohara, A., Shubayev, V., Santucci, C., Hefferan, M., Marsala, M., Hua, X-Y., *PLoS One*, **2012**, *7* (3), e32581.

Beierle, J. M., Yoshimatsu, K., Chou, B., Mathews, M. A. A., Lesel, B. K., Shea, K. J., *Angew. Chem. Int. Ed.*, **2014**, *53* (35), 9275 – 9279.

Weisman, A., Chou, B., O'Brien, J., Shea, K. J., *Adv. Drug. Deliver. Rev.*, **2015,** *90*, 81–100.

Chou, B., Coating or polish removable by an aqueous amino acid solution, UC Patent Disclosure: 2015-142-0, **2015**, Irvine, CA.

Chou, B., Mirau, P., Jiang, T., Wang, S-W., Shea, K. J., Tuning Hydrophobicity in an Abiotic Affinity Reagent. Polymer Hydrogel Affinity Reagents for Molecules with Lipid-like Domains. *Biomacromolecules,* **2016**, *17* (5), 1860 – 1868.

Chou, B., Dalal, R., Shea, K. J., Polymer Hydrogel Nanoparticles as Artificial Heat-Shock Proteins for Immunoglobulin G. **2016**, In preparation.

Chou, B., Shea, K. J., Novel End-Cap for Self Immolative Polymers. **2016**, In preparation.

Presentations.

Chou, B., Dalal, R., Shea, K. J., *Division of Polymeric Materials Science and Engineering*, *251st ACS National Meeting & Exposition*, March 13-17, 2016, San Diego, CA.

Chou, B., Shea, K. J., *Division of Polymer Chemistry*, *251st ACS National Meeting & Exposition*, March 13-17, 2016, San Diego, CA.

Chou, B., *Division of Colloids and Surface Chemistry, ACS 2015 Western Regional Meeting,* November 6-8, 2015, San Marcos, CA.

Chou, B., *UCI Graduate Student and Post-Doctoral Colloquium*, May 8, 2015, Irvine, CA.

Chou, B., Wang, S. W., Shea, K. J., *Division of Polymeric Materials Science and Engineering*, *248th ACS National Meeting & Exposition*, August 10-14, 2014, San Francisco, CA.

***Awards*.**

Beall Innovation Award (2014).

Outstanding Contributions to the Chemistry Department Teaching Program by a TA – Lower Division (2014).

Graduate Award for Departmental Service (2013).

***Professional affiliations*.**

American Chemical Society (2014 – Present)

American Association for the Advancement of Science: Science Program for Excellence in Science (2012 – Present)

ABSTRACT OF THE DISSERTATION

The Role of Hydrophobicity in Biomacromolecular Interactions with Abiotic Affinity Agents

By

Beverly Chou

Doctor of Philosophy in Chemistry

University of California, Irvine, 2016

Professor Kenneth J. Shea, Chair

The interactions between synthetic affinity agents and biomacromolecules are reported to be due to the various intermolecular interactions that occur between them during binding. Among them, hydrophobic interactions play a large role. Changes in hydrophobicity, either due to changes in incorporation or in hydrophobicity of the monomers used, can often change more than just biomacromolecular affinity. By changing the chemical composition, the physical properties and structure of the abiotic affinity agents can also be affected. It is therefore important to study how changes in hydrophobicity can affect the polymer affinity reagents and their biomacromolecular targets. This information can then be used to enhance and optimize binding to biomacromolecules. In Chapter 1, I discuss the effect of hydrophobicity on the structure and affinity of synthetic affinity agents, and how the structure and function of the biomacromolecules that interact with them are affected.

In Chapter 2, we describe how NiPAm based copolymer nanoparticles (NPs) containing C4 – C8 hydrophobic groups were used to optimize affinity to molecules with lipid-like

domains. Using NMR spectroscopy, we found that optimizing interactions between NPs and lipopolysaccharides require maximizing hydrophobicity while avoiding side chain aggregation.

In Chapter 3, we describe how these NPs can be engineered as autonomous polymer heat shock proteins that prevent denaturation of biomacromolecules. By studying the effect of different hydrophobic monomers, we found that hydrophobic interactions can affect not only affinity, but activity of the synthetic affinity agents against biomacromolecules.

In Chapter 4, we discuss a novel end-cap for self immolative polymers that is active against cysteine. We tested this novel end-cap as a protective group on a monomer and oligomer, in solution and as a film, and found that it was selective for cysteine, and could remain stable in atmospheric conditions.

Chapter 1

Polymer Hydrophobicity and Biomacromolecules. How hydrophobicity of synthetic affinity agents can affect intra and intermolecular interactions with themselves and biomacromolecules.

A. Introduction

Polymer-biomacromolecule affinity agents have gained importance in recent years, since they may provide useful functions in therapeutics,[1] diagnostics,[2] and separations.[3] The fact that they are abiotic materials that are manufactured inexpensively make them attractive materials to study. Because of this, understanding fundamental polymer-biomacromolecule interactions are important to advance their use. Hydrophobic interactions are an important component of protein-protein and protein-polymer interactions and contribute to biomacromolecular affinity.[4] It is therefore important to study the physical properties and structure of an abiotic biomacromolecular affinity reagent and understand the interactions that occur between the synthetic affinity agents and their biomacromolecular targets.

Changes in chemical composition and structural features are reported to affect the size of synthetic affinity agents and their interactions with biomacromolecules. It is important to note that changing the chemical composition of the polymer affinity agent can not only affect biomacromolecular affinity, but it also will affect their physical structure. Since changes in a single variable can lead to any number of unintended changes, a study of the effects of a systematic change of functional groups can provide insight as to the nature of the interaction

of affinity agents with biomacromolecules. It is hoped that this information can be used to enhance and optimize binding to biomacromolecules. In the following sections, I discuss how hydrophobicity can affect the structure and affinity of synthetic affinity agents, and how these changes affect the structure and function of the biomacromolecules that interact with them.

B. Hydrophobic Contributions to NP-Protein Interactions

There are a number of things to take into account when designing a polymer affinity agent. The first thought is to find an affinity agent with functionalities that will be complementary to the biomacromolecular target. A general starting point in designing an affinity agent, is to take inspiration from natural affinity agents. In nature, two proteins bind together through a mixture of various intermolecular interactions.[5] Among them, hydrophobic interactions are often an important driving force in causing protein-protein binding or protein folding. Hydrophobic binding is typically an entropically driven phenomena.[6] Despite the fact that individual hydrophobic interactions are not as strong as some noncovalent interactions, like hydrogen bonding or electrostatic interactions, the cumulative hydrophobic surface area between two biomacromolecules can add up to a very strong binding interaction.

Many groups have studied the importance of hydrophobic functional groups in creating synthetic affinity agents, by either functionalizing solid nanoparticles (NPs) with hydrophobic ligands, or by synthesizing a polymer with hydrophobic functional monomers, that can contribute to affinity to a biomacromolecule. De *et al.* studied how adding different L-amino acid ligands to the surface of gold NPs would affect binding to chymotrypsin (ChT),

histone, and cytochrome C (cyt C) using isothermal titration calorimetry (ITC).[7] They found that affinity of the functionalized NPs is highly dependent on the protein being studied. For example, when binding to ChT, they found that NPs with glutamic acid (NP-Glu) had the weakest binding, while NPs with leucine (NP-Leu) had higher affinity, and NPs with phenylalanine (NP-Phe) had the greatest affinity. Binding was also found to be sensitive to pH and ionic strength.

Overall, an increase in hydrophobicity of the NPs produced an increase in affinity towards the proteins tested. NP-Phe had consistently higher affinity than NP-Leu to all proteins tested. This was attributed to the higher surface area of phenylalanine compared to leucine, which would contribute more hydrophobic surface area. The increased hydrophobic surface area provides more potential hydrophobic interactions, which could increase affinity to proteins. Further testing showed that hydrophobic interactions alone were not sufficient to maintain affinity at higher ionic strengths where the contributions of electrostatic interactions are diminished, thus a combination of intermolecular interactions are needed for favorable NP-protein affinity.

Chen *et al.* modified gold NPs with different hydrophobic ligands to enhance selectivity between two isoforms of β-lactoglobulin (BLG).[8] The gold NPs were functionalized with four ligands with different hydrophobicities, an alkyl (aliphatic) alcohol, a benzene, a cyclohexane, and a n-decyl hydrocarbon chain (Figure 1.1A). All NPs had a net positive charge by incorporating a tertiary ammonium group. The ligands were attached to the gold NPs through a tetra(ethylene glycol) spacer to isolate the head group from the gold NP surface. BLG was chosen as the model protein because its two isoforms (BLGA or BLGB) vary

in only two amino acids, and thus would be a good way to study if changing functional monomers can help tune selectivity for very similar proteins.

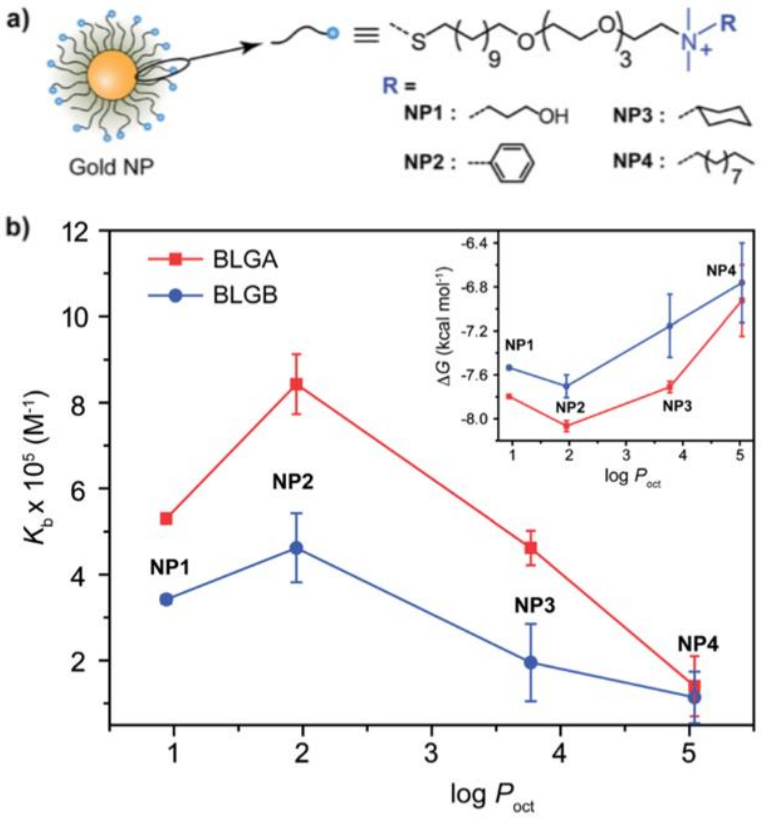

Figure 1.1. A. The chemical structures of functional monomers attached to cationic gold NPs. B. Binding constants (K_b) determined by ITC compared to the partition coefficients (log P_{oct}) of the functional monomers used. Adapted with permission from reference [8]. Copyright 2014 Royal Society of Chemistry.

Using ITC, NPs with the alkyl alcohol ligand was found to bind exothermically with a slight loss in entropy to both proteins, while the NPs functionalized with the three more hydrophobic ligands bound endothermically with large gain in entropy. The use of increasingly hydrophobic ligands, resulted in increased binding affinity to both isoforms of BLG. Overall, NPs with less hydrophobic side chains could discriminate between BLGA and BLGB better, but had lowered overall affinity to both isoforms (Figure 1.1B). This selectivity

was suspected to arise due to the extra carboxyl group present in BLGA, which would encourage additional electrostatic interactions with NPs containing more polar groups. This would lead to greater differentiation between the two BLG isoforms. These results show that, although hydrophobicity can be an important contributor to affinity, contributions to selectivity is highly dependent on a combination of intermolecular interactions.

Using NiPAm copolymer NPs, Lindman *et al.* studied how addition of the hydrophobic tBAm (tert-butylacrylamide) monomer affected affinity to human serum albumin (HSA).[9] NPs were screened for HSA affinity at 5 ^{o}C using ITC because the NPs used for the study aggregated at room temperature. NP-HSA binding was observed to be an exothermic interaction, with a very small enthalpy change associated with adsorption. More HSA was needed to reach saturation with the more hydrophobic particles compared to the more hydrophilic ones. This implies that there was a higher capacity for HSA with hydrophobic particles. Overall, HSA affinity did not vary much with increasing addition of the hydrophobic tBAm monomer to the NPs, but the more hydrophilic NPs (less tBAm) had a slightly higher affinity towards HSA. These results show that hydrophobicity can have a profound effect on both selectivity and capacity, often at the expense of affinity.

- NP Size and affinity.

In addition to studying the importance of hydrophobicity to HSA affinity, Lindman *et al.* wanted to see how NP size could affect affinity to HSA by varying sizes of the NPs from 70 – 700 nm (Figure 1.2).[9] They observed that smaller NPs had a lower capacity for HSA than larger particles. Based on the size of HSA, 31 HSA molecules could bind to the surface of a 70 nm particle, while 53 HSA molecules could in principle bind to a 120 nm particle. The strain

associated with the larger surface curvature of the smaller NPs could lead to fewer HSA molecules that could theoretically fit around the surface of the NP. This could explain why the smaller NPs resulted in lower HSA capacity, despite having similar affinities to HSA.

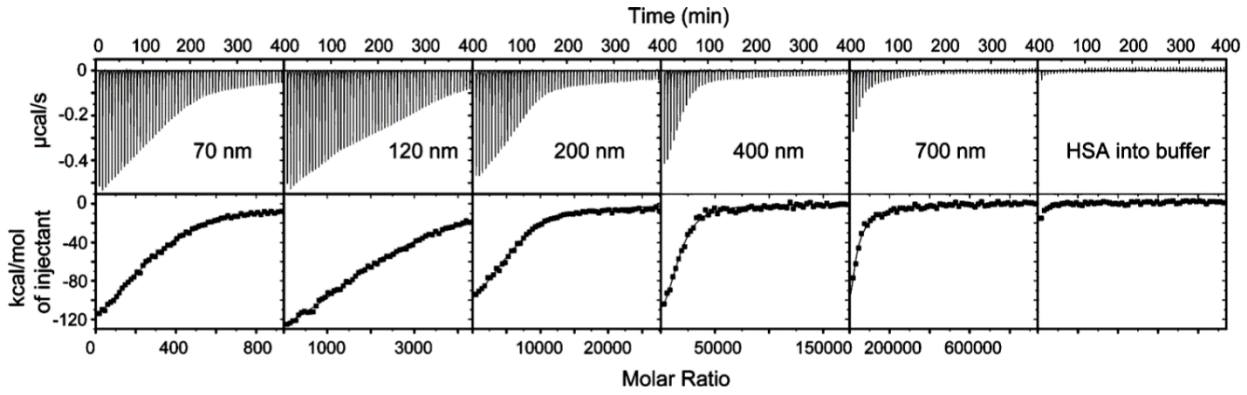

Figure 1.2. ITC binding data for NP-HSA binding of 50:50 NiPAm/tBAm NPs of varying sizes. Particle concentration in the cell was 1 mg/mL, with protein concentration in the syringe at 40 µM. Adapted with permission from reference [9]. Copyright 2007 American Chemical Society.

C. Contribution of Hydrophobicity to Hydrogel Structure

Changing functional monomers can help optimize affinity of a synthetic polymer for a biomacromolecular target. However, it is important to keep in mind how the functional group variations will affect the structure of the synthetic affinity agents. Often, the end groups are affected by solvents and other environmental conditions, which may limit their availability for intermolecular interactions with biomacromolecular targets. The incorporation of a functional monomer in a polymer does not mean that it will be available for intermolecular interactions. Its availability could be influenced by intramolecular

interactions within the polymer itself. To this end, many groups have studied the structure and intramolecular interactions of the synthetic affinity agents and how different functional monomers can affect the structure.

- NP structure

To this end, Saunders studied the internal structure of a *N*-isopropylacrylamide (NiPAm) NPs with either 1 or 10 wt% loading of *N,N'*-methylenebisacrylamide (BIS) crosslinker.[10] These microgels had a mass of ~6 x 10^9, which was in agreement with the poly(NiPAm) microgels without crosslinker reported by others.[11-12] The NiPAm-Bis microgels (~1050 nm) were found to form a fairly uniform structure, but with a thin shell (~20 nm) that was not affected by temperature (30 – 50 ^{o}C). (Figure 1.3).

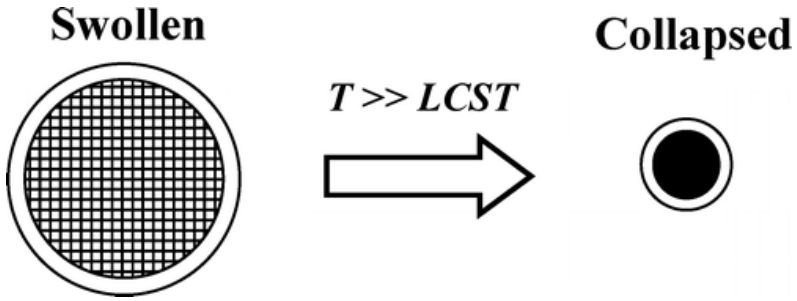

Figure 1.3. Structure of NiPAm-BIS NPs above and below their temperature controlled transition (LCST). Adapted with permission from reference **[10].** Copyright 2004 American Chemical Society.

Expanding upon this, Clara-Rahola *et al.* studied the structure of a NiPAm microgels with a more hydrophilic poly(ethylene glycol diacrylate) (PEG) crosslinker (2%).[13] Using dynamic light scattering (DLS) and static light scattering (SLS), they studied the r_h (hydrodynamic

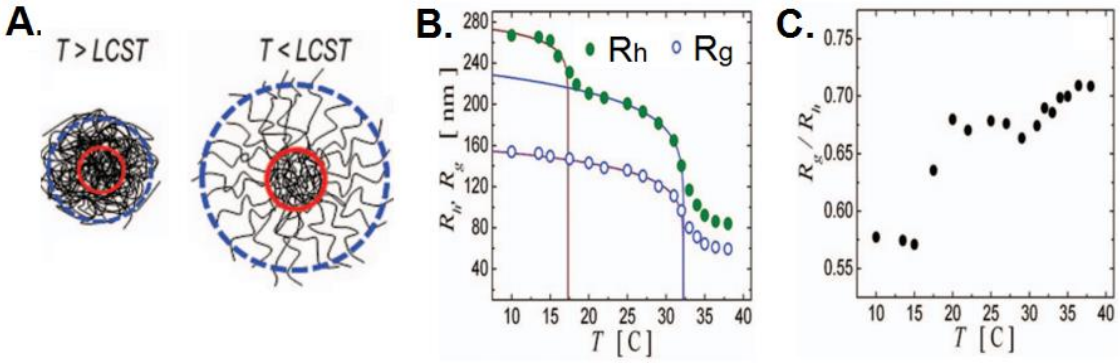

Figure 1.4. A. Shows the difference in organization of the monomer chains above and below LCST. B. Shows the r_g and r_h determined by SLS and DLS over a range of temperatures. C. Shows the r_g/r_h ratios calculated at various temperatures, as determined by the data found in B. Adapted with permission from reference [13]. Copyright 2012 American Institute of Physics.

radius), which defines the radius of the microgel under observation as the equivalent to a hard sphere that diffuses at the same rate, and r_g (radius of gyration), which is defined by the mass weighted average distance from the core to each mass element in the microgel under observation,[14] of each microgel to see how they changed as a function of temperature (Figure 1.4B), passing through the lower critical solution temperature (LCST). By finding the r_g and r_h of each microgel above and below the LCST, they can evaluate how the ratio of r_g/r_h is affected by temperature, determine the general topology of the microgel, and determine how the functional monomers are distributed. A typical r_g/r_h ratio for a hard sphere system is 0.775, while a soft sphere system has a ratio of r_g/r_h of 0.61. They found that for the NiPAm-

PEG copolymer microgels, the ratio of r_g/r_h above LCST was ~0.71, while below LCST, the r_g/r_h ratio was reduced to ~0.67 (Figure 1.4C). This implies that above LCST, the NP follows soft sphere model with a dense core and shell. When below LCST, the NP morphology changes and begins to follow a star polymer model, with a dense core and swollen shell (Figure 1.4A).

To confirm the core/shell property of these NiPAm NPs, Smith *et al.* studied how crosslinkers were incorporated into NiPAm based NPs.[15] To accomplish this, they incorporated a chemically labile cross-linker (1,2-dihydroxyethylene)bisacrylamide (DHEA) into either a NiPAm polymer and monitored how the cross-linked structure deconstructed. These NPs were synthesized using similar precipitation polymerizations to yield particles with comparable sizes to other NiPAm NPs with the methylenebisacrylamide (BIS) crosslinker. Using multiangle light scattering (MALS), they studied the size and density of the NPs as they degraded in the presence of sodium periodate. They found that the NP started with ratio of r_g/r_h of 0.63, which is indicative of a radially inhomogeneous mass distribution with a denser, more heavily crosslinked core, and a swollen, less crosslinked shell.

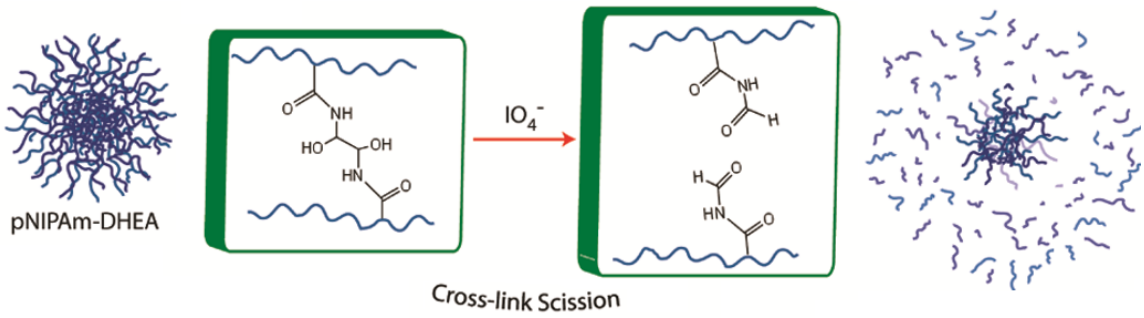

Figure 1.5. Structure and suspected depolymerization scheme of NiPAm-DHEA NPs. Adapted with permission from reference [15]. Copyright 2011 American Chemical Society.

Upon addition of sodium periodate, they found that the NiPAm NPs experienced mass loss in the exterior of the network, which eventually proceeded towards the interior (Figure 1.5). They found an immediate decrease in r_g upon cleavage of the crosslinker. They associated this decrease in r_g with mass loss proceeding from the exterior of the particle toward the interior. This showed that the crosslinker was distributed with high incorporation in the interior of the NP, and low incorporation in the outer shell of the NP. These studies show the how crosslinker incorporation affected the structure of the NiPAm based NPs, and imply that the physical property of the NPs is likely affected by temperature.

- How changes in temperature, buffer pH, and salt concentration affect polymer structure.

The structure of synthetic affinity agents is often influenced by environmental conditions. Changes in temperature, buffer pH, and salt concentration can affect not only their size, but also their intra and intermolecular interactions within and between NPs and biomacromolecules. It is therefore important to study how synthetic affinity agents are affected by these changes in environmental conditions. To this extent, Smith *et al.* studied how different ionic strengths could affect swelling in NiPAm-acrylic acid (AAc) microgel networks with 2% BIS crosslinker content.[16] After synthesizing the NiPAm-AAc microgels, they confirmed incorporation of AAc through titration against NaOH, and determined microgel size and density using MALS. The r_h and M_w of the microgels were shown to decrease with increasing ionic strength. This was attributed to charge screening of the polyanionic network. The reduced charge repulsion results in shrinkage of the microgel.

Next, Smith *et al*. studied how the changes to their microgel structure influenced binding to cytochrome C (Cyt C). To accomplish this, they titrated Cyt C into a microgel solution, and observed density changes in the microgel by MALS.[16] In solutions of high ionic strength, NPs and microgels will experience more charge screening. Smith *et al.* found that their NiPAm copolymers with 30% AAc were swollen in water, allowing proteins to be distributed throughout the microgel. The concentration of Cyt C bound to each microgel (24 μM) exceeded the solubility of Cyt C in water, which suggests the microgel network facilitates solubilization of the proteins. Microgels with lower AAc content (10 and 20 mol%) were less swollen in water, which decreased accessibility of Cyt C to the charged groups on the polymer chains (Figure 1.6), limiting loading of Cyt C to the microgel exterior with the less swollen particles. This in turn resulted in a lowered affinity and capacity to Cyt C.

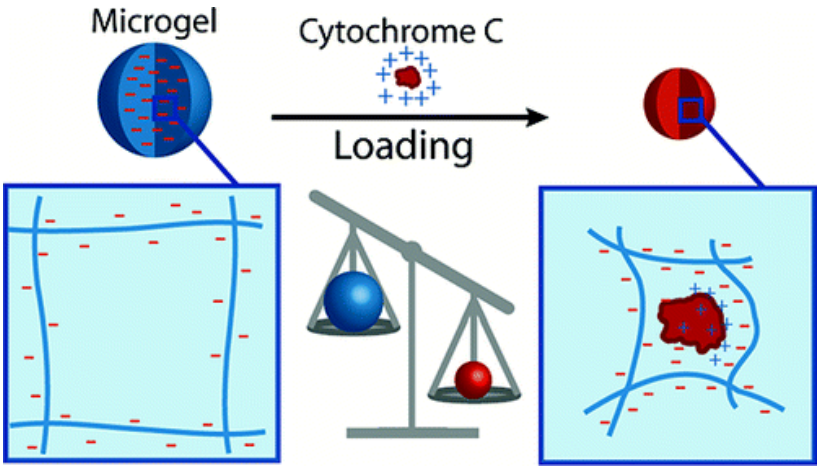

Figure 1.6. Scheme demonstrating the how the physical properties of microgels change upon cytochrome C loading. Adapted with permission from reference **[16].** Copyright 2011 American Chemical Society.

NiPAm based polymer hydrogel NPs exhibit a temperature induced volume change, the lower critical solution temperature (LCST). This temperature responsive phenomenon has been reported to be connected to biomacromolecular affinity.[17-18] Above the LCST, the

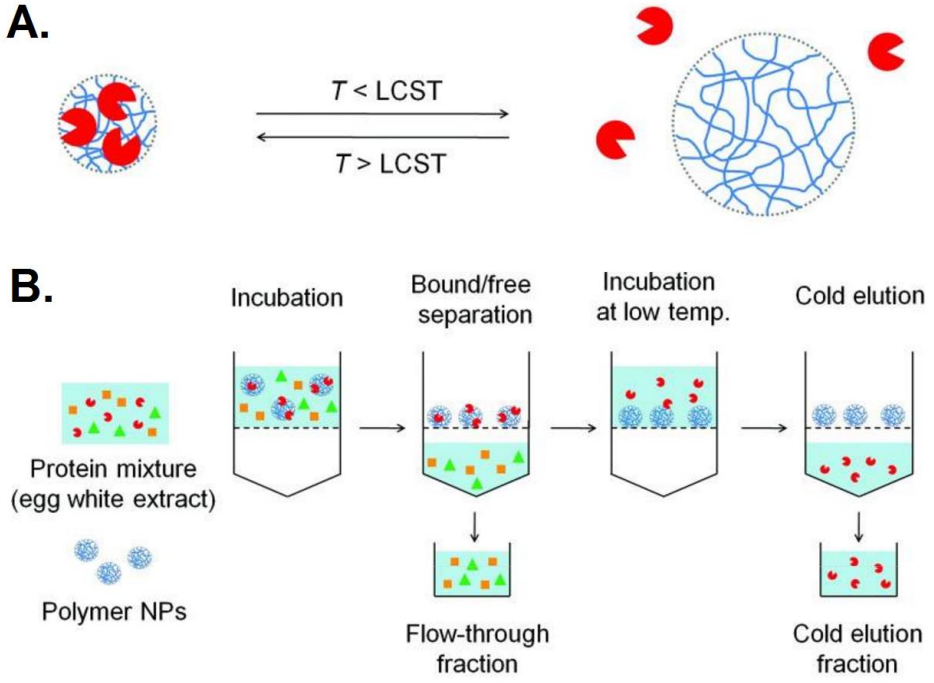

Figure 1.7. A. Schematic of the temperature responsiveness of NiPAm based NPs to protein targets. B. Schematic of the "catch-and-release" experiment of the selective capture of lysozyme from egg white. Adapted with permission from reference [18]. Copyright 2012 Wiley-VSH Verlag GmbH & Co. KGaA, Weinheim.

NiPAm copolymer NPs go through an entropically driven collapse and desolvation, resulting in an increase in biomacromolecular affinity (Figure 1.7A). The temperature responsive behavior of NiPAm based hydrogel NPs to melittin,[17] lysozyme,[18-19] and other biomacromolecular targets[20] has been exploited for a number of applications. Yoshimatsu *et al.* studied the effects of LCST on lysozyme affinity.[18] They found that a NiPAm-tBAm-AAc

copolymer NP showed high affinity to lysozyme at RT. Using centrifugation filtration (Figure 1.7B), they found that a NP bound up to 90% of lysozyme in PBS. The same NP was found to inhibit nearly all of the lysozyme activity *in situ*, suggesting that binding blocked access to the active site of lysozyme to a *Micrococcus lysodeikticus* cell suspension. They next tested if the NP could selectively capture lysozyme from a complex protein mixture. For this, they mixed their NP in a chicken egg-white mixture. After equilibration, the NP-lysozyme mixture was cooled below the NP LCST (<10 ^{o}C), and the released lysozyme was recovered from the NP complex. This demonstrated a temperature responsive "catch and release" capability of these NiPAm based NPs, showing how changes to environmental conditions can influence biomacromolecular affinity. It also demonstrates how these materials may be used for protein purification.

The LCST can be tuned by changing the hydrophobicity of the NPs by either changing the feed ratio of functional monomers, or by using a functional monomer of a different hydrophobicity. A NP with more hydrophobic content has a lower LCST, as the core of the NP becomes less water soluble, leading to a hydrophobic collapse at lower temperatures. A less hydrophobic NP has a higher LCST, as the overall NP core would become less hydrophobic and more water soluble, thus more energy would be required to force an entropically favored dehydration. This property is useful for engineering the temperature at which a polymer captures and releases a protein, and has been used to design a polymer that protects a protein from thermal stress.

To protect a protein from thermal stress, the polymer affinity agent would ideally bind to and hinder aggregation or denaturation of a protein at temperatures above its' denaturation temperature (T_m), while having little affinity to the protein at temperatures

below its LCST. Beierle *et al.* utilized this concept to tune the LCST of a NiPAm copolymer NP to create a polymer affinity agent with high affinity to lysozyme at elevated temperatures, but with little affinity to the protein at room temperature.[19] To achieve this, the NP formulation optimized by Yoshimatsu *et al.*[18] was modified by decreasing the tBAm content in an effort to raise the LCST of the NP. In doing so, they were able to increase the LCST of their NPs to 42 ^{o}C. Using centrifugation filtration, they found that their NPs had high affinity for lysozyme above 42 ^{o}C, with significantly lowered affinity for lysozyme at room temperature. When heating the NP-lysozyme mixture up to 80 ^{o}C (10 ^{o}C above lysozyme's denaturation temperature) for 20 min, they found that they could recover lysozyme upon cooling the NP-lysozyme complex back to room temperature. The recovered lysozyme was tested for activity against a *Micrococcus lysodeikticus* cell suspension, and found to retain ~80% of activity. These results establish that both affinity and LCST of NiPAm based NPs can be tuned, allowing these properties to be used for biomacromolecule stabilizations. An understanding of how changes in temperature can affect the structure and biomacromolecular affinity of synthetic affinity agents provides a molecular based explanation and can expand the possible applications of these synthetic affinity agents.

- Location of protein binding in a polymer affinity agent.

Proteins can bind in different configurations and into different locations on the synthetic affinity agents depending on the protein type and the monomer composition, size, and porosity of the NP. Studies of protein-NP interactions have found that proteins can either bind within the polymer network,[11] on the surface of the polymer, or both[16, 21] depending on the physical properties of the polymers (surface curvature, mesh size, etc.) and size, shape

and chemical composition of the biomacromolecule. Using micromanipulator-assisted light microscopy, Johansson *et al.* observed changes in a single polyAAc microgel upon lysozyme adsorption (Figure 1.8).[21] Lysozyme was found to initially bind to the outer portion of the microgel ("shell"), which resulted in microgel shrinkage. After saturation of lysozyme on the microgel shell, further addition of protein did not cause further microgel shrinkage. This was interpreted as lysozyme now binding throughout the interior of the microgel ("core").

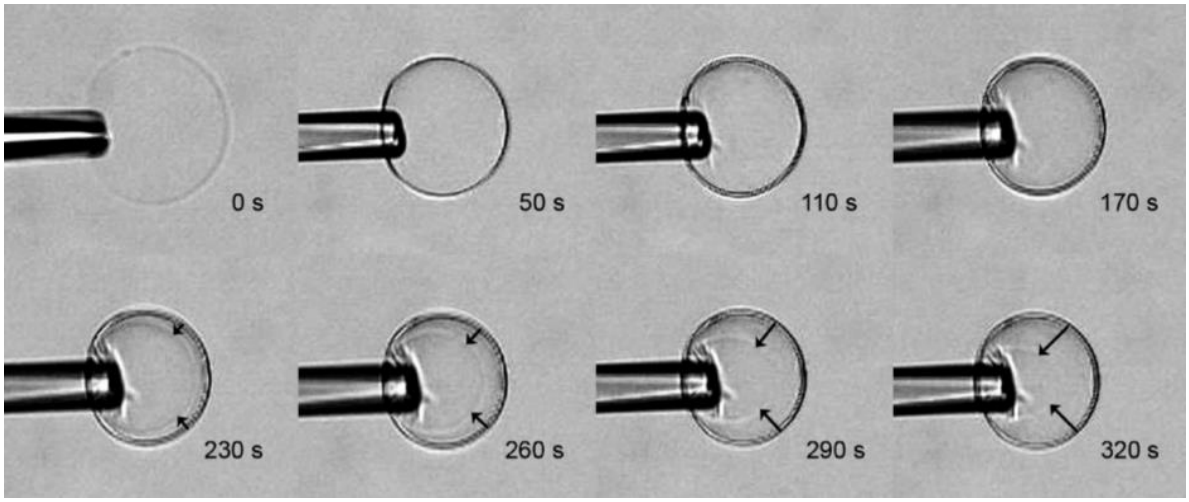

Figure 1.8. Micromanipulator-assisted light microscopy images showing a microgel, sucked onto the tip of a micropipet. The different time points show a titration of lysozyme into the microgel solution. Adapted with permission from reference [21]. Copyright 2009 American Chemical Society.

To explain why the microgel stopped shrinking and confirm continuing lysozyme adsorption, Johansson *et al.* added lysozyme labelled with two different fluorophores and different time points, and studied their uptake using confocal microscopy. They observed that lysozyme initially adsorbed to the outer shell, causing formation of a lysozyme shell.

This initial adsorption caused the microgel to shrink, likely due to charge neutralization that occurred upon binding, reducing charge repulsion in the polymer chains.[16] The lysozyme added later tended to diffuse into the core, as evidenced by a greater concentration of the second labelled lysozyme found in the core than in the shell. The authors suggested that this was possibly due to a slight aggregation of the lysozyme that bound in the outer shell, which stabilized the shell structure. The stabilization of the shell then allowed the lysozyme to diffuse through into the core without causing the microgel to shrink any further.

The same binding pattern was observed with Cyt C binding to a NiPAm-AAc copolymer.[16] Smith *et al.* found that Cyt C (pI ~10) bound initially to the polymer shell in pH 7.0 phosphate buffer (10 mM, ionic strength 20 mM). The Cyt C that bound formed a protein shell, which stabilized the microgel due to repulsion between the bound Cyt C molecules in the polymer shell. This stability then enabled diffusion of subsequent Cyt C through the collapsed protein shell, which resulted in a uniform distribution of Cyt C throughout the microgel at equilibrium.

Using near-infrared surface plasmon resonance microscopy (SPRM), Cho *et al.* monitored the uptake of the peptide melittin into NiPAm based copolymer NPs.[11] Relatively hydrophobic NPs (40% tBAm, 5% AAc, Figure 1.9C) were adsorbed to a hydrophobized (C11) gold surface so they could monitor changes in the point diffraction patterns on the surface plasmon polaritons across the gold surface to determine the average single NP SPRM reflectivity change ($<\Delta\%R_{NP}>$, Figure 1.9D). They found that melittin (0 to 2.5 μM) adsorbed to their NPs (20 pM) with an increase in $<\Delta\%R_{NP}>$ of 1.04 ± 0.03% over a 10 min period. In contrast, addition of the FLAG peptide and BSA to their NPs showed no change in $<\Delta\%R_{NP}>$ over a 10 min period (Figure 1.9B), showing some selectivity of their NP for melittin.

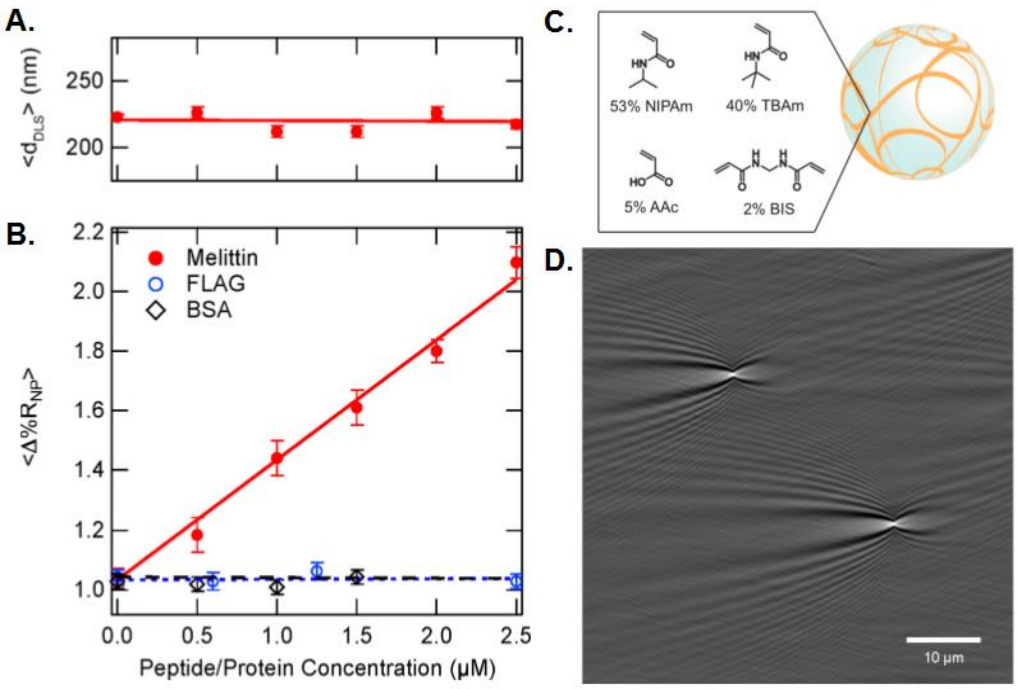

Figure 1.9. A. The mean r_H obtained by DLS and B. <Δ%R_{NP}> determined by SPRM of the NPs (30 pM) in the presence of melittin (0 – 2.5 μM). C. The NP composition used for the SPRM experiment. D. A 58.5 μm x 58.5 μm Fourier filtered SPRM 3 s differential reflectivity image showing the adsorption of 2 NPs onto a C11-functionalized gold film. Adapted with permission from reference [11]. Copyright 2015 American Chemical Society.

To ensure this reflectivity change was not due to an increase in NP volume over this time period, they tested the r_H of their NPs using DLS upon addition of melittin to their NP and found no change in r_H over the concentration range measured with SPRM (Figure 1.9A). This result establishes that melittin adsorbs into the NPs in a way that affects the refractive index of the NPs but not the size. Therefore, melittin binds to interior of the NP replacing PBS, which has a lower refractive index than melittin, in the NP core. From these studies, it

becomes apparent that binding location is dependent on the biomacromolecule studied and the polymer affinity agent used.

D. Stability and Activity of Proteins after Adsorption

Once biomacromolecular affinity to a NP affinity agent has been optimized, it is important to note how the bound biomacromolecules interact with the NP. For many applications, maintaining secondary and tertiary structure of biomacromolecules is necessary. Any denaturation or distortion will cause loss of function of enzymes, and block or otherwise impede active or binding sites on proteins, which would render the protein ineffective. It is therefore important to understand how introduction of functional groups affect the interactions of the synthetic affinity agents with biomacromolecules.

- Biomacromolecule stability upon binding to synthetic affinity agents.

Many groups have researched how and why hydrophobic groups can affect protein stability. However, it has also been observed that hydrophobic groups can be effective in increasing affinity to biomacromolecules. Therefore, finding a balance between increasing the intermolecular impact of a hydrophobic interaction while avoiding protein denaturation is of interest. Roach *et al.* used silica spheres of different sizes (15 – 165 nm) decorated with hydrophilic (hydroxy) and hydrophobic (alkane) surface chemistries to learn how surface curvature and functionality can affect the orientation of proteins upon binding.[22] They focused on targeting two proteins based on their shapes, bovine serum albumin (BSA), a globular protein, and bovine fibrinogen, a rodlike protein. Using infrared spectroscopy (IR)

with an attenuated total reflectance (ATR) accessory, they were able to examine the secondary structure of the bound proteins to determine how the silica NPs affected the bound proteins.

They found that less BSA absorbs to hydrophobic surfaces than to hydrophilic surfaces. In addition, more BSA is adsorbed as particle size increases with both hydrophobic and hydrophilic particles, due to the greater surface area availability per particle for binding. Upon binding, they observed that hydrophobic surfaces caused a higher amount of disorder and loss of native structure than hydrophilic surfaces. These trends were visible at all NP sizes. In addition, a large change in secondary structure for BSA was observed with NPs with radii from 10 - 40 nm, while larger sized particles saw a higher retention of native structure (Figure 1.10).

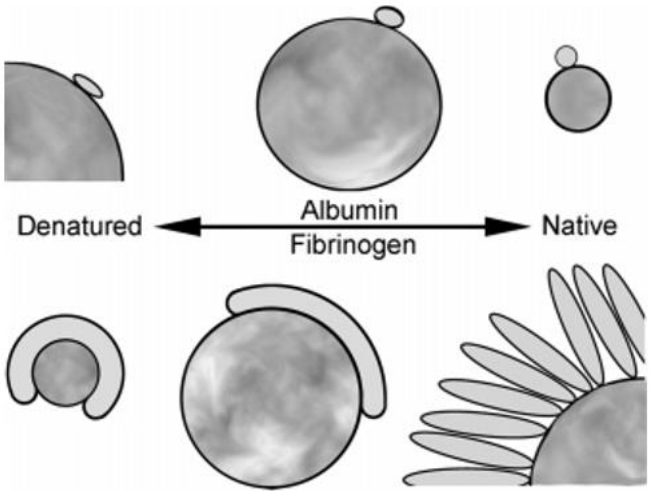

Figure 1.10. Schematic showing conformation and orientation of binding of albumin and fibrinogen depending on surface curvature. Adapted with permission from reference [22]. Copyright 2006 American Chemical Society.

Using the same technique, they found that less fibrinogen bound to hydrophobic surfaces. They attributed this to surface-induced deformation, which caused fibrinogen to spread onto the hydrophobic surface upon binding. This reduced the surface area available for interaction with the particle, leading to a lowered capacity for fibrinogen. They also found that the bound fibrinogen became more disordered on smaller particles, with little conformational change with larger particles. This trend was observed for both hydrophilic and hydrophobic spheres, but more disorder was observed with hydrophobic spheres in all sizes.

They were also able to observe that binding orientation of the fibrinogen depended on the size of the particles and the surface curvature (Figure 1.10). Fibrinogen has a rodlike structure, so it can either bind on its longer side (side-on), or on its short end (end-on). Using IR, they found that with particles with radii less than ~20 nm, the amount of fibrinogen bound corresponded with the theoretical amount expected for a side-on monolayer. In contrast, particles with radii greater than 20 nm bound more fibrinogen than expected for a side-on monolayer, but less than expected for an end-on monolayer. They associated this with constraints of close packing that would prevent a monolayer of end-on oriented fibrinogen. This study shows that controlling surface curvature and particle size is important, as it could influence protein affinity, stability, and binding orientation.

Using polystyrene NPs (220 d.nm), Kelly *et al.* studied the binding orientation, stability, and function of transferrin adsorption.[23] First, the size of the NP-transferrin complex was determined by differential centrifugal sedimentation (DCS). Next, they titrated in immunogold labels to detect available binding epitopes. Monoclonal labels were added initially, until saturation was observed by DCS, at which point polyclonal labels were titrated

in until saturation was observed. Once labeled, the complex was imaged using transmission electron microscopy (TEM) to detect where transferrin was attached to the polystyrene NPs, and in what orientation they bound. They found that transferrin is adsorbed onto the polystyrene particles with negligible directional preference for the adsorption.

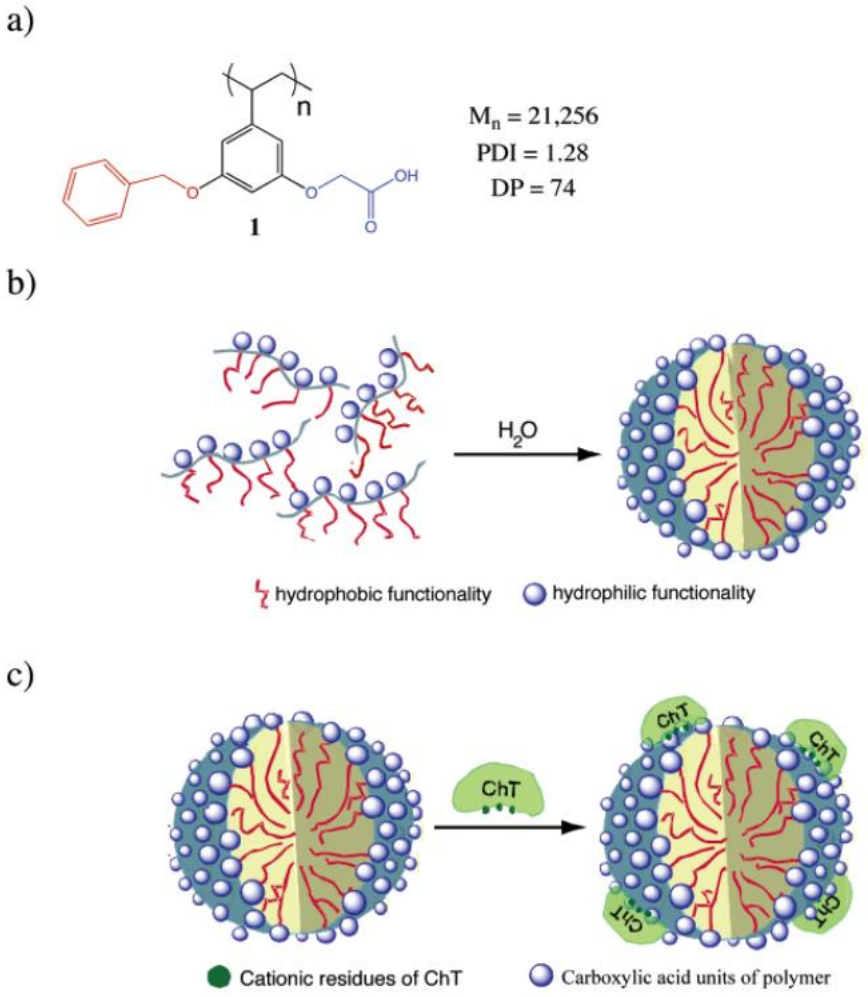

Figure 1.11. A. Chemical structure of polymer used. B. Formation of micellar structure of synthetic affinity agents in water. C. Schematic representation of polymer affinity agent interaction with ChT. Adapted with permission from reference [24]. Copyright 2005 American Chemical Society.

Using a different polymer system, Sandanaraj *et al.* studied polymer micelles formed from amphiphilic homopolymers containing carboxylic acid ligands on the surface, for affinity to chymotrypsin (ChT) (Figure 1.11).[24] They thought that the flexibility of this polymer system would allow the polymer to adapt to the surface of the protein, compared to gold NPs, which are rigid and may favor denaturation of protein. To determine how their amphiphilic homopolymers affected the structure of ChT, they analyzed the change in tryptophan fluorescence of ChT upon adsorption. They observed that there was a conformational change associated with polymer-ChT adsorption. To determine if this conformational change permanently affected the native structure, they analyzed ChT using circular dichroism (CD) to observe the secondary structure of ChT after binding to the polymer. They found that structural integrity is maintained, meaning the conformational change observed did not lead to denaturation of the native structure.

Using silica NPs, Lundqvist *et al.* studied how NPs of various sizes interacted with different variants of human carbonic anhydrase (HCA), and how this interaction affected the secondary structure of HCA.[25-26] Using 2D NMR (TROSY), they monitored the interactions between their NPs and different HCA variants, HCAI, HCAII, and a truncated version of HCAI (trunc5HCAI), and tracked any changes in the NMR spectrum. HCAI was seen as a "hard" variant, due to the higher stability of the protein along with the lower flexibility of the protein structure. Trunc5HCAI and HCAII were seen as the "soft" variant, due to lower stability of the protein and higher flexibility of the protein structure. They were able to observe how the structure of the different HCA variants were affected upon binding to a silica NP.

Initially, they observed complete loss of all the peaks in the NMR spectrum when their NPs begin interacting with HCA. The authors associate this phenomenon with the random

nature of the protein-polymer binding. Inexplicitly, after several days bound HCA became "visible" on NMR. As time passes, the NMR spectrum disappears again as the proteins lose their native structure and aggregate. The interaction of the protein-polymer complex in this case exhibits a complicated time dependent behavior and further study is needed to understand in more detail.

- Change in biomacromolecular activity upon binding to synthetic affinity agents.

Different compositions of synthetic affinity agents could not only change biomacromolecular conformation, but also the activity of bound biomacromolecules. Kelly *et al.* found that upon binding to polystyrene NPs, many binding sites on the bound transferrin were blocked by the particle surface or adjacent proteins.[23] Despite this, the transferrin bound to polystyrene NPs still bind iron, suggesting that some receptor binding sites were still accessible. Analysis of tryptophan fluorescence of the particle-transferrin complex showed that the adsorbed transferrin was not denatured. The loss of certain binding sites was therefore likely due to the random nature of transferrin binding to the particles blocking some iron binding sites.

With a slightly modified system, Welsch *et al.* studied how a NiPAm-AAc copolymer coating on polystyrene NPs (~85 d.nm) affects adsorbed lysozyme.[27] They studied the affinity of their coated NPs to lysozyme using ITC. They found that NP-lysozyme binding was strongly influenced by electrostatics. Despite this, the NPs still had affinity to lysozyme in buffer with high concentrations of salt. This was perhaps due to contributions of hydrophobic interactions to the NP-lysozyme binding. Interestingly, they found an increase in enzymatic activity of lysozyme by a factor of ~3.5 after binding of the protein to the NP.

They found, using ITC, that upon NP-lysozyme binding at pH 7.2, the bound lysozyme becomes protonated and exists in a similar protonation state as free lysozyme at pH 5, the pH for optimum lysozyme activity. Thus, the increased activity observed was likely due to protonation of lysozyme upon NP binding, which puts lysozyme in the optimal configuration for enzymatic activity.

The polystyrene based polymer micelles (~41 d.nm, Figure 1.11) studied by Sandanaraj *et al.* for affinity to chymotrypsin (ChT) were thought to be an alternative to gold NPs.[24] Binding to the stiff gold NPs showed loss of ChT activity upon release, possibly due to a partial denaturation of ChT upon Au NP binding. They thought that the more flexible polymer systems would perhaps be a better alternative to solid gold NPs for binding to and releasing native proteins. Addition of their polymer caused a loss in ChT activity, with one polymer binding approximately 10 ChT molecules. However, titration of NaCl into the polymer-ChT complex, caused loss in affinity of the polymer to ChT. ChT was able to regain its activity after release from the polymer.

Beyond just the basic crosslinked NiPAm NP, Cabaleiro-Lago *et al.* studied the interaction of NiPAm copolymer NPs containing tert-butylacrylamide (tBAm) with amyloid β (Aβ) fibrils in an effort to prevent fibrillation.[28] To establish if NPs could inhibit Aβ fibril formation, they studied the absence or presence of amyloid aggregates using a continuous thioflavin T (ThT) binding assay. They detected interactions between the amyloid fibrils and protofibrils by monitoring a red shift in the excitation spectrum of ThT. They found that the NPs inhibit fibrillation of Aβ differently depending on the concentration and hydrophobicity of the NPs. Less hydrophobic NPs (less tBAm and more NiPAm) could prevent Aβ fibrillation for longer times. They associated this phenomenon with hydrogen bonding between the NPs and Aβ

peptides. Hydrogen bonding between the β strands of Aβ fibrils has been shown to be an important structural feature.[29] Decrease in tBAm content increases the hydrogen bonding ability of NPs.[30] The increased hydrogen bonding between the NP and the Aβ fibrils are thus expected to inhibit hydrogen bonding between the Aβ fibrils, thus inhibiting Aβ fibrillation.

The author hypothesized that Aβ binding to NPs and inhibition of fibrillation could occur in two ways. The NPs could bind to the Aβ monomer and inhibit fibrillation by decreasing the amount of free monomer in solution. Trapping the Aβ monomers would disturb the monomer-oligomer equilibrium, thus causing early aggregates to dissociate to maintain the equilibrium. Another possible mechanism would be that the NPs bind to the Aβ oligomer. This would lead to depletion of sub and near-critical oligomers needed for fibrillation. By reducing oligomer concentration in solution, the nucleation step would be delayed. The NPs would then hinder the elongation process by blocking sites for monomer addition on the aggregates.

To determine which mechanism might be occurring, they tested the NPs using pyrene fluorescence analysis. Previous studies reported that the Aβ monomers bind preferentially to hydrophobic and positively charged surfaces to hinder the fibrillation process.[31] By analyzing the NPs using pyrene fluorescence, Cabaeiro-Lago *et al.* deduced that the NPs provide a more hydrophobic environment than water, thus leading to stronger affinity to Aβ monomers. They deduced that the NPs were likely associating with the Aβ monomers, thus disturbing the monomer-oligomer equilibrium hindering fibrillation (Figure 1.12). These studies show that changing the hydrophobic content of synthetic affinity agents can often have unintended effects on the stability or enzymatic activities of the biomacromolecules bound.

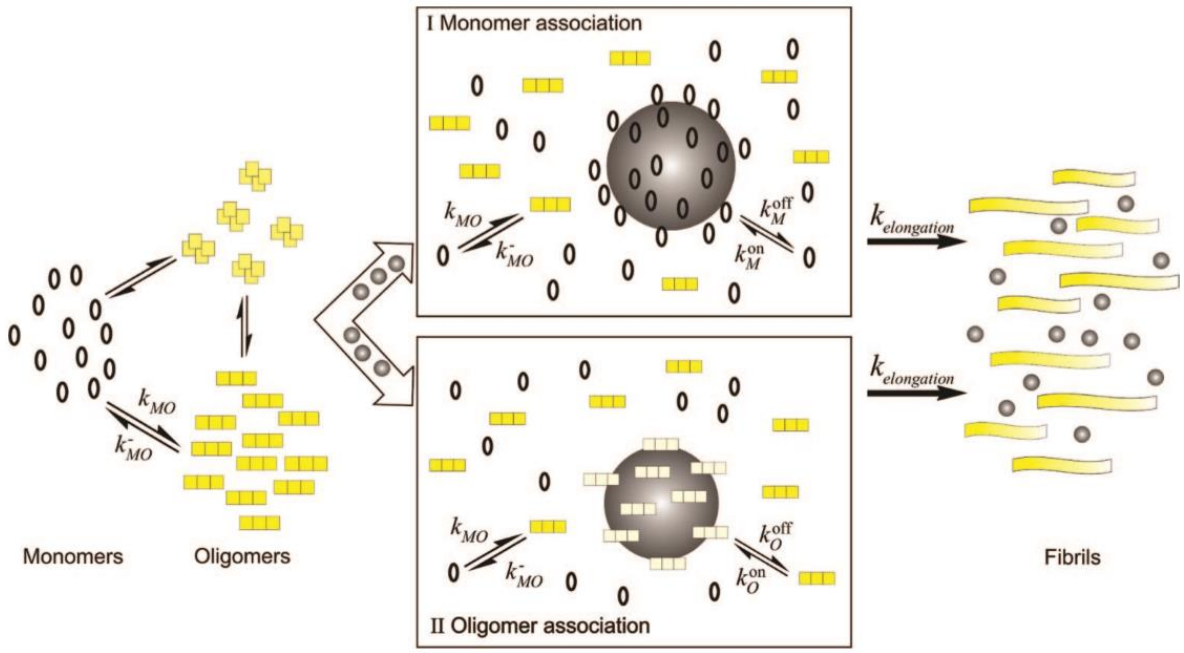

Figure 1.12. Scheme showing possible mechanisms of inhibition of fibrillation by NPs. Adapted with permission from reference [28]. Copyright 2008 American Chemical Society.

E. Conclusions

There are many types of intermolecular interactions that take place between polymers and biomacromolecules. Among them, hydrophobic interactions play a very important role. However, when a polymer affinity agent interacts with a biomacromolecular target, the observed effect can arise from many factors. The introduction of hydrophobic groups in the polymer can produce changes in the polymer itself, which in turn will influence its interaction with the biomacromolecule. It is therefore important to study not only how the composition of synthetic affinity agents influences biomacromolecular affinity, but also how the hydrophobic group influences the NP structure to gain a complete understanding of the interaction. It is also important to note how the synthetic affinity agents will respond to biomacromolecules under different environmental conditions, and how different

compositions will affect that response. Studying these responses can help determine which factors are important in optimizing affinity and activity towards biomacromolecular targets.

F. References

1. Hamidi, M.; Azadi, A.; Rafiei, P., Hydrogel nanoparticles in drug delivery. *Adv Drug Deliv Rev* **2008,** *60* (15), 1638-49.

2. Chen, G.; Roy, I.; Yang, C.; Prasad, P. N., Nanochemistry and Nanomedicine for Nanoparticle-based Diagnostics and Therapy. *Chem Rev* **2016,** *116* (5), 2826-85.

3. Franzreb, M.; Siemann-Herzberg, M.; Hobley, T. J.; Thomas, O. R., Protein purification using magnetic adsorbent particles. *Appl microbiol biot* **2006,** *70* (5), 505-16.

4. Dyson, H. J.; Wright, P. E.; Scheraga, H. A., The role of hydrophobic interactions in initiation and propagation of protein folding. *P Natl Acad Sci USA* **2006,** *103* (35), 13057-13061.

5. Ross, P. D.; Subramanian, S., Thermodynamics of Protein Association Reactions - Forces Contributing to Stability. *Biochemistry* **1981,** *20* (11), 3096-3102.

6. Moreira, I. S.; Fernandes, P. A.; Ramos, M. J., Hot spots-A review of the protein-protein interface determinant amino-acid residues. *Proteins* **2007,** *68* (4), 803-812.

7. De, M.; You, C. C.; Srivastava, S.; Rotello, V. M., Biomimetic interactions of proteins with functionalized nanoparticles: A thermodynamic study. *J Am Chem Soc* **2007,** *129* (35), 10747-10753.

8. Chen, K. M.; Rana, S.; Moyano, D. F.; Xu, Y. S.; Guo, X. H.; Rotello, V. M., Optimizing the selective recognition of protein isoforms through tuning of nanoparticle hydrophobicity. *Nanoscale* **2014,** *6* (12), 6492-6495.

9. Lindman, S.; Lynch, I.; Thulin, E.; Nilsson, H.; Dawson, K. A.; Linse, S., Systematic investigation of the thermodynamics of HSA adsorption to N-iso-propylacrylamide/N-tert-butylacrylamide copolymer nanoparticles. Effects of particle size and hydrophobicity. *Nano Lett* **2007,** *7* (4), 914-920.

10. Saunders, B. R., On the structure of poly(N-isopropylacrylamide) microgel particles. *Langmuir* **2004,** *20* (10), 3925-3932.

11. Cho, K.; Fasoli, J. B.; Yoshimatsu, K.; Shea, K. J.; Corn, R. M., Measuring Melittin Uptake into Hydrogel Nanoparticles with Near-Infrared Single Nanoparticle Surface Plasmon Resonance Microscopy. *Anal Chem* **2015,** *87* (9), 4973-4979.

12. Gao, J.; Frisken, B. J., Cross-linker-free N-isopropylacrylamide gel nanospheres. *Langmuir* **2003,** *19* (13), 5212-5216.

13. Clara-Rahola, J.; Fernandez-Nieves, A.; Sierra-Martin, B.; South, A. B.; Lyon, L. A.; Kohlbrecher, J.; Barbero, A. F., Structural properties of thermoresponsive poly(N-isopropylacrylamide)-poly(ethyleneglycol) microgels. *J Chem Phys* **2012,** *136* (21).

14. Leszczyszyn, O. Hydrodynamic Radius Vs Radius of Gyration.

15. Smith, M. H.; Herman, E. S.; Lyon, L. A., Network Deconstruction Reveals Network Structure in Responsive Microgels. *J Phys Chem B* **2011,** *115* (14), 3761-3764.

16. Smith, M. H.; Lyon, L. A., Tunable Encapsulation of Proteins within Charged Microgels. *Macromolecules* **2011,** *44* (20), 8154-8160.

17. Hoshino, Y.; Haberaecker, W. W.; Kodama, T.; Zeng, Z. Y.; Okahata, Y.; Shea, K. J., Affinity Purification of Multifunctional Polymer Nanoparticles. *J Am Chem Soc* **2010,** *132* (39), 13648-13650.

18. Yoshimatsu, K.; Lesel, B. K.; Yonamine, Y.; Beierle, J. M.; Hoshino, Y.; Shea, K. J., Temperature-Responsive "Catch and Release" of Proteins by using Multifunctional Polymer-Based Nanoparticles. *Angew Chem Int Edit* **2012,** *51* (10), 2405-2408.

19. Beierle, J. M.; Yoshimatsu, K.; Chou, B.; Mathews, M. A. A.; Lesel, B. K.; Shea, K. J., Polymer Nanoparticle Hydrogels with Autonomous Affinity Switching for the Protection of Proteins from Thermal Stress. *Angew Chem Int Edit* **2014,** *53* (35), 9275-9279.

20. Serpe, M. J.; Yarmey, K. A.; Nolan, C. M.; Lyon, L. A., Doxorubicin uptake and release from microgel thin films. *Biomacromolecules* **2005,** *6* (1), 408-13.

21. Johansson, C.; Hansson, P.; Malmsten, M., Mechanism of Lysozyme Uptake in Poly(acrylic acid) Microgels. *J Phys Chem B* **2009,** *113* (18), 6183-6193.

22. Roach, P.; Farrar, D.; Perry, C. C., Surface tailoring for controlled protein adsorption: Effect of topography at the nanometer scale and chemistry. *J Am Chem Soc* **2006,** *128* (12), 3939-3945.

23. Kelly, P. M.; Aberg, C.; Polo, E.; O'Connell, A.; Cookman, J.; Fallon, J.; Krpetic, Z.; Dawson, K. A., Mapping protein binding sites on the biomolecular corona of nanoparticles. *Nat Nanotechnol* **2015,** *10* (5), 472-479.

24. Sandanaraj, B. S.; Vutukuri, D. R.; Simard, J. M.; Klaikherd, A.; Hong, R.; Rotello, V. M.; Thayumanavan, S., Noncovalent modification of chymotrypsin surface using an amphiphilic polymer scaffold: Implications in modulating protein function. *J Am Chem Soc* **2005,** *127* (30), 10693-10698.

25. Lundqvist, M.; Sethson, I.; Jonsson, B. H., Protein adsorption onto silica nanoparticles: Conformational changes depend on the particles' curvature and the protein stability. *Langmuir* **2004,** *20* (24), 10639-10647.

26. Lundqvist, M.; Sethson, I.; Jonsson, B. H., High-resolution 2D H-1-N-15 NMR characterization of persistent structural alterations of proteins induced by interactions with silica nanoparticles. *Langmuir* **2005,** *21* (13), 5974-5979.

27. Welsch, N.; Becker, A. L.; Dzubiella, J.; Ballauff, M., Core-shell microgels as "smart'' carriers for enzymes. *Soft Matter* **2012,** *8* (5), 1428-1436.

28. Cabaleiro-Lago, C.; Quinlan-Pluck, F.; Lynch, I.; Lindman, S.; Minogue, A. M.; Thulin, E.; Walsh, D. M.; Dawson, K. A.; Linse, S., Inhibition of Amyloid beta Protein Fibrillation by Polymeric Nanoparticles. *J Am Chem Soc* **2008,** *130* (46), 15437-15443.

29. Nelson, R.; Sawaya, M. R.; Balbirnie, M.; Madsen, A. O.; Riekel, C.; Grothe, R.; Eisenberg, D., Structure of the cross-beta spine of amyloid-like fibrils. *Nature* **2005,** *435* (7043), 773-778.

30. Lynch, I.; Blute, I. A.; Zhmud, B.; MacArtain, P.; Tosetto, M.; Allen, L. T.; Byrne, H. J.; Farrell, G. F.; Keenan, A. K.; Gallagher, W. M.; Dawson, K. A., Correlation of the adhesive properties of cells to N-isopropylacrylamide/N-tert-butylacrylamide copolymer surfaces with changes in surface structure using contact angle measurements, molecular simulations, and Raman spectroscopy. *Chem Mater* **2005,** *17* (15), 3889-3898.

31. Ban, T.; Morigaki, K.; Yagi, H.; Kawasaki, T.; Kobayashi, A.; Yuba, S.; Naiki, H.; Goto, Y., Real-time and single fibril observation of the formation of amyloid beta spherulitic structures. *J Biol Chem* **2006,** *281* (44), 33677-33683.

Chapter 2

Tuning hydrophobicity in an Abiotic Affinity Reagent. Polymer hydrogel affinity reagents for molecules with lipid-like domains.

A. Introduction

Affinity reagents are molecules that bind specifically to a target biomolecule to track, detect, capture, or mediate its activity. Many affinity reagents such as proteins, nucleic acids and antibiotics, are biological in origin. Despite a variety of new strategies for generating biological affinity reagents, the time needed for their discovery, development and production, and reagent cost, provide a strong motivation to identify non-biological (abiotic) alternatives.[1, 2] Our program has focused on developing synthetic polymer affinity reagents that can function as alternatives to more traditional biological based reagents. Synthetic polymers have many features that make them attractive candidates as affinity reagents. Their size and conformational flexibility can be controlled, which can aid in interacting with a target biomacromolecule surface. In addition, polymers are relatively simple and inexpensive to produce and can be prepared rapidly on a large scale. Since these NPs are not synthesized in living organisms, biological contamination is avoided. Organic polymers are robust and can function under a variety of conditions. Importantly, a broad range of chemical functionality is available to optimize affinity. In some cases, the size, physical properties, and biomacromolecule affinity of polymers can be influenced by external stimuli (temperature, pH, ionic strength) providing an extra dimension of control.[3,4] There is now a number of

examples of synthetic linear polymers[5-7], dendritic polymers[8], and polymer nanoparticles (NPs) that have been engineered to exhibit affinity for a range of target peptides[9, 10], proteins[11, 12], and polysaccharides[11]. In these cases, polymer affinity was realized by incorporating functional groups that mimic side chains of amino acids that are complementary to the biomacromolecule target. These abiotic synthetic polymers offer alternatives to the corresponding biological affinity ligands.

In this report, we describe our efforts to develop abiotic synthetic polymers with affinity for lipid and lipid-like macromolecules, an important family of biomacromolecules. Our study focuses on lipopolysaccharides (LPS), the lipophilic component of the outer membrane of Gram-negative bacterial membranes. Their structure is distinct from peptides and proteins and present unique challenges for developing capture reagents that function in water.[13] LPS are released during cell growth, division, and death, can induce shock at 1 ng/mL in mammals, and can be toxic to primary cells at concentrations as low as 100 ng/mL.[13-15] Their presence is of great concern in the production of biologics, as LPS can be a major source of contamination, particularly with recombinant protein preparations.

LPS are comprised of four distinct domains. The conserved hydrophobic lipid A region incorporates into the bacterial cell membrane and is responsible for LPS-induced toxicity.[15] The inner and outer core regions, which are varied in composition among different bacteria, contain phosphates that give the LPS membrane an overall negative charge and help stabilize the outer membrane through interactions with divalent cations (Figure 2.1). The fourth region is the O-specific antigen region, which has a bacterial strain specific composition projecting from the LPS surface.[15]

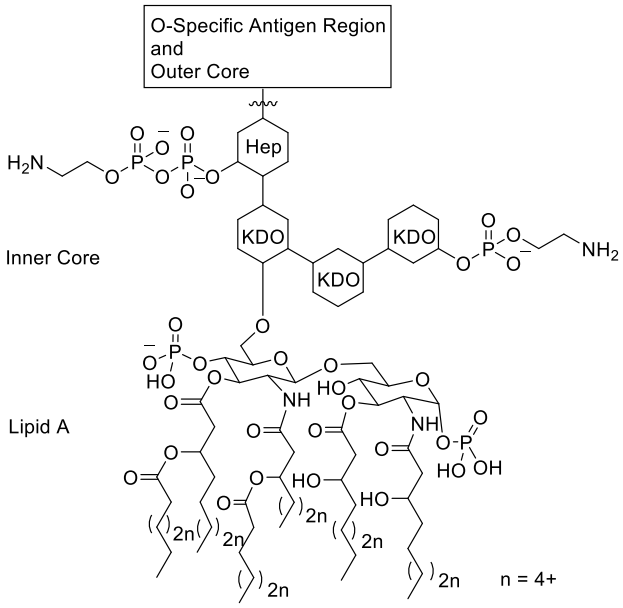

Figure 2.1. The inner core and lipid A portions of LPS. These are the portions being targeted by polymer hydrogel NPs.[16] KDO: 3-Deoxy-D-manno-oct-2-ulosonic acid, Hep: Heptose.

To develop a capture agent for lipid and lipid-like macromolecules, we evaluated a small library of synthetic polymer NPs incorporating a range of functional monomers. Insight into the choice of functional monomers used in the NP synthesis was drawn from known LPS affinity agents, such as polymyxin B (PMB). PMB is a basic peptide antibiotic derived from *Bacillus polymyxa* and has been shown to have high affinity for LPS.[13, 17] Commercial products incorporating PMB for LPS removal are commonly used to reduce LPS concentration. By systematically deleting functional groups from PMB, LPS affinity could be attributed to the side chains of several hydrophobic amino acids.[13] In addition, it was found that several charged groups also contributed to the initial recognition of PMB to LPS. With this information, the chemical composition of the NP library was varied to examine the contributions of both hydrophobic and electrostatic interactions to NP-LPS affinity in water. NP-biomacromolecule interactions were evaluated by fluorescence

polarization spectroscopy and affinity chromatography. A combination of 1D and 2D NMR was used to provide insight to the origins of affinity trends, in particular, the importance of hydrophobic group solvation in the NP to LPS binding. Our results provide guidelines for engineering NPs as lipophilic affinity reagents.

B. Synthesis and characterization of NiPAm based co-polymer nanoparticles.[29]

Table 2.1. A summary of NP compositions. All NPs contain 2 mol% BIS with the indicated amounts of functional monomer. The remainder was comprised of NiPAm (see Table S1 for complete data). Hydrodynamic diameters (Z-avg) were determined at 25 °C.

NP	tBAm (mol%)	OAm (mol%)	HAm (mol%)	BAm (mol%)	APM (mol%)	Z-avg (d.nm)
BAm20APM5	---	---	---	20	5	62
BAm30APM5	---	---	---	30	5	63
tBAm10	10	---	---	---	---	98
OAm10	---	10	---	---	---	56
HAm10	---	---	10	---	---	58
BAm10	---	---	---	10	---	131
BAm20	---	---	---	20	---	94
BAm30	---	---	---	30	---	79

A small library of synthetic polymer NPs was prepared using a modified precipitation polymerization. The NPs were synthesized with monomers that had physicochemical characteristics complementary to the different functional regions of the LPS molecule. We note, however, that we could not explore all of compositional space in NP synthesis. For example, at high feed ratios of *N*-alkylacrylamide monomers (BAm past 30%, HAm and OAm past 10%), the NPs aggregated, and are polydisperse by dynamic light scattering (DLS). Within this constraint, the compositions of the NPs discussed in this paper are summarized in Table 2.1. Full details of the complete NP library are given in Table 2.S1.

DLS experiments were conducted to assess the polydispersity (PDI), physical stability, and average hydrodynamic diameter (Z-avg) of the particles. Most NPs were monomodal (DLS) and behaved as stable colloidal suspensions (Table 2.1, 2.S1).

NiPAm based polymers can exhibit a temperature dependent phase transition (lower critical solution temperature, LCST). This phenomenon results in a change in NP size and density. In this entropically driven phenomenon, NPs will desolvate and collapse in size at temperatures above the LCST, but expand and become more water swollen below LCST.[4, 12, 30] The z-average hydrodynamic diameter of the NPs was determined from 15 – 40 °C (Figure 2.2, Table 2.S2); LCSTs of the NPs studied ranged from ~23 – 33 °C (Figure 2.2). A slight decrease in LCST with an increase in hydrophobic monomer content was noted for HAm and OAm copolymers, but a slight decrease was noted for BAm copolymers.

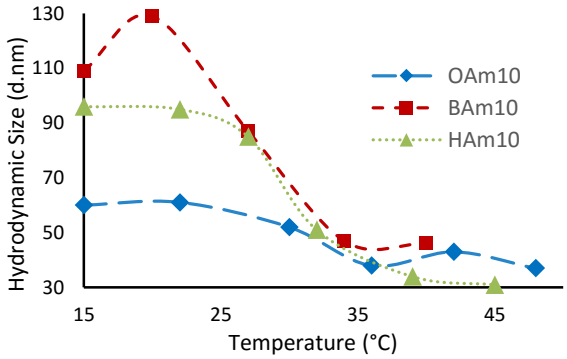

Figure 2.2. DLS hydrodynamic size (z-average) measurements taken of three NPs (♦ = **OAm10**, ▲ = **HAm10**, ■ = **BAm10**) at various temperatures from 15 – 50 °C to measure approximate LCST.

In some cases, we have observed that NP - biomacromolecular affinity is influenced by the degree of solvation of the NiPAm NP; measurements therefore can be influenced by

temperature, depending on whether the measurement is above or below the LCST.[12, 31] In the present study, LCSTs of the NPs ranged from ~23 – 33 °C and the affinity measurements were made at 25 °C. However we have established that there is a negligible difference in LPS affinity when measured at 25 °C or 37 °C (Figure 2.S1). Since there are a number of factors that contribute to NP-LPS affinity, and each of these may have a temperature dependence, the influence of NP size (hydration) does not contribute importantly in the 25 – 37 °C range in this study.

C. Fluorescence polarization analysis of NP-LPS interaction as a function of the hydrophobic monomer.

LPS binding to the NP library was evaluated by fluorescence polarization spectroscopy (FP) using a fluorescein modified LPS (FITC-LPS). Since hydrophobic interactions are related to the exposed surface area of the hydrophobic group, we were particularly interested in how the size and shape of the hydrophobic groups in the NP influence LPS binding. Our initial working hypothesis was that LPS affinity could be improved by an increase in the size of the hydrophobic functional group, providing the polymer NPs remained as stable collodial solutions. Within this constraint, a NP library comprising of NiPAm, BIS, and varying amounts of C4 (tBAm, BAm), C6 (HAm), and C8 (OAm) hydrocarbon groups were evaluated for LPS affinity.

A preliminary investigation revealed that NPs containing various levels of the tBAm monomer had no affinity to FITC-LPS (no effect on FP), so these NPs were not studied further. For the remaining hydrophobic monomers, NPs with a 10% loading of BAm (**BAm10**) exhibited the greatest increase in anisotropy when compared to NPs containing

10% HAm or OAm (**HAm10** and **OAm10**, Figure 2.3). We also found that increasing the feed ratio of the BAm monomer from 10 to 30% (Figure 2.S2A) resulted in a further increase in anisotropy. However, a further increase produced NPs that were no longer stable in water. The fluorescence polarization results imply that NPs containing an *n*-butyl (BAm) group have a stronger interaction with LPS compared to *n*-hexyl (HAm) or *n*-octyl (OAm) containing NPs. The results establish that simply increasing the surface area of the alkyl chain does not result in greater affinity to LPS. We sought to provide an explanation for this observation.

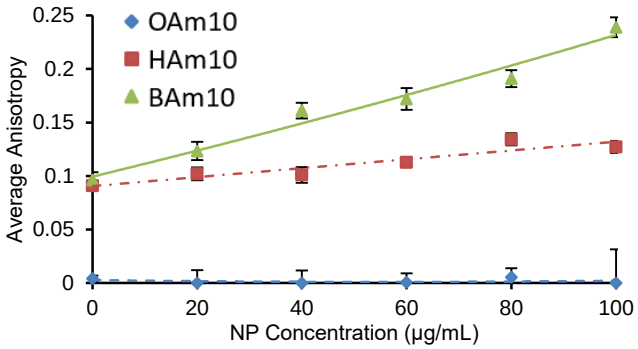

Figure 2.3. Fluorescence polarization study of NPs titrated into a solution of LPS (500 ng/mL) in 10 mM SPB at pH 6.8 at 25 °C. This figure shows the results of three NPs, each containing 10% of a *N*-alkylacrylamide monomer (♦ = **OAm10**, ■ = **HAm10**, ▲ = **BAm10**). A greater slope indicates higher LPS binding.

Several factors could contribute to the trends observed in Figure 2.3. The NP-LPS association arises from a balance between free energy of solvation of the polymer chains, self association of the polymer chains, or NP-LPS association. First, there is a progression of hydrophobicity in the *N*-alkylacrylamide monomers used in this study. The partition

coefficients (log *P,* water/octanol) of tBAm, BAm, HAm, and OAm have values of 0.8, 1.5, 2.5, and 3.5 respectively. The lower log *P* value of the BAm monomer compared to HAm and OAm monomers suggests a greater degree of solvation in water of BAm containing NPs. This could result in a greater accessibility to LPS resulting in greater LPS binding. The more hydrophobic monomers (HAm and OAm) on the other hand could have a greater degree of inter and intra chain association of hydrophobic groups. These aggregates would have a lower degree of water solvation, making them less favorable for LPS interaction. We turned to NMR spectroscopy to provide insight as to the mobility and degree of solvation and/or aggregation of the polymer chains in each NP.

D. NMR Investigations of NPs - Compositional analysis.

The NPs are lightly crosslinked and form globular structures with flexible polymer segments, allowing analysis by solution NMR spectroscopy. The ^{1}H NMR spectra of the polymers in $CDCl_3$ provided a semi-quantitative analysis of monomer incorporation (Figure 2.4, 2.S3). Incorporation of the hydrophobic monomers (OAm, HAm, BAm) was confirmed by the presence of a peak at 0.9 ppm corresponding to the terminal methyl group of the alkyl chain (Peak A). NiPAm was identified by a peak at 4.1 ppm, which corresponds to the methine proton associated with the isopropyl group of NiPAm (Peak B). The percent incorporation of BIS crosslinker (2%) was below the limit of detection and thus could not be established by NMR. APM signals were difficult to assign because of significant overlap in the ^{1}H NMR spectra of the other functionality present, but incorporation of these monomers under similar polymerization conditions was found to be >60% of the theoretical amount.[32] ^{1}H NMR analysis of the ratio of hydrophobic to NiPAm monomer

incorporation was confirmed by integration of peaks A and B. This ratio was consistent with the monomer feed ratio (Table 2.2).

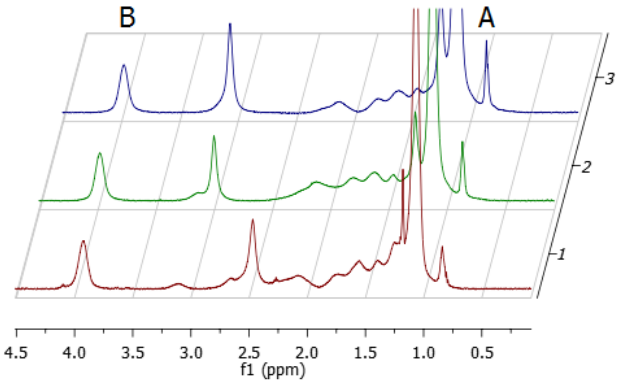

Table 2.

NP	A%	B%
BAm10	13	87
HAm10	11	89
OAm10	11	89
Feed Ratio	10	88

Figure 2.4. ^{1}H NMR's taken in $CDCl_3$ at 25 °C for NPs containing 10% *N*-alkylacrylamide, NiPAm, and BIS copolymers (1: **BAm10**, 2: **HAm10**, 3: **OAm10**). Peak A is a broad singlet at ~0.9 ppm representing the terminal methyl group in the hydrophobic monomers (BAm, HAm, OAm), and peak B is the broad singlet at ~4.1 ppm assigned to the methine proton of the isopropyl group in NiPAm.

Table 2.2. Incorporation ratios of **BAm10**, **HAm10**, and **OAm10**. These values were obtained by integration of peaks A and B in Figure 2.4. The feed ratio in all cases were 10:88 hydrophobic monomer to NiPAm.

E. NMR Investigations of NPs - 1D and 2D NMR spectra of NPs.

1D and 2D NMR experiments were performed to obtain information about intra-particle association. The NMR spectra were analyzed in water and chloroform to determine the influence of solvent on intra particle association. With increasing hydrophobicity of the monomers, there is an anticipated reduction in solubility of the NP polymer chains in water. This increase in hydrophobicity can result in a decrease in water solubility of the entire NP and/or an increase in self-association of the hydrophobic side chains, an intramolecular event. It is well known that relatively high resolution spectra can be obtained for swollen hydrogels under a variety of conditions.[33] Although the polymer chains are covalently associated in 2% cross-linked hydrogels, the individual chains are solvated, leading to averaging of the local dipolar interactions and relatively sharp lines. Aggregation of polymer chains in a hydrogel can lead to the water exclusion and restricted chain dynamics, leading to the disappearance of lines from the spectrum as they are broadened beyond detection. A partial collapse or strong self-association can cause the lines to broaden without completely disappearing from the spectra.

The two most basic probes for the structure and dynamics of hydrogels are the line widths and the dipolar interactions measured by NOESY NMR and relaxation methods. The terminal methyl groups in the copolymer side chains are of particular interest as the lines are sharpened by fast methyl group rotation and are usually the sharpest lines in the spectra. The effect of copolymer sequence on the line widths is illustrated in Figures 2.4, 2.5, which compares the NMR spectra of **BAm10, HAm10**, and **OAm10** in chloroform and water, respectively. The expected behavior of fully solvated NPs is that the terminal methyl groups for longer side chains would be sharper, since the methyl is separated by more

rotatable bonds from the more restricted main chain.[34] This is evident from the NMRs in chloroform, shown in Figure 2.4, which show fully solvated polymer chains with increasingly sharp peaks for the terminal methyls of the hydrophobic side chains with increasing chain length for BAm, HAm, and OAm. The NMRs of these same NPs in water, as shown in Figure 2.5, show quite different behavior. The lines from the BAm side chain are sharpest while the peaks from the HAm and OAm side chains are too broad to observe. This behavior can be explained by clustering of the more hydrophobic side chains in water. In such clusters the side chains are restricted and molecular motion insufficient to average the dipolar interactions. It is interesting to note that the NiPAm methine signals (3.9 ppm) do not appear to significantly increase in line width in all three NPs. This suggests that the hydrophobic side chains associate into small clusters in **HAm10** and **OAm10**, and do not affect the dynamics of the NiPAm, while **BAm10** side chains remain solvated in water.

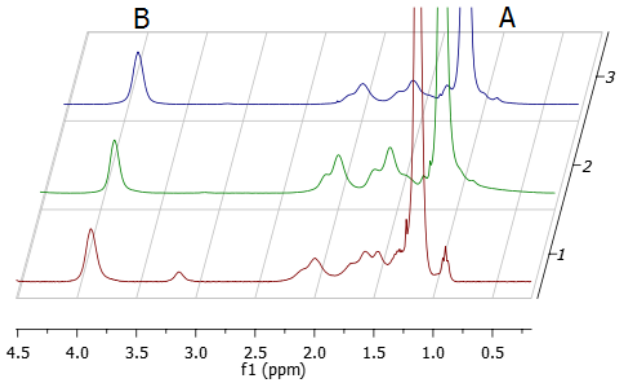

Figure 2.5. The 400 MHz spectra of 1. **BAm10**, 2. **HAm10**, and 3. **OAm10** in 90:10 H_2O:D_2O. Peak A refers to the side chain methyl and peak B refers to the side chain methylene protons.

A second measure of the structure of NPs are the dipolar interactions measured by the nuclear Overhauser effects (NOEs).[27] The NOE cross peaks are inversely proportional to the sixth power of the inter-nuclear separation and are difficult to observe between pairs of protons separated by more than 5 Å. This sensitivity to short distances makes the NOE an excellent tool to study the local molecular structure. In both synthetic and natural polymers in a random coil conformation it is possible to observe NOEs between nearest neighbor monomers by 2D NOESY.[35] These cross peaks may be absent in cases where the local structure is perturbed by self-association.

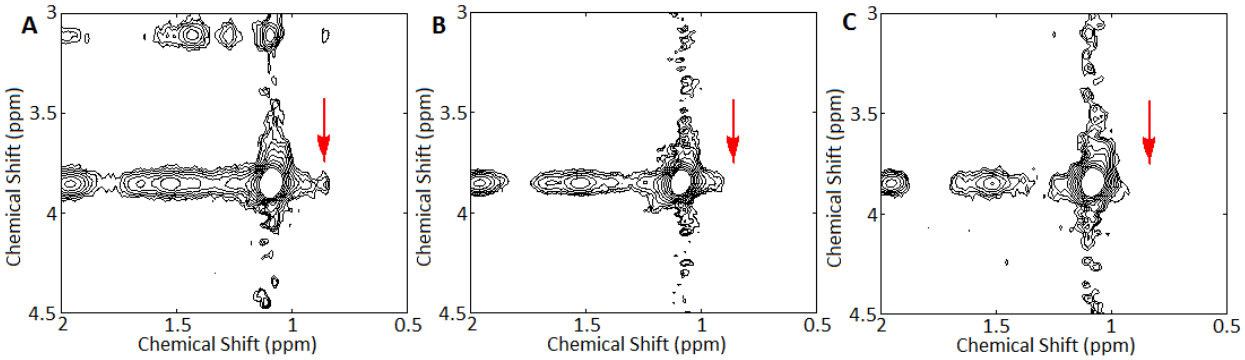

Figure 2.6. Truncated 2D NOESY spectrum showing the interaction between the terminal methyl group (0.9 ppm) of A. BAm, B. HAm, and C. OAm, and the methine (3.9 ppm) of NiPAm. The NP spectrums (A. **BAm10,** B. **HAm10**, C. **OAm10**) were acquired in 90:10 H_2O:D_2O with a 0.4 s mixing time. For full spectra, see Figure 2.S4.

2D NMR studies of NPs with 10% feed ratio of hydrophobic monomer (**BAm10**, **HAm10**, **OAm10,** Figure 2.6, 2.S4) are evaluated for intra-particle associations between the side chains present in the NPs. The results show that the least hydrophobic monomers (BAm and tBAm) exhibit intra-particle interactions between the NiPAm isopropyl group

(methine hydrogen) and the terminal methyl of BAm (0.9 ppm, Figure 2.6A and 2.64B) and tBAm (1.3 ppm, Figure 2.S4A). The more hydrophobic monomer, HAm (0.9 ppm, Figure 2.6B and 2.S4C), shows decreased interaction between the terminal methyl of HAm and the NiPAm methine hydrogen, while the most hydrophobic monomer, OAm (0.9 ppm, Figure 2.6C and 2.S4D), shows no association between the terminal methyl and NiPAm methine hydrogen. This result is consistent with the 1D data, and supports the analysis that increasing hydrocarbon chain length increases clustering of hydrophobic side chains in water, reducing their mobility and availability to participate in intermolecular association. All things being equal, increasing hydrophobicity of the monomer will increase the hydrophobicity of the overall NP with an inverse effect on water solubility of the hydrophobic side chains. At some critical point, this will lead to an increase in clustering of the hydrophobic side chains. Clustering or aggregation of side chains results in their desolvation, decreasing their availability to contact and bind to LPS. This clustering is related to the ability of the NPs to interact with and sequester compounds of interest since the alkyl groups must first disaggregate, a process that requires energy.

The observation that 10% tBAm containing NPs were ineffective at binding LPS suggests that chain branching of the hydrophobic group contributes significantly to affinity. The more compact C4 (tBAm) has less surface area than the linear C4 *n*-butyl ligand (BAm) and hence a lower degree of solvation. The net free energy gain by interacting with either self or LPS is less than **BAm10**, **HAm10**, and **OAm10**. Tuning a polymer by incorporating hydrophobic groups for LPS affinity requires hydrophobic groups that are on the cusp of aggregation. Much like the critical micelle concentration (CMC) of surfactant molecules in water, increasing the chain length of hydrophobic monomers will result in a decrease in the

intramolecular polymer CMC (pCMC) within the hydrogel network.[36, 37] This pCMC would be some local concentration of monomers that would encourage intramolecular aggregation of nonpolar functional groups to minimize contact with water. To optimize the interaction with hydrophobic targets, hydrophobic monomers within the NP must be at an optimal surface area, concentration and chain length to operate just below it's internal pCMC.

F. Influence of charged monomers on NP-LPS capacity.

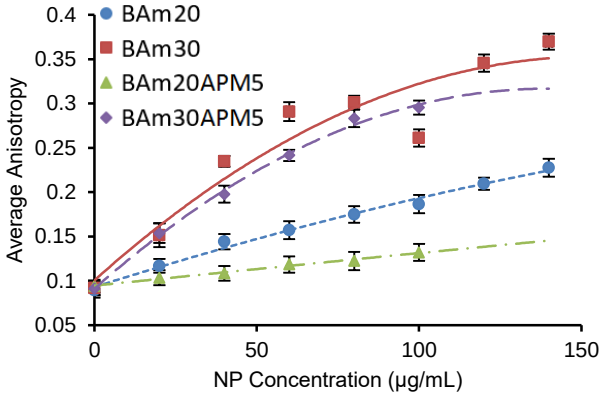

G.

Figure 2.7. Fluorescent polarization study of four NPs, with and without 5% APM (▲ = **BAm20APM5**, ♦ = **BAm30APM5**, ● = **BAm20**, ■ = **BAm30**), titrated into a solution of LPS (500 ng/mL) in 10 mM SPB at pH 6.8.

LPS carries a net negative charge, so the contribution of NP charge on LPS affinity was evaluated. NPs incorporating positively charged monomers (APM or GUA), together with NiPAm, BIS, and BAm, were incorporated into NPs and evaluated for LPS affinity. Interestingly, fluorescence polarization studies suggest that the addition of a charged monomer does not increase LPS binding, and in some cases even decreased binding. For

example, 30% BAm containing NPs with (**BAm30APM5**) and without 5% APM (**BAm30**) showed comparable affinity, but APM containing NPs with lower BAm content (**BAm20APM5**) had a reduced affinity for LPS compared to those without APM (**BAm20,** Figure 2.7 and 2.S2D). This data is consistent with the results reported by Srimal, *et al,* who observed that removing charged substituents on PMB did not greatly influence binding to LPS.[13]

Finally, to confirm that the binding observed in the fluorescence polarization studies was due to the LPS-NP interaction, rather than the LPS-fluorescein interaction, NPs with LPS affinity were tested against fluorescein itself. Addition of **BAm20** resulted in an increase in anisotropy when added to a solution of FITC-LPS, while no change in anisotropy was observed when **BAm20** was added to a solution of fluorescein itself (Figure 2.S2E). The anisotropy change is due to a NP-LPS interaction rather than a NP-fluorescein interaction.

H. Polymer Coated Agarose Beads – Evaluation of Clearance Effectiveness.

After establishing the NP composition with the highest LPS binding (BAm NPs), we evaluated the effectiveness of these polymers for clearing LPS from solution. The optimized formulations that incorporated BAm, NiPAm, and BIS were copolymerized onto agarose beads (Table 2.3) according to a protocol by Muller *et al.* Conjugation to the relatively-large agarose beads (40 – 165 μm) enables a method to separate the polymer-bound LPS from solution. Since polymer coating of beads is no longer bound by the constraints of forming uniform, stable NP solutions, a somewhat broader range of polymer compositions could be explored in this study.

Table 2.3. Monomer Feed Ratio of Polymers Coated onto Agarose

Sample	NiPAm %	BAm %	BIS %	% Monomers Functionalized
ABAm10	90	10	--	45
ABAm20	80	20	--	47
ABAm30	70	30	--	53
ABAm30B2	68	30	2	75
ABAm40	60	40	--	50
ABAm40B2	58	40	2	100
ABAm50	50	50	--	10
ABAm50B2	48	50	2	12

Table 2.4. Raw Data from Elemental Analysis.

Element	Agarose CL-4B	**ABAm40**	**ABAm40B2**
C	47%	53%	59%
H	6%	8%	9%
N	0%	6%	9%
Bead to Polymer Molar Ratio	100:0	53:47	25:75

The amount of polymer coated onto the agarose beads was evaluated by elemental analysis of coated and uncoated agarose beads. The theoretical percentages, along with the experimental mass percent data from the elemental analysis, were used to determine the ratio of agarose to polymer. Since nitrogen is only present in the polymers, the polymer loadings in **ABAm40** and **ABAm40B2** were estimated based on the increase in nitrogen content from elemental analysis (Table 2.4). The higher nitrogen content in **ABAm40B2** (9%) compared to **ABAm40** (6%) implied higher polymer loadings were obtained when BIS (2%) was added to the monomer mixture (Table 2.4).

The mass of polymer grafted onto the agarose beads was also confirmed by analysis of the washings from the polymerization step. Solvent was removed from the washings of

ABAm40 and **ABAm40B2**. The theoretical maximum of monomers polymerized onto the beads is assumed to be half of the feed ratio since half the initiators are not covalently attached to the bead. The trend observed from the washings (Table 2.3) showed that **ABAm40B2** (100%) had a higher polymerization yield than for **ABAm40** (50%). This data was supported by results obtained by elemental analysis of the samples (Table 2.4), which showed that **ABAm40** was 47% polymer by weight, and **ABAm40B2** was 75% polymer by weight.

However, efforts to prepare polymer coatings with higher loadings of hydrophobic monomer (> 40% BAm) resulted in low levels of polymer bound to the agarose beads. Most of the monomers were recovered in the washing steps. With 50% BAm loading (**ABAm50** and **ABAm50B2**), only a 10% coating by weight was observed. In addition, the polymer coated beads at this composition tended to aggregate and sediment rather than remain in suspension. Since these polymers aggregated in water, only beads loaded with 40% or less BAm could be successfully tested under aqueous conditions.

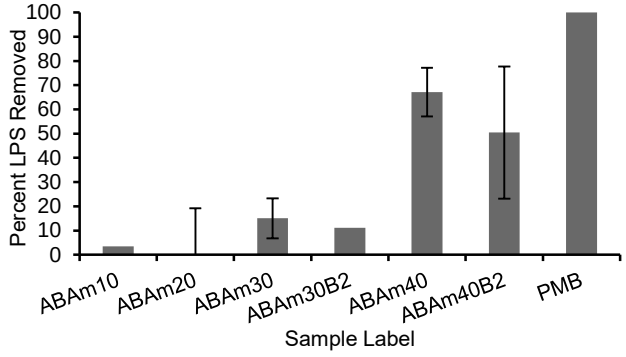

Figure 2.8. Fluorescence results from FITC-LPS solutions incubated in polymer coated agarose beads (n ≥ 3). PMB represents the commercially available polymyxin B column.

Polymer coated agarose beads (1 mL) were packed into a column and evaluated for their ability to remove FITC-LPS (1 μg/mL) from solution. The results of the LPS removal were compared to the commercially available PMB columns. **ABAm10** and **ABAm20**, showed no LPS removal from solution, while **ABAm30** and **ABAm30B2** saw 10 – 15% LPS removal from solution (Figure 2.8). **ABAm40** and **ABAm40B2** on the other hand, which had the maximum BAm loading (40%), removed substantially more LPS, with **ABAm40B2** clearing up to 50% and **ABAm40** clearing nearly 70% of LPS from solution. These results demonstrate that an increase in the feed ratio of BAm monomer (above what could be achieved in the NP study) produced a synthetic polymer coating that efficiently removed LPS from solution. By increasing BAm, LPS binding is improved. However, an effective removal system requires interaction between the polymer and the biomacromolecule. When the BAm feed composition exceeded 40%, the agarose beads became white and aggregated in aqueous solution and exhibited no ability to remove LPS from solution. This suggests that once the polymer coating on the agarose beads reached a critical "internal" concentration of BAm, it could no longer be solvated, and the wettability of the beads was lost, along with the potential to remove LPS. The ideal system balances maximum hydrophobic surface area with solvation. In a comparison with a commercially available PMB column, the synthetic polymer coated agarose beads have somewhat lower clearance, but at a significantly lower cost to produce. By identifying the factors that are important for LPS affinity, it is now possible to further enhance performance. Work towards this goal is currently underway.

I. Conclusions.

A library of synthetic copolymer NPs containing branched and linear C4-C8 hydrophobic N-alkyl acrylamide monomers, positively charged monomers, N-isopropylacrylamide (NiPAm) and N,N-methylenebisacrylamide (BIS) was synthesized using a modified precipitation polymerization technique. The compositional boundaries for realizing monodisperse NP formation were established. The stable colloidal suspension of NP copolymers were screened for LPS binding using fluorescence polarization of fluorescein modified LPS (FITC-LPS). Optimal affinity was found for NPs incorporating a linear C4 hydrocarbon group. Branched C4 and linear C6 and C8 hydrocarbons were substantially less effective. Increasing the BAm content resulted in a further increase LPS affinity, with a NP composition of BAm 30%, NiPAm 68%, BIS 2% (**BAm30**) having the greatest LPS affinity. To understand these observations, 1D and 2D ^{1}H NMR studies in water revealed that the longer chain (C6 and C8) alkyl groups in the hydrogel NPs were engaged in intrachain association, a phenomena that can be ascribed to an intraparticle CMC, analogous to the more common solution CMC. The intrachain association of hydrophobic groups renders them less available to interact with LPS. The results establish that although hydrophobicity plays an important role in LPS binding, optimal LPS-NP interaction requires a solvated hydrophobic group that is just below its "internal" CMC so as to avoid aggregation. Finally, since addition of charged monomers had little influence on NP-LPS binding, hydrophobic interactions play a much larger role in binding of lipophilic molecules than electrostatic interactions. Polymer compositions with high LPS binding were grafted onto agarose beads and evaluated for LPS clearance from solution; samples containing linear C4 groups also showed the highest LPS clearance capacity, a result

consistent with both fluorescence polarization and NMR studies. This study provides a guideline for optimizing performance of affinity reagents for binding lipophilic biomacromolecules.

J. Experimental procedures.

- Materials.

The following materials were obtained from commercial sources: *N*-isopropylacrylamide (NIPAm), 2,2'-azobisisobutyronitrile (AIBN), Sepharose CL-4B, acryloyl chloride, cetyltrimethylammonium bromide (CTAB), *N*-butylamine, *N*-hexylamine, *N*-octylamine, and lipopolysaccharides from *Escherichia coli* 0111:B4 (FITC conjugate, bound to primary amine associated with the phosphate groups) were obtained from Aldrich; *N*-(3-amidopropyl) methacrylamido (APM) was obtained from Polysciences Inc.; *N,N*'-methylenebisacrylamide (BIS) was from Fluka. All other solvents and compounds were obtained from Fisher Scientific Inc. or VWR International LLC. NIPAm was crystallized from hexane before use. Other chemicals were used as received. Water used in polymerization and characterization was purified using a Barnstead Nanopure Diamond™ system. Labconco Freezone 2.5 was used for lyophilization.

- Nuclear Magnetic Resonance (NMR) spectroscopy.

NMRs were run using two Bruker instruments with either a BBO or TCI probe, both at 500MHz, and analysis was done using the XwinNMR and MestReNova programs. NP solutions were lyophilized, then redispersed into a solution of deuterated chloroform for analysis.

- Dynamic Light Scattering (DLS).

Nanoparticle zetapotential, diameter, and polydispersity were determined with a Malvern ZEN3600 dynamic light scattering (DLS) instrument. Freshly dialyzed NPs were diluted 10 times in nanopure water for analysis.

- Elemental analysis.

The functionalized beads (20 mg) were dried using vacuum filtration, then left in a vacuum desiccator overnight. The beads were then sent out to Atlantic Microlab, Inc. for elemental analysis of C, H, and N. The results were then compared to a theoretical composition of C, H, and N to determine the relative incorporation of polymer to beads.

- Synthesis of N-octylacrylamide.[18]

Alkyl acrylamides were prepared from literature procedures. Briefly, acryloyl chloride (5.1 mmol, 850 µL) was mixed into a solution of dry CH_2Cl_2 (75 mL), and slowly dripped into a solution of *N*-octylamine (6.1 mmol, 1010 µL) in triethylamine (6.1 mmol, 410 µL) at 0 ^{0}C for 1 h with stirring. The resulting solution was warmed to room temperature with stirring, and left overnight. The solution was washed with saturated solutions of NH_4Cl (100 mL), $NaHCO_3$ (100 mL), then NaCl (100 mL). The organic layer was dried over $MgSO_4$, and the solvent was evaporated to yield a white powder. The product was recrystallized in hexanes to yield a white crystalline product, *N*-octylacrylamide. (88%) ESMS *m/z*: 183.1[(M) calc'd for $C_{11}H_{21}NO$: 183.32]. T_m: 34°C (Lit T_m 35-36°C). ^{1}H NMR (500 MHz, $CDCl_3$): δ 0.88 (t, *J* = 13.8 Hz, 3H, CH_3), 1.29 [m, 10H, $(CH_2)_5$], 1.54 (m, 2H, CH_2), 3.35 (q, *J* =

6.7 Hz, 2H, CH_2), 5.52 (s, 1H, NH), 5.64 (dd, *J* = 10.3, 1.4 Hz, 1H, =CH), 6.08 (dd, *J* = 16.9, 10.3 Hz, 1H, $=CH_2$), 6.27 (dd, *J* = 17.0, 1.0 Hz, 1H, $=CH_2$).

- Synthesis of N-hexylacrylamide.[18]

A yellow waxy product was synthesized using the same procedures as for *N*-octylacrylamide, but with *N*-hexylamine. (85%) ESMS *m/z*: 155.1[(M) calc'd for $C_9H_{17}NO$: 155.27] T_m: 27°C (Lit. T_m: 31-32°C). ^{1}H NMR (500 MHz, $CDCl_3$): δ 0.89 (t, *J* = 13.7 Hz, 3H, CH_3), 1.30 [m, 6H, $(CH_2)_3$], 1.54 (m, 2H, CH_2), 3.33 (q, *J* = 6.8 Hz, 2H, CH_2), 5.52 (s, 1H, NH), 5.64 (dd, *J* = 10.3, 1.4 Hz, 1H, =CH), 6.08 (dd, *J* = 16.9, 10.3 Hz, 1H, $=CH_2$), 6.28 (dd, *J* = 17.0, 1.4 Hz, 1H, $=CH_2$).

- Synthesis of N-butylacrylamide.[18]

Using the procedure described above, a clear oil was obtained using *N*-butylacrylamide, rather than *N*-octylamine. The product was purified using column chromatography with hexanes:ethyl acetate as eluent. (93%) ESMS *m/z*: 127.1[(M) calc'd for $C_{11}H_{21}NO$: 127.2]. ^{1}H NMR (500 MHz, $CDCl_3$): δ 0.92 (t, *J* = 14.7 Hz, 3H, CH_3), 1.36 [m, 2H, -CH_2-], 1.53 [m, 2H, -CH_2-], 3.32 (q, *J* =6.7 Hz, 2H, N-CH_2-), 5.60 (dd, *J* = 10.2, 1.9 Hz, 1H, =CH), 5.91 (s, 1H, NH), 6.10 (dd, *J* = 17.0, 10.25 Hz, 1H, $=CH_2$), 6.25 (dd, *J* = 17.0, 1.43 Hz, 1H, $=CH_2$).

- Synthesis of NiPAm copolymer nanoparticles.

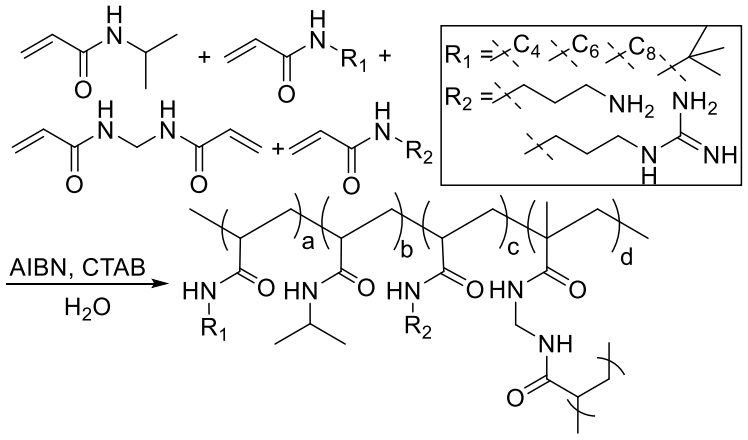

Scheme 2.1. Synthesis of NiPAm based co-polymer NPs.

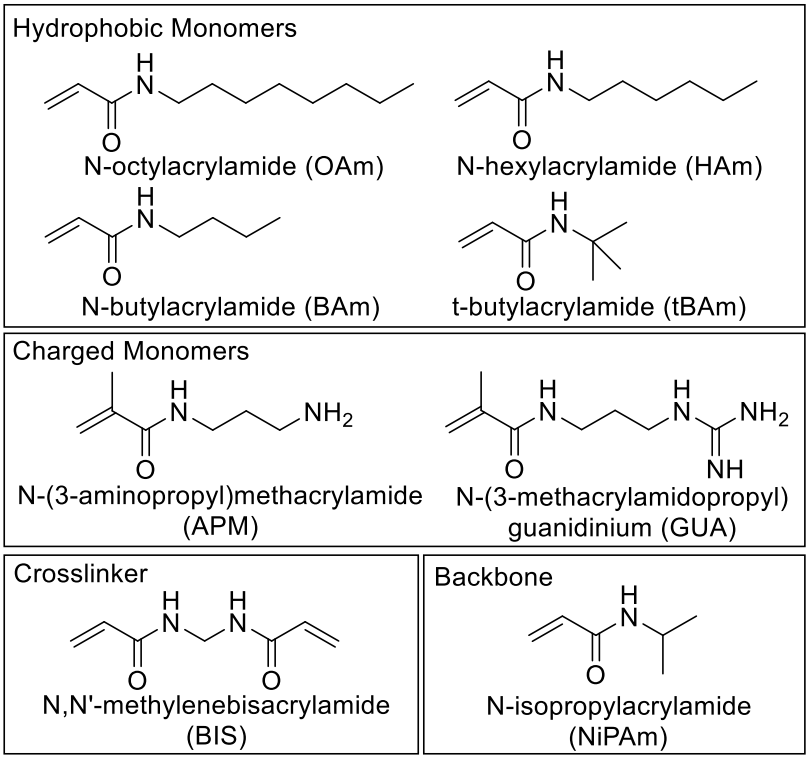

Figure 2.9. Monomers used for the synthesis of polymer NPs. NiPAm and BIS were used as the backbone and crosslinker of the synthetic polymers, respectively.

NPs were synthesized by a modified precipitation polymerization in an aqueous solution of functional monomers (Scheme 2.1, Figure 2.9).[9, 19-23] Briefly, stock solutions of NiPAm (A mol%), APM (B mol%), GUA (C mol%), BIS (2 mol%), and CTAB (0.2 mg/mL) were prepared by dissolving in the compounds in nanopure water. The OAm, HAm, BAm, and tBAm (D mol%) stock solutions were prepared by dissolving the compounds in a minimal amount of ethanol. Monomers were added in the desired ratios to generate a total monomer concentration of 65 mM in 50 mL of water. The solutions were degassed for 30 min with nitrogen while stirring. The initiator (AIBN, 0.6 mg/mL) was dissolved in minimal volume of acetone (~200 μL). The initiator was then injected into the reaction mixture after degassing, and the flask was immersed into an oil bath at 60 °C for 3 h with stirring under a nitrogen atmosphere. The polymer solutions were purified by dialysis against deionized water (4 L for 200 mL crude NP) using a 12 – 14 kDa MWCO regenerated cellulose membrane, and changing the water twice daily for 4 d. After dialysis, 5 mL of the NP solution was lyophilized to determine weight based concentration and yield.

- Synthesis of copolymer coated agarose beads.

Commercially available agarose beads were modified to display an initiator, from which monomers were copolymerized. (Scheme 2.2).[24] Briefly, Sepharose CL-4B beads (20 mL gel volume, 40 – 165 μm bead diameter), were washed thoroughly with water and dried by vacuum filtration. The beads were then resuspended in a NaOH solution (50% v/v, 0.4 M) and stirred (30 min at 40 °C). Epichlorohydrin (5% v/v) was injected into the mixture, and the reaction was stirred for 2 h. The beads were then washed with water and dried by vacuum filtration. The beads were resuspended in ammonia (2 M, 57% v/v) and warmed

overnight (30 °C) with stirring. The beads were then washed (water, ethanol) and dried by vacuum filtration. A Kaiser test was used to establish the presence of primary amines.[25] The beads were then resuspended in DMF (1:1 DMF:H_2O) containing 2-ethoxy-1-ethyoxycarbonyl-1,2-dihydroquinoline (EEDQ, 150 mM) and 4,4'-azobis(4-cyanovaleric acid) (ACV, 75 mM) under N_2 for 6 h at RT. Following filtration and washing (DMF, ethanol), the beads were vacuum filtered. The beads were resuspended in ethanol-water (1:1 v/v) with the monomer mixture (808 mM) and heated to 80 °C overnight with stirring. Following cooling, washing (EtOH, water), and drying by vacuum filtration the beads were stored in an ethanol-water mixture (1:4 v/v) until use.

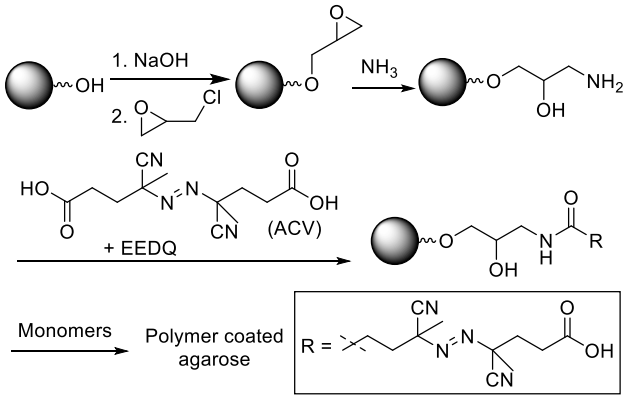

Scheme 2.2. Functionalization of agarose beads.

- Percent yield of agarose bead functionalization.

To determine relative yield, the washings from the polymerization step were saved and the solvent was removed using rotary evaporation. The residue was then weighed to determine yield.

- Kaiser test.

The Kaiser test was used after the epoxide opening step. Around 5 mg of beads were dried by vacuum filtration and placed in a vial. Stock solutions of 0.5 g ninhydrin in 10 mL ethanol and 0.4 mL of 0.001 M KCN in 20 mL of pyridine were made up, and 100 μL of each solution was mixed in with the dried beads. The mixture was then heated up to 100 °C for 5 min. A sample of unfunctionalized Sepharose CL-4B beads was run concurrently as a negative control.[1] The samples were then removed from heat, and the color of the solution was observed. A purple solution indicated the presence of primary amines, and an orange solution indicated a lack of primary amines in solution.

- Lower Critical Solution Temperature (LCST) measurements.

The NP hydrodynamic diameter was determined between 15 – 40 °C using a Malvern ZEN3600 DLS instrument. NPs were diluted in nanopure water to 1 mg/mL for analysis. The NPs were allowed to incubate at each temperature for 10 min prior to each measurement.

- Fluorescence polarization.

FITC-LPS molecules were shown to bind nonspecifically to filters, and thus LPS and NPs were not easily separated. As the presence of NPs will affect most assays used to detect presence of LPS, a solution based technique like fluorescence polarization was ideal in this instance. Fluorescence was determined with a SPEX Fluorolog1680 0.22m Double Spectrometer, and fluorescent polarization was determined with the ISS Photon Counting Spectrofluorometer. Stock solutions of NPs (2 mg/mL) and fluorescein tagged LPS (FITC-

LPS, 50 μg/mL) were diluted using SPB (sodium phosphate buffer, 10 mM, pH 6.8). FITC-LPS (Sigma) was diluted with SPB to a final concentration of 500 ng/mL. The mixture was incubated in the dark at 25 °C for ~5 to 10 min and transferred into a quartz cuvette, and the FITC-LPS content was analyzed at an excitation wavelength of 500 nm, with an emission filter at 525 nm. A solution of NPs (0 – 200 μg/mL) was then titrated into the cuvette, allowing ~5 min to equilibrate. Each experiment was repeated at least 3 times, with the final results averaged and plotted against final concentration of NP in each solution. A polymer EC_{50} (pEC_{50}) was calculated using a four parameter logistic equation with a sigmoidal fit of change in anisotropy versus log [NP], assuming the NPs act as a receptor, and the change in anisotropy represents the activity measured.

- NMR Characterization of NPs.

Proton NMR spectra were acquired at 298 °K on a 400 MHz or 500 MHz Bruker Advance NMR spectrometer using the WATERGATE pulse sequence for water suppression.[26] NP solutions were lyophilized, then redispersed into a solution of deuterated chloroform for analysis or were used in the original water solution at 5 mg/mL and contained 10% D_2O for NMR field frequency locking. The NOESY spectra[27] were acquired with 6 kHz sweep widths in the direct and indirect dimensions with mixing times of 0.4 s. The collected data matrix of size 512 x 2048 was zero filled to 2048 x 2048 and quadrature detection in the indirect dimension was achieved using time-proportional phase incrementation.[28]

- Evaluation of modified agarose beads for LPS capacity.

The polymer coated agarose beads were tested for their ability to remove LPS from a SPB solution using FITC-LPS. The experiment was performed by equilibrating the polymer coated agarose beads (1 mL, vacuum filtered) in sodium phosphate buffer (SPB, 10 mM, pH 6.8). A solution of FITC-LPS (1 μg/mL, 1 mL), diluted in the same buffer, was mixed with the beads and incubated for 1 h. The supernatant was then collected and analyzed at emission wavelength of 513 nm after excitation at 485 nm.

K. Supplementary Information.

Table 2.S1A. Summary of sizes, PDI's, yields, log[NP], and pEC_{50} of all the OAm containing NPs synthesized.

NP	OAm (mol%)	NiPAm (mol%)	Bis (mol%)	APM (mol%)	Z-avg (d.nm)	PDI	Yield (%)	Log ([NP])	pEC_{50} (nM)
OAm2.5APM5	2.5	90.5	2	5	102	0.38	49	NC	NC
OAm5APM5	5	88	2	5	91	0.28	45	NC	NC
OAm10APM5	10	83	2	5	96	0.25	70	NC	NC
OAm20APM5	20	73	2	5	97	0.24	41	ND	ND
OAm2.5	2.5	95.5	2	---	83	0.06	56	-8.0	10.4
OAm5	5	93	2	---	75	0.05	57	NC	NC
OAm10	10	88	2	---	56	0.02	60	NC	NC

Table 2.S1B. Summary of sizes, PDI's, yields, log[NP], and pEC_{50} of all the HAm containing NPs synthesized.

NP	HAm (mol%)	NiPAm (mol%)	Bis (mol%)	APM (mol%)	Z-avg (d.nm)	PDI	Yield (%)	Log ([NP])	pEC_{50} (nM)
HAm2.5APM	2.5	90.5	2	5	90	0.36	47	NC	NC
HAm5APM5	5	88	2	5	90	0.26	54	ND	ND
HAm10APM5	10	83	2	5	91	0.26	55	ND	ND
HAm20APM5	20	73	2	5	96	0.24	48	-6.5	290.3
HAm2.5	2.5	95.5	2	---	66	0.08	63	NC	NC
HAm5	5	93	2	---	65	0.09	66	ND	ND
HAm10	10	88	2	---	58	0.06	62	-7.7	18.4

Table 2.S1C. Summary of sizes, PDI's, yields, log[NP], and pEC_{50} of the BAm containing NPs synthesized.

NP	BAm (mol%)	NiPAm (mol%)	Bis (mol%)	APM (mol%)	Z-avg (d.nm)	PDI	Yield (%)	Log ([NP])	pEC_{50} (nM)
BAm5APM5	5	88	2	5	101	0.28	51	NC	NC
BAm10APM5	10	83	2	5	81	0.22	51	NC	NC
BAm20APM5	20	73	2	5	62	0.2	47	ND	ND
BAm30APM5	30	63	2	5	63	0.23	59	-8.0	10.2
BAm5	5	93	2	---	231	0.03	74	ND	ND
BAm10	10	88	2	---	131	0.0	62	-7.8	15.7
BAm20	20	78	2	---	94	0.03	66	-7.7	22.2
BAm30	30	68	2	---	79	0.03	67	-8.0	10.4

Table 2.S1D. Summary of sizes, PDI's, yields, log[NP], and pEC_{50} of the BAm-GUA containing NPs synthesized.

NP	BAm (mol%)	NiPAm (mol%)	Bis (mol%)	GUA (mol%)	Z-avg (d.nm)	PDI	Yield (%)	Log ([NP])	pEC_{50} (nM)
BAm10GUA5	10	83	2	5	118	0.31	51	ND	ND
BAm20GUA5	20	73	2	5	70	0.33	57	ND	ND
BAm30GUA5	30	63	2	5	83	0.32	49	-7.1	79.3

Table 2.S1E. Summary of sizes, PDI's, yields, log[NP], and pEC_{50} of the tBAm containing NP synthesized.

NP	tBAm (mol%)	NiPAm (mol%)	Bis (mol%)	Z-avg (d.nm)	PDI	Yield (%)	Log ([NP])	pEC_{50} (nM)
tBAm10	10	88	2	98	0.02	97	NC	NC

Supporting Table 2.S1. A, B, C, D, E. Details of which nanoparticles were synthesized, and their sizes, determined by dynamic light scattering (DLS) at 25 °C, diluted 1:10 in nanopure water. NP were synthesized using an AIBN initiator and CTAB surfactant. All monomer solutions were flushed with N_2 for 15 minutes prior to addition of initiator. All NPs were stirred for 3 h at 60 °C. Yields were determined by lyophilizing 5 - 10 mL of solution, and weighing the product to determine mass percentage. The polymer EC_{50}'s (pEC_{50}) was calculated using a four parameter logistic equation with a sigmoidal fit of anisotropy change in FP against log (NP concentration), with the polymers acting as the receptor, and the anisotropy change being the activity observed. The molecular weight of each NP was estimated to be 5000 kDa based off averages of previous molecular weight calculations. The raw data is shown in Figure 2.3, and 2.S2. ND = Not Determined, NC = No Change in anisotropy.

Table 2.S2A.

T (°C)	OAm2.5APM5 (d.nm)	OAm5APM5 (d.nm)	OAm10APM5 (d.nm)
15	*86*	64	*65*
20	*85*	67	63
25	*92*	*71*	70
32	*81*	60	64
38	*73*	*57*	60
44	*73*	51	54

Table 2.S2B.

T (°C)	HAm2.5APM5 (d.nm)	HAm5APM5 (d.nm)	HAm10APM5 (d.nm)	HAm20APM5 (d.nm)
15	46	52	44	43
21	46	52	44	43
25	45	54	46	48
32	37	46	40	42
40	*36*	*44*	38	39
44	*36*	43	37	36

Table 2.S2C.

T (°C)	BAm5APM5 (d.nm)	BAm10APM5 (d.nm)	BAm20APM5 (d.nm)	BAm30APM5 (d.nm)
10	---	---	82	83
15	95	92	73	73
20	94	88	65	62
25	92	81	57	58
30	73	63	57	56
35	59	56	54	54
40	58	53	51	52
45	55	49	49	49

Table 2.S2D.

T (°C)	NiPAm 98% (d.nm)	OAm2.5 (d.nm)	OAm5 (d.nm)	OAm10 (d.nm)
15	125	82	87	60
22	135	89	82	61
30	156	83	73	52
36	113	47	45	38
42	57	42	42	43
48	63	43	40	37

Table 2.S2E.

T (°C)	HAm2.5 (d.nm)	HAm5 (d.nm)	HAm10 (d.nm)
15	67	63	96
22	67	66	95
27	59	62	85
32	55	52	51
39	31	34	34
45	33	34	31

Table 2.S2F.

T (°C)	BAm5 (d.nm)	BAm10 (d.nm)	BAm20 (d.nm)
15	102	109	135
20	94	129	132
27	45	87	117
34	40	47	59
40	40	46	58

Supporting Table 2.S2 A-F: Lower critical solution temperature (LCST) study on DLS data showing trends in size of various NPs based on changing temperature. NPs were diluted with nanopure water in 1:10 dilution from stock solutions. The study was done using disposable cuvettes. Each sample was equilibrated for 10 minutes prior to each reading. The italicized values represent values with PDI's that were too high for the particles to be considered monodisperse. All values are determined by the Z-avg of the samples.

Figure 2.S1.

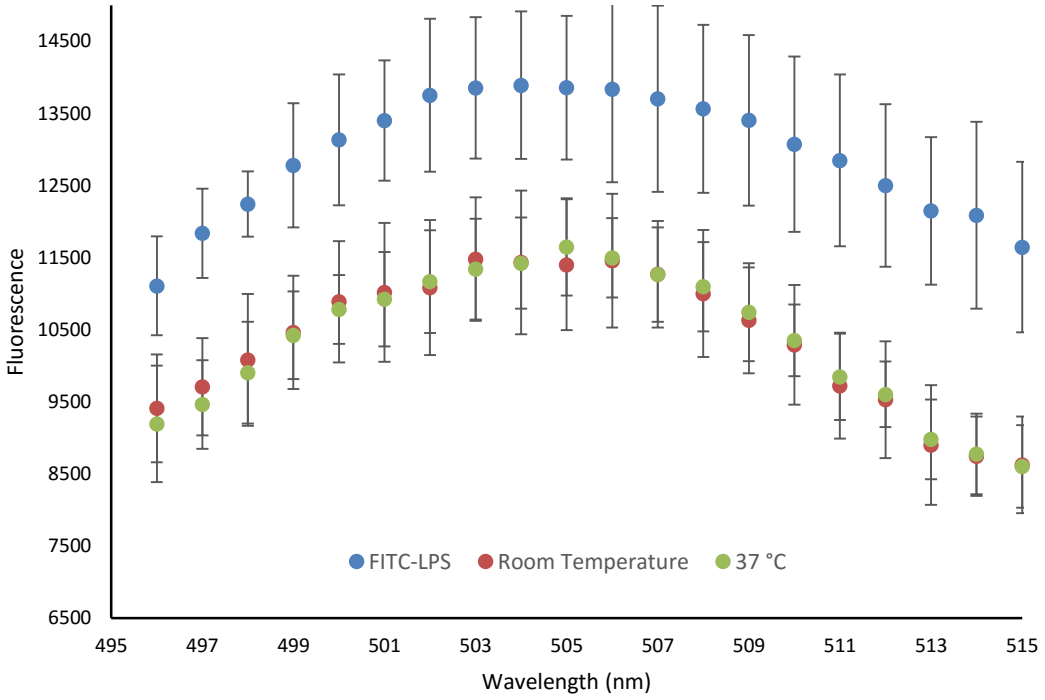

Supporting Figure 2.S1: Fluorescence data on BAm30 NP interaction with FITC-LPS. NPs (1 mg/mL) were incubated in a FITC-LPS solution (1 µg/mL) for 30 min at either 25 °C or 37 °C in SPB (10 mM, pH 7.0) with two controls (FITC-LPS only and NP only). The NPs were then pelleted (15,000 rpm, 45 min), and the supernatent was measured for presence of FITC-LPS (Ex: 495 nm, Em: 496 – 515 nm). The background fluoresence from the NP only solution was subtracted from the samples containing NPs.

Fig. 2.S2A

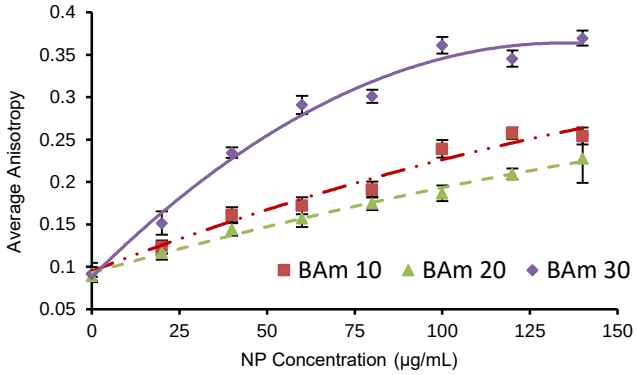

Fig. 2.S2B

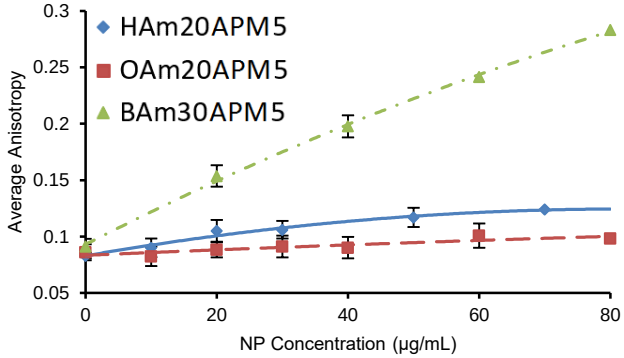

Fig. 2.S2C

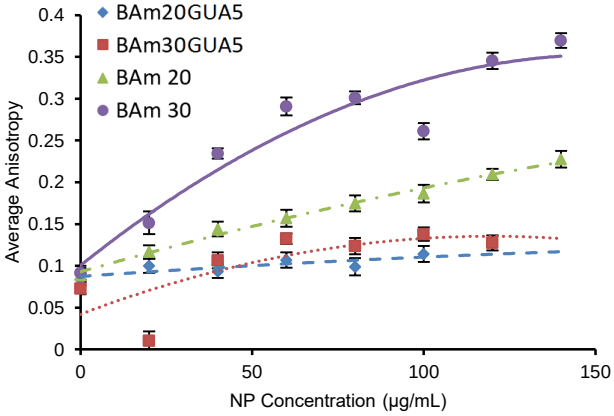

Fig. 2.S2D

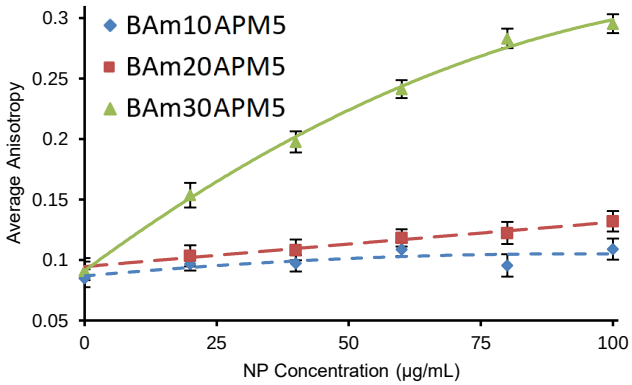

Fig. 2.S2E

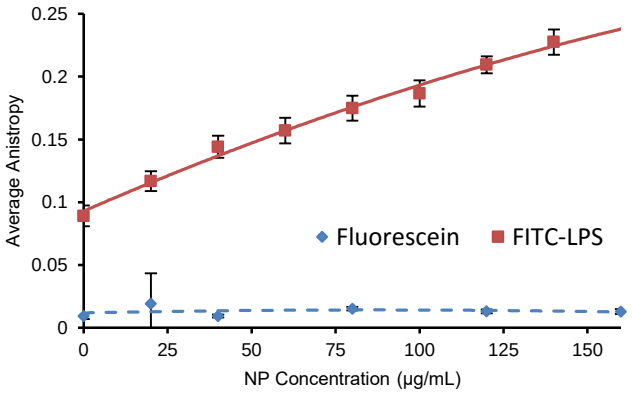

Supporting Figure 2.S2: Fluorescence polarization study on NPs. NPs were titrated into a solution of 500 ng/mL FITC-LPS in 10 mM sodium phosphate buffer at pH 6.8. A: ■ = BAm10, ▲ = BAm20, ♦ = BAm39. B: ■ = OAm20APM5, ♦ = HAm10APM5, ▲ = BAm30APM5. C: ♦ = BAm20GUA5, ■ = BAm30GUA5, ▲ = BAm20, ● = BAm30. D: ♦ = BAm10APM5, ■ = BAm20APM5, ▲ = BAm30APM5. E: ♦ = Fluorescein, ■ = FITC-LPS.

Figure 2.S3A.

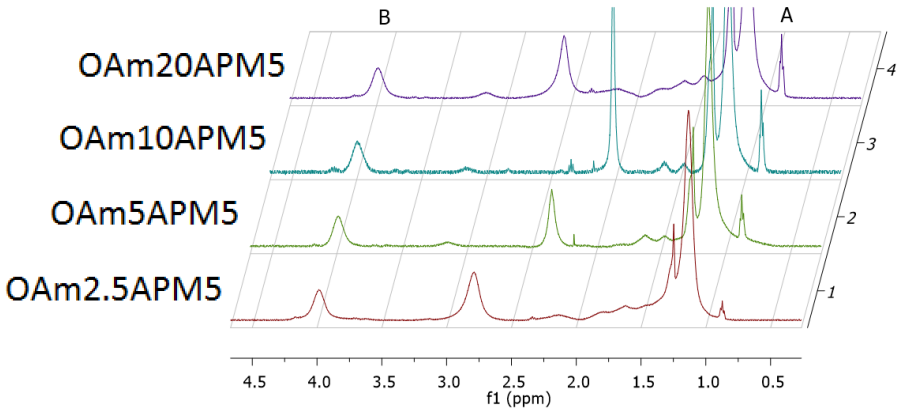

Figure 2.S3B.

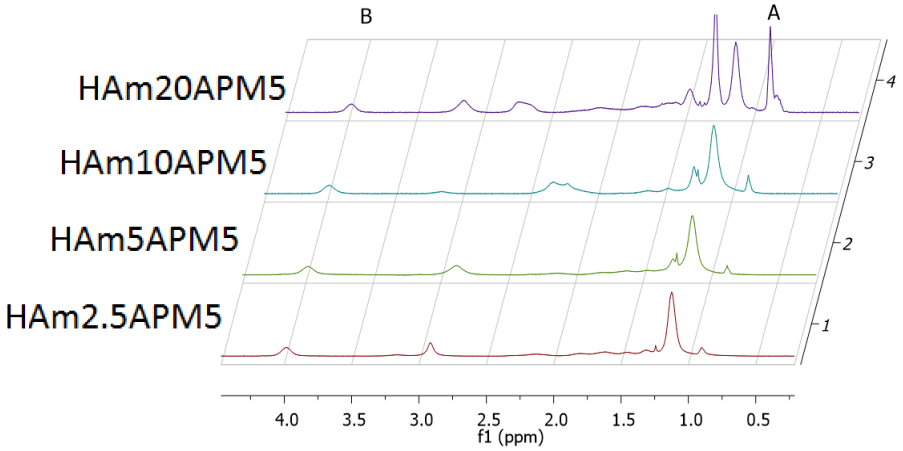

Figure 2.S3C.

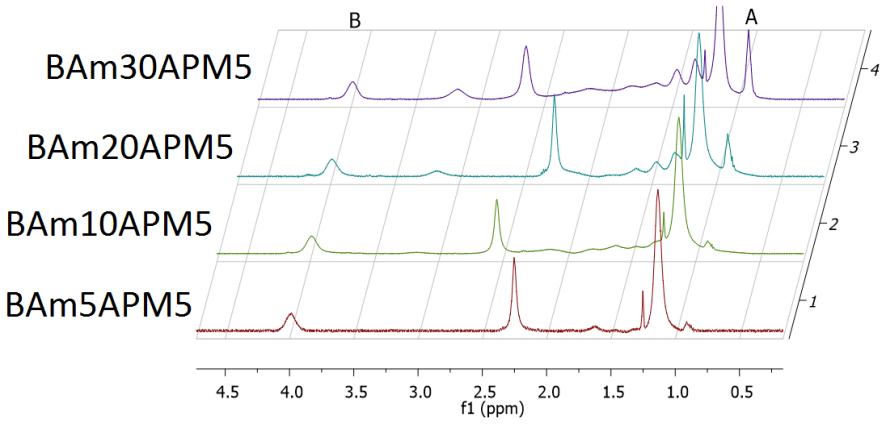

Figure 2.S3D.

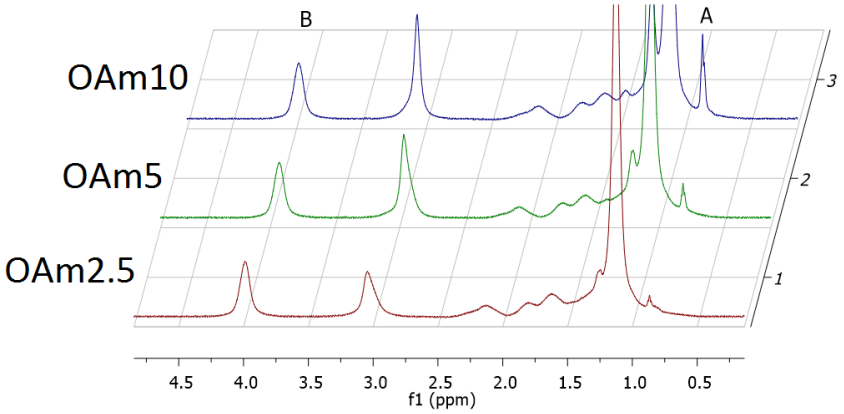

Figure 2.S3E.

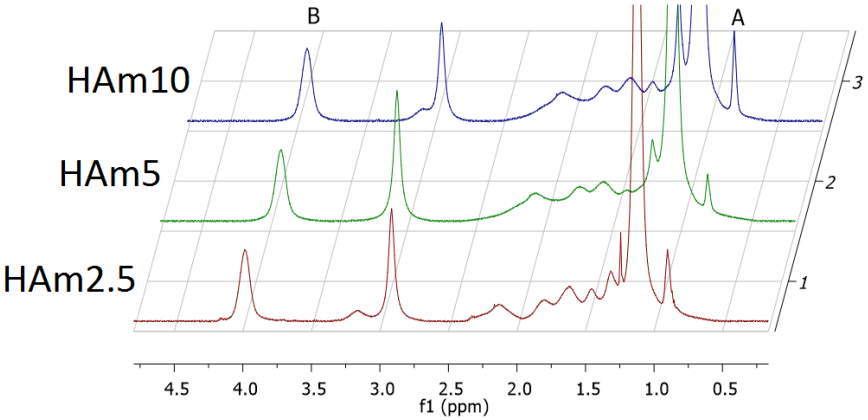

Figure 2.S3F.

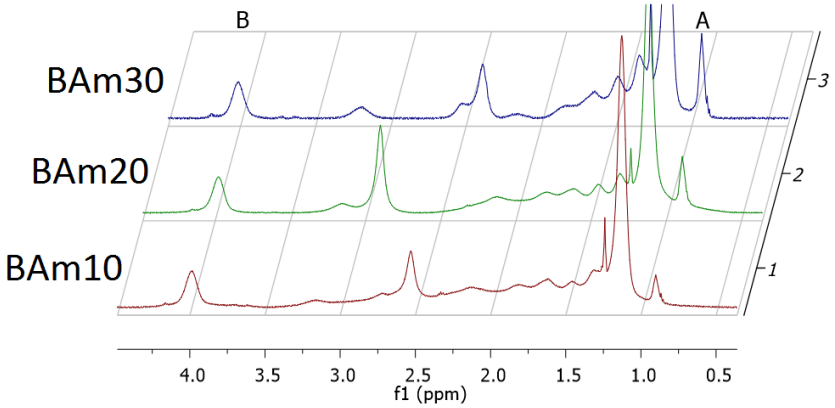

Supplementary Figure 2.S3 (A-F): These represent the ^{1}H NMR's taken for most of the NPs in the library. The incorporation ratios are qualitatively deduced from observing the change in peaks A and B, with a change in feed ratio of the monomers. Peak A is a broad singlet around 0.9 ppm representing the terminal methyl group in the new hydrophobic

monomers (BAm, HAm, OAm), and peak B is the broad singlet at ~4.1 ppm representing the methine of the isopropyl group in NiPAm.

Figure 2.S4A.

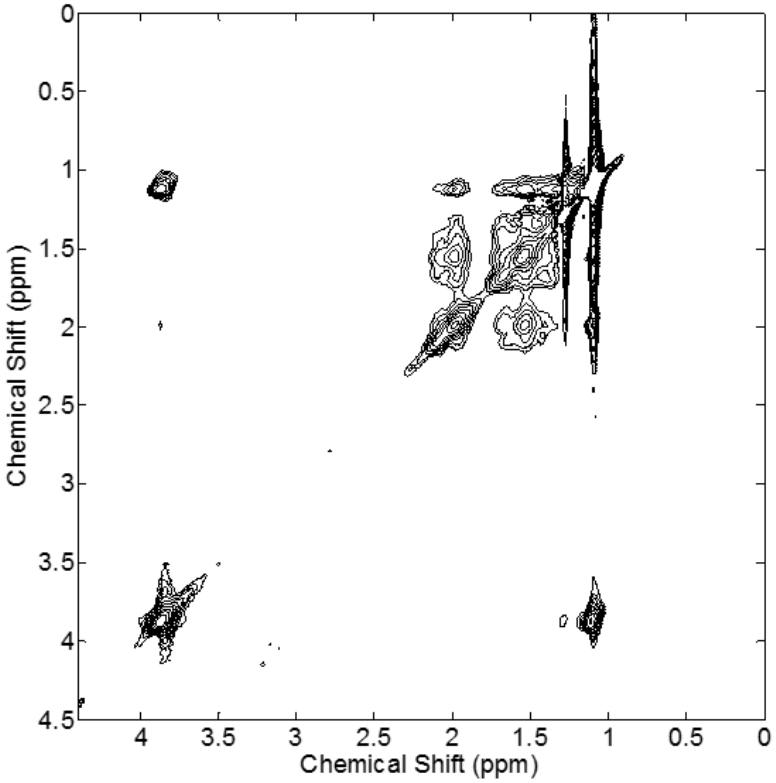

Figure 2.S4B.

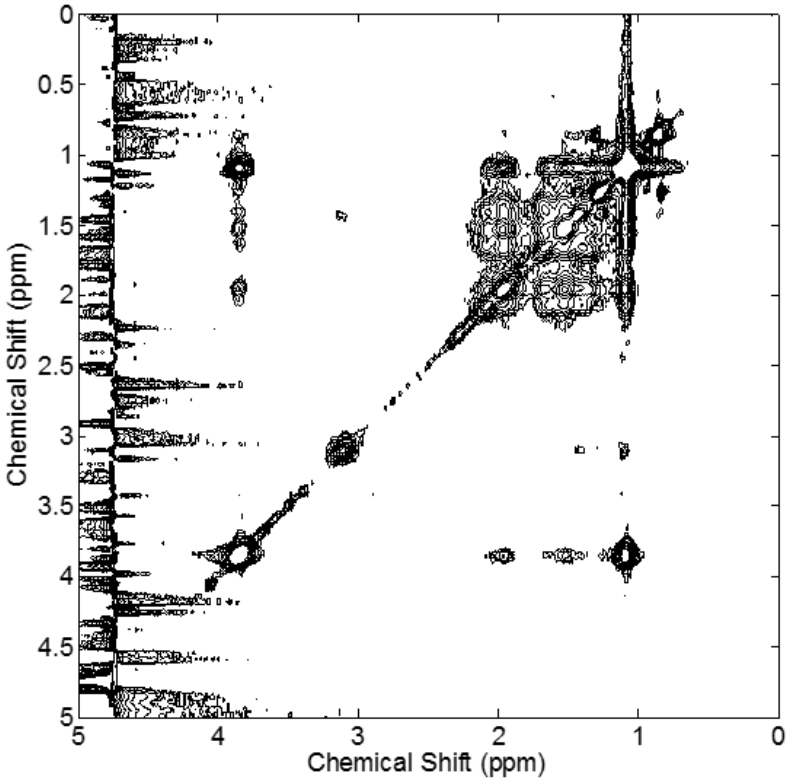

Figure 2.S4C.

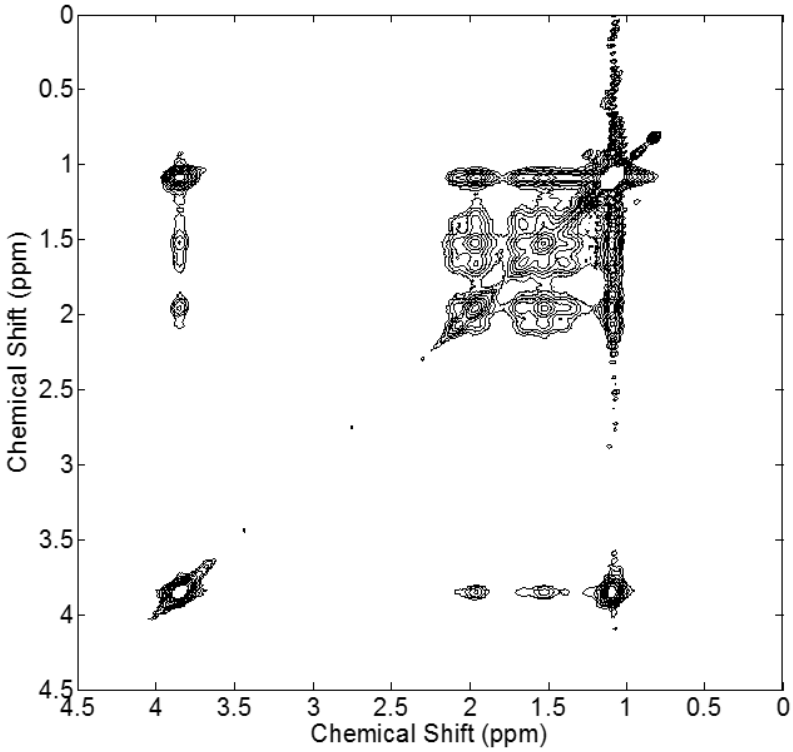

Figure 2.S4D.

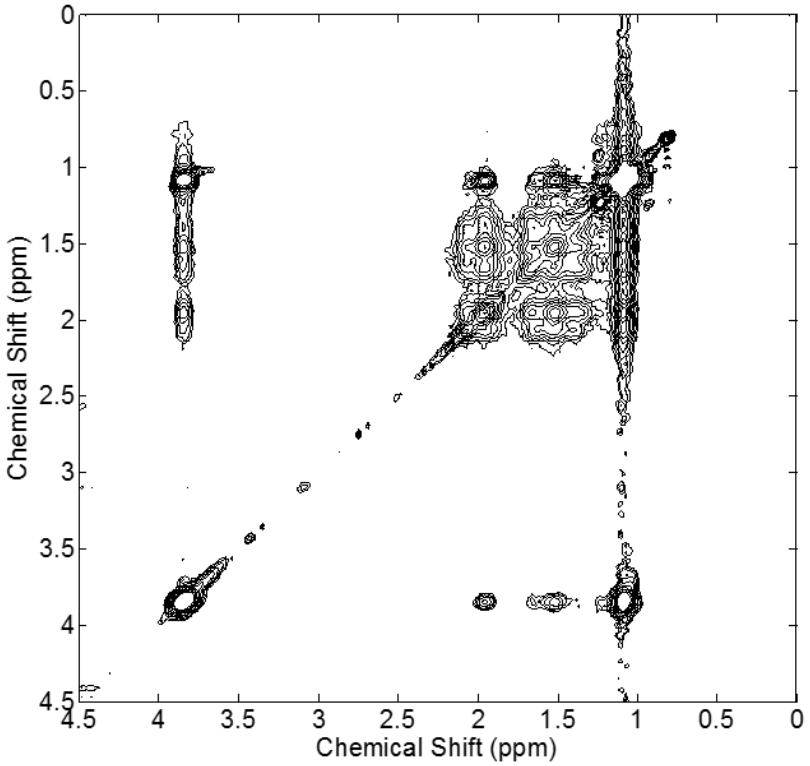

Supplementary Figure 2.4. 2D NOESY NMR of three NPs, A. tBAm10, B. BAm10, C. HAm10, D. OAm10, in 90:10 H_2O: D_2O.

L. References

1. Koide, H.; Asai, T.; Hatanaka, K.; Akai, S.; Ishii, T.; Kenjo, E.; Ishida, T.; Kiwada, H.; Tsukada, H.; Oku, N., T cell-independent B cell response is responsible for ABC phenomenon induced by repeated injection of PEGylated liposomes. *Int J Pharm* **2010,** 392, (1-2), 218-23.

2. Koide, H.; Asai, T.; Kato, H.; Ando, H.; Shiraishi, K.; Yokoyama, M.; Oku, N., Size-dependent induction of accelerated blood clearance phenomenon by repeated injections of polymeric micelles. *Int J Pharm* **2012,** 432, (1-2), 75-9.

3. Klinger, D.; Landfester, K., Stimuli-responsive microgels for the loading and release of functional compounds: Fundamental concepts and applications. *Polymer* **2012,** 53, (23), 5209-5231.

4. Schild, H. G., Poly (N-Isopropylacrylamide) - Experiment, Theory and Application. *Prog Polym Sci* **1992,** 17, (2), 163-249.

5. Christman, K. L.; Vazquez-Dorbatt, V.; Schopf, E.; Kolodziej, C. M.; Li, R. C.; Broyer, R. M.; Chen, Y.; Maynard, H. D., Nanoscale Growth Factor Patterns by Immobilization on a Heparin-Mimicking Polymer. *J Am Chem Soc* **2008,** 130, (49), 16585-16591.

6. Oh, Y. I.; Sheng, G. J.; Chang, S. K.; Hsieh-Wilson, L. C., Tailored Glycopolymers as Anticoagulant Heparin Mimetics. *Angew Chem, Int Ed* **2013,** 52, (45), 11796-11799.

7. Nguyen, T. H.; Kim, S. H.; Decker, C. G.; Wong, D. Y.; Loo, J. A.; Maynard, H. D., A heparin-mimicking polymer conjugate stabilizes basic fibroblast growth factor. *Nat Chem* **2013,** 5, (3), 221-227.

8. Dernedde, J.; Rausch, A.; Weinhart, M.; Enders, S.; Tauber, R.; Licha, K.; Schirner, M.; Zugel, U.; von Bonin, A.; Haag, R., Dendritic polyglycerol sulfates as multivalent inhibitors of inflammation. *Proc Natl Acad Sci USA* **2010,** 107, (46), 19679-19684.

9. Hoshino, Y.; Koide, H.; Furuya, K.; Haberaecker, W. W.; Lee, S. H.; Kodama, T.; Kanazawa, H.; Oku, N.; Shea, K. J., The rational design of a synthetic polymer nanoparticle that neutralizes a toxic peptide in vivo. *Proc Natl Acad Sci USA* **2012,** 109, (1), 33-38.

10. Koch, S. J.; Renner, C.; Xie, X. L.; Schrader, T., Tuning linear copolymers into protein-specific hosts. *Angew Chem, Int Ed* **2006,** 45, (38), 6352-6355.

11. Lee, S. H.; Hoshino, Y.; Randall, A.; Zeng, Z. Y.; Baldi, P.; Doong, R. A.; Shea, K. J., Engineered Synthetic Polymer Nanoparticles as IgG Affinity Ligands. *J Am Chem Soc* **2012,** 134, (38), 15765-15772.

12. Yoshimatsu, K.; Lesel, B. K.; Yonamine, Y.; Beierle, J. M.; Hoshino, Y.; Shea, K. J., Temperature-Responsive "Catch and Release" of Proteins by using Multifunctional Polymer-Based Nanoparticles. *Angew Chem, Int Ed* **2012,** 51, (10), 2405-2408.

13. Srimal, S.; Surolia, N.; Balasubramanian, S.; Surolia, A., Titration calorimetric studies to elucidate the specificity of the interactions of polymyxin B with lipopolysaccharides and lipid A. *Biochem J* **1996,** 315, 679-686.

14. Cardoso, L. S.; Araujo, M. I.; Goes, A. M.; Pacifico, L. G.; Oliveira, R. R.; Oliveira, S. C., Polymyxin B as inhibitor of LPS contamination of Schistosoma mansoni recombinant proteins in human cytokine analysis. *Microb Cell Fact* **2007,** 6.

15. Magalhaes, P. O.; Lopes, A. M.; Mazzola, P. G.; Rangel-Yagui, C.; Penna, T. C. V.; Pessoa, A., Methods of endotoxin removal from biological preparations: a review. *J Pharm Pharm Sci* **2007,** 10, (3), 388-404.

16. Anspach, F. B., Endotoxin removal by affinity sorbents. *J Biochem Biophys Methods* **2001,** 49, (1-3), 665-681.

17. Hou, K. C.; Zaniewski, R., The Effect of Hydrophobic Interaction on Endotoxin Adsorption by Polymeric Affinity Matrix. *Biochim Biophys Acta* **1991,** 1073, (1), 149-154.

18. Chiesl, T. N.; Shi, W.; Barron, A. E., Poly(acrylamide-co-alkylacrylamides) for electrophoretic DNA purification in microchannels. *Anal Chem* **2005,** 77, (3), 772-9.

19. Hoshino, Y.; Urakami, T.; Kodama, T.; Koide, H.; Oku, N.; Okahata, Y.; Shea, K. J., Design of Synthetic Polymer Nanoparticles that Capture and Neutralize a Toxic Peptide. *Small* **2009,** 5, (13), 1562-1568.

20. Hoshino, Y.; Haberaecker, W. W.; Kodama, T.; Zeng, Z. Y.; Okahata, Y.; Shea, K. J., Affinity Purification of Multifunctional Polymer Nanoparticles. *J. Am. Chem. Soc.* **2010,** 132, (39), 13648-13650.

21. Zeng, Z. Y.; Hoshino, Y.; Rodriguez, A.; Yoo, H. S.; Shea, K. J., Synthetic Polymer Nanoparticles with Antibody-like Affinity for a Hydrophilic Peptide. *ACS Nano* **2010,** 4, (1), 199-204.

22. Hoshino, Y.; Koide, H.; Oyama, D.; Yonamine, Y.; Lee, S. H.; Oku, N.; Shea, K. J., Design of polymer nanoparticles that are capable of neutralizing toxicity of fetal proteins. *Abstr Pap, Jt Conf - Chem Inst Can Am Chem Soc* **2011,** 241.

23. Mcphee, W.; Tam, K. C.; Pelton, R., Poly(N-Isopropylacrylamide) Latices Prepared with Sodium Dodecyl-Sulfate. *J Colloid Interface Sci* **1993,** 156, (1), 24-30.

24. Mueller, T. K. H.; Cao, P.; Ewert, S.; Wohlgemuth, J.; Liu, H. Y.; Willett, T. C.; Theodosiou, E.; Thomas, O. R. T.; Franzreb, M., Integrated system for temperature-controlled fast protein liquid chromatography comprising improved copolymer modified

beaded agarose adsorbents and a travelling cooling zone reactor arrangement. *J Chromatogr A* **2013,** 1285, 97-109.

25. Coin, I.; Beyermann, M.; Bienert, M., Solid-phase peptide synthesis: from standard procedures to the synthesis of difficult sequences. *Nat Protoc* **2007,** 2, (12), 3247-3256.

26. Piotto, M.; Saudek, V.; Sklenar, V., Gradient-Tailored Excitation for Single-Quantum NMR Spectroscopy of Aqueous Solutions. *J Biomol NMR* **1992,** 2, 661-665.

27. Cavanagh, J.; Fairbrother, W. J.; Parlmer III, A. G.; Rance, M.; Skelton, N. J., *Protein NMR Spectroscopy: Principles and Practice*. Elsevier Academic Press: Burlington, MA, 2007.

28. Marion, D.; Wuthrich, K., Application of Phase Sensitive Two-Dimensional Correlated Spectroscopy (COSY) for Measurement of ^{1}H-^{1}H Spin-Spin Coupling Constants in Proteins. *Biochem Biophys Res Comm* **1983,** 113, 967.

29. Yoshimatsu, K.; Koide, H.; Hoshino, Y.; Shea, K. J., Preparation of abiotic polymer nanoparticles for sequestration and neutralization of a target peptide toxin. *Nat Protoc* **2015,** 10, (4), 595-604.

30. Debord, J. D.; Lyon, L. A., Synthesis and characterization of pH-responsive copolymer microgels with tunable volume phase transition temperatures. *Langmuir* **2003,** 19, (18), 7662-7664.

31. Beierle, J. M.; Yoshimatsu, K.; Chou, B.; Mathews, M. A. A.; Lesel, B. K.; Shea, K. J., Polymer Nanoparticle Hydrogels with Autonomous Affinity Switching for the Protection of Proteins from Thermal Stress. *Angew Chem, Int Ed* **2014,** 53, (35), 9275-9279.

32. Yonamine, Y.; Yoshimatsu, K.; Lee, S. H.; Hoshino, Y.; Okahata, Y.; Shea, K. J., Polymer Nanoparticle-Protein Interface. Evaluation of the Contribution of Positively Charged Functional Groups to Protein Affinity. *ACS Appl Mater Interfaces* **2013,** 5, (2), 374-379.

33. Shapiro, Y. E., Structure and Dynamics of Hydrogels and Organogels: An NMR Spectroscopy Approach. *Prog Polym Sci* **2011,** 36, (9), 1184-1253.

34. Levy, G. C.; Axelson, D. E.; Schwartz, R.; Hochmann, J., Interpretation of Complex Molecular Motions in Solution. A Variable Frequency Carbon-13 Relaxation Study of Chain Segmental Motions in Poly(alkyl methacrylates). *J Am Chem Soc* **1978,** 100, 410-423.

35. Mirau, P. A., A Practical Guide to the NMR of Polymers. *John Wiley & Sons: Hoboken* **2004**, 418.

36. Araos, M. U.; Warr, G. G., Structure of nonionic surfactant micelles in the ionic liquid ethylammonium nitrate. *Langmuir* **2008,** 24, (17), 9354-9360.

37. Ilavsky, M.; Sedlakova, Z.; Bouchal, K.; Plestil, J., Phase-Transition in Swollen Gels .21. Effect of Acrylamide Quaternary-Salts with Various Alkyl Lengths on the Collapse, Mechanical, and Saxs Behavior of Poly(Acrylamide) Networks. *Macromolecules* **1995,** 28, (20), 6835-6842.

Chapter 3

Designing *N*-isopropylacrylamide Thermal Protectants for Immunoglobulin G. A Functional Synthetic Analog of HSP60

A. Introduction.

Chaperone proteins play an important role in nature. They assist in non-covalent folding or unfolding and assembly or disassembly of macromolecules.[1-2] Heat shock proteins, a subclass of this group, prevent newly synthesized polypeptide chains and assembled subunits from aggregating. The production of heat shock proteins is triggered by environmental stress. Stress upregulates the production of heat shock proteins (HSPs) to assist in the folding and establishment of proper protein conformation preventing unwanted protein aggregation and loss of function. One in particular, HSP60, works by binding proteins in their hydrophobic chamber. Once bound, a second protein closes off the hydrophobic chamber in an ATP driven event, causing HSP60 to undergo a conformational change, in which the hydrophobic binding pocket is transformed into a more hydrophilic microenvironment. The isolated denatured protein is allowed to refold into its native state, without the opportunity to aggregate with other unfolded denatured proteins.[3] Many groups have attempted to mimic this behavior using noncovalent associations with polymers to protect lysozyme,[4] carbonic anhydrase,[5-6] citrate synthase,[7] phytase,[8] chymotrypsin,[9] horseradish peroxidase,[10] and other biomacromolecules[11] from thermal denaturation. These studies have proposed the use of synthetic affinity agents as thermal protectants and

encouraged mechanistic studies of how synthetic affinity agents work to protect biomacromolecules from thermal stress.

In this study, our goal was to develop abiotic thermal protectants for immunoglobulin G (IgG). Antibodies comprise one of the most important types of protein affinity reagents for drug and diagnostic products on the market. Their biomacromolecular specificity has been exploited for use in therapeutics and for protein purification.[12] Of these, IgG is the most common type of therapeutic antibody. IgG's are 150 kDa molecules composed of two identical heavy chains bonded through disulfide bonds to each other, and to one of two identical light chains. The IgG molecule is comprised of two segments, designated as the antigen binding fragment (Fab) and the crystallizable fragment (Fc). The variable Fab region is the antigen binding domain. The Fc domain is highly conserved across all IgG's, and binds to Fc receptors as part of the immune system.[13-15]

IgG unfolds when heated above its denaturation temperature (T_m, ~60 °C) and undergoes irreversible aggregation and loss of function.[14-15] An effective heat protectant for IgG would entail association of the NP to IgG at elevated temperatures to protect against thermal stress, but having low affinity to IgG at low temperatures to allow for easy recovery of native IgG. Since many NP-protein interactions result in denaturation of the protein,[16-20] the interaction of the polymer with the protein must at the very least not denature the protein, but should allow refolding (renaturation) of the protein upon cooling.[21] Ideally the NP-protein interaction could stabilize the protein. To stabilize a protein, the polymer could bind to and stabilize thermally vulnerable domains of the protein by inhibiting protein unfolding (increasing the T_m), or alternatively, could sequester and isolate the protein to prevent

aggregation above its' T_m, in analogy to HSP60. The polymer could also function by some combination of the aforementioned mechanisms to limit denaturation.

There have been several reports of IgG affinity agents[13-15], but there have been few methods that have offered protection against thermal stress. Martin *et al.* have reported the use of short linear poly(acrylate) copolymers that reduce aggregation of IgG above its T_m. They suspect their copolymers are complexing with IgG, which hinders interprotein contact and slows down or possibly prevents the formation of IgG aggregates. However, their approach did not report removal of their polymers from IgG.[15] We are not aware of other polymers that can stabilize IgG at above their T_m, which can also be easily removed without accompanying denaturation.

An ideal thermal protectant for proteins would function only in the event of thermal stress, and would not affect normal biomacromolecular function under physiological conditions. We report a method to stabilize IgG at elevated temperatures using stimuli responsive NiPAm based hydrogel polymers that have been engineered with autonomous affinity to IgG. Most thermally responsive NiPAm NPs collapse at temperatures above their LCST and are more hydrophobic, but are more hydrophilic and solvent swollen below their LCST. This property has been observed to affect NP-biomacromolecular affinity.[4, 22] In some cases, the collapsed NPs above LCST have been reported to have increased biomacromolecular affinity, while the biomacromolecular affinity below LCST is significantly diminished. We hope to utilize the autonomous affinity of these NiPAm based NPs to capture IgG in a denatured state before it suffers from aggregation.

Our strategy takes advantage of the fact that protein-protein interactions are the result of a cumulative effect of individually weak interactions including hydrogen bonding,

hydrophobic, and electrostatic interactions. To bind IgG, we took inspiration from the binding interface between IgG and protein A, a known IgG affinity agent. Protein A has been reported to bind specifically to the conserved Fc domain of IgG. Based on analysis of the X-ray crystal structure of the protein A-Fc complex[14], negatively charged acrylic acid (AAc) was introduced to encourage electrostatic interactions with the positively charged side chains in IgG (isoelectric point (pI) of 6.4 to 9.0)[23] (Figure 3.1). Also, we have observed that engineering NP-protein affinity reagents often require incorporation of hydrophobic functional monomers to achieve high affinity.[24] Thus, our library of NPs included three hydrophobic monomers, t-butylacrylamide (tBAm), *N*-octylacrylamide (OAm), and *N*-hexylacrylamide (HAm), in lightly crosslinked NiPAm based NPs, to interact with the exposed hydrophobic residues in IgG.

A small library of polymer NPs were screened for their affinity to fluorescently tagged polyclonal IgG (FITC-IgG) using an immunoprecipitation assay. Following identification of lead NPs and the critical functional groups that contribute to their affinity, NP-IgG binding was improved by optimizing the monomer composition in an iterative process. In addition to the NP composition, NP-IgG binding was also found to be dependent on temperature and buffer conditions. Optimized NPs were evaluated for their effect on IgG during thermal stress, and to understand the mechanisms of binding their functioning and as a thermal protectants. The results of this study show how small changes in composition of NiPAm copolymer hydrogel NPs can affect inter and intrachain interactions of the polymer, and how these inter and intrachain interactions help tune protein affinity and mechanism of action, and ultimately affect how the NPs interact with biomacromolecules.

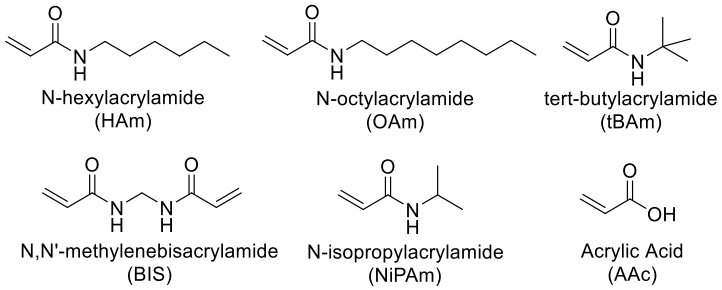

Figure 3.1. Monomers used in this study.

B. NP Synthesis and Characterization.

Table 3.1A. Summary of NP compositions used and their yields. For full table, see Table 3.S1.

Sample name	tBAm (mol%)	OAm (mol%)	HAm (mol%)	AAc (mol%)	NiPAm (mol%)	BIS (mol%)	Yield (%)
tBAm5AAc20	5	---	---	20	73	2	84
tBAm5AAc35	5	---	---	35	58	2	68
OAm5AAc20	---	5	---	20	73	2	52
OAm5AAc35	---	5	---	35	58	2	56
HAm5AAc20	---	---	5	20	73	2	59
HAm5AAc35	---	---	5	35	58	2	42

Table 3.1B. Summary of NP analysis data obtained by DLS, MALS, and RI.

Sample name	r_H (nm, DLS)	r_g (nm, MALS)	r_g/r_H	ρ (x10^{-2} g/mL)	PDI (DLS)	MW_{MALS} (x10^6)	dndc
tBAm5AAc20	414	248	0.60	0.01	0.07	18 ± 16	0.135
tBAm5AAc35	126	81	0.64	0.11	0.24	5.6 ± 2.7	0.163
OAm5AAc20	83	*177*	*2.17*	*1.6*	0.18	23 ± 2.9	0.149
OAm5AAc35	118	74	0.63	0.75	0.09	31 ± 1.9	0.189
HAm5AAc20	142	104	0.62	0.64	0.08	46 ± 6.9	0.170
HAm5AAc35	139	100	0.67	0.87	0.08	59 ± 4.0	0.175

Combinations of functional monomers (Figure 3.1) were copolymerized together with NiPAm, a monomer chosen for its history at the biological interface and its known thermal responsiveness (LCST). The NPs were synthesized by a modified precipitation

polymerization in aqueous solvent and purified by dialysis in DI water.[25] The NPs formed stable colloidal suspensions, which were analyzed by MALS, RI, and DLS to determine radius of gyration (r_g), hydrodynamic radius (r_h, z-avg), and weight-averaged molecular weight (Mw) (Table 3.1A, 3.1B). The ratio of r_g/r_H was calculated to determine the general topology of the NPs (Table 3.1B). An r_g/r_H ratio of 0.778 would suggest the NPs exists as a sphere with a uniform internal structure.[26-28] NPs with a denser inner core and a less dense outer shell, a "core-shell" NP, would have an r_g/r_H ratio less than 0.778.[26, 29] Most of our NPs had r_g/r_H values of approximately 0.6, which is similar to previously reported NiPAm NP[29], suggesting these NPs exist with a somewhat denser core, the result of a higher crosslinking density in the interior of the NP.[29-30]

The densities of the NPs were also calculated from MW and size measurements (Table 3.1B). The low densities (ρ) of the NPs calculated (0.006 - 0.009 g/mL) are typical of acrylamide hydrogels.[29-30] These NPs were all made with reduced surfactant to create larger NPs. The NPs ranged in size from 165 – 284 d.nm by DLS, with the exception of **tBAm5AAc20**, which was used at 827 d.nm, as we were unable to find conditions to form smaller NPs with this composition. These NPs were then tested to establish the time and RPM needed for them to be centrifuged. All NPs were pelleted in as little as 10 min at 15,000 RPM.

The LCSTs of each NP were determined by evaluating NP hydrodynamic size by DLS between 10 – 50 °C. The LCST was determined by the approximate inflection point in the curve (Table 3.S1B). All NiPAm based NPs present chemical compositions with engineered affinity for biomacromolecules. The NPs had LCSTs ranging from 27 – 32 °C, suggesting that

all NPs would have the highest affinity at temperatures above 32 °C, while losing affinity below 27 °C. Knowing this, all screens for NP affinity were performed at 37 °C.

C. Hydrophobic Contributions to IgG Binding.

The amount of IgG captured by each member of a small library of NPs was screened using a fluorescently tagged polyclonal IgG (FITC-IgG). This assay was used to evaluate the contribution of various hydrophobic groups to NP-IgG binding. NPs (250 μg/mL) were mixed with fluorescently tagged IgG (FITC-IgG, 20 μg/mL) in water and incubated at 37 °C for 30 min. The NPs were centrifuged at 15,000 rpm for 1 h and the supernatant was analyzed to quantify the non-bound FITC-IgG. There are several trends that are noteworthy. The results (Figure 3.2, 3.S1) show that NPs with decreasing amounts of the hydrophobic monomer bind more IgG. For example, decreasing the feed ratio of tBAm from 40% to 20%, resulted in a 175% increase in the amount of IgG bound (**tBAm40AAc10** vs. **tBAm20AAc10**) (Figure 3.2). Furthermore, when linear rather than branched groups were used as the hydrophobic monomer, less of the hydrophobic monomer was needed to capture similar amounts of IgG. For example, **OAm10AAc20** and **tBAm20AAc20** both bound 95% of IgG (Figure 3.S1). Although this initial screen allowed us to identify several requirements for binding, it did not include sufficient variables to determine the optimal NP composition. Since combinations of both hydrophobic and charged groups were found to provide synergistic contributions to protein affinity, hydrophobic groups alone are insufficient to identify NP compositions with the highest protein affinity.

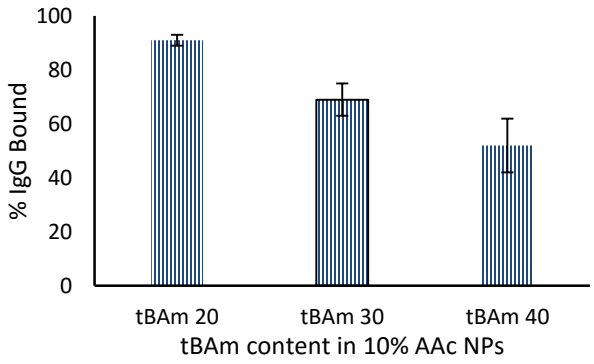

Figure 3.2. Capture of FITC-IgG (20 μg/mL) using tBAm NPs (250 μg/mL) with 10% AAc in water at 37 °C after 30 min incubation.

D. Electrostatic Contributions to IgG Binding.

After determining that hydrophobicity was important to NP-IgG binding, we next analyzed the contribution of electrostatics to NP-IgG binding. The copolymerization of AAc into NiPAm copolymers was found to be a function of polymerization conditions. To confirm the incorporation of AAc with increased feed ratio, the average amount of AAc incorporated in the NPs was determined by titration of the carboxylic acid groups against NaOH (Table 3.S2). The amount of AAc incorporated was determined from the total volume of NaOH added at the inflection point of the titration per mass of NP. The theoretical mol AAc/g NP was calculated from the stoichiometric amount of AAc added to the polymerization mixture over total mass of all monomers added. AAc incorporation was found to scale quantitatively with the amount of AAc added into the polymerization reaction. The results correlate well with other studies of AAc incorporation into NiPAm based polymer hydrogel NPs, under similar polymerization conditions.[29]

Most IgG have been found to have a net positive charge in neutral and acidic pH, thus increasing the feed ratio of the negatively charged monomer should lead to an increase in

NP-IgG binding. Indeed, the results (Figure 3.3, 3.S1) show that increasing the feed ratio of negatively charged carboxylate groups (AAc) in the NPs, results in an increase in amount of NP-IgG binding. When the mol% of AAc is increased from 5% to 10% (**tBAm40AAc5** compared to **tBAm40AAc10**) there is approximately 250% increase in IgG binding (Figure 3.3A). When the mol% of AAc is further increased from 10% to 20% (**tBAm40AAc10** compared to **tBAm40AAc20**), there is an additional 130% increase in IgG bound. The same trend was observed with the OAm NPs (Figure 3.3B). An increase from 0% AAc (**OAm10**) to 5% AAc (**OAm10AAc5**) increases NP-IgG binding by over 1000%. These results demonstrate a remarkable sensitivity of NP-IgG binding to small changes in NP feed ratio. By systematically changing the amount and type of hydrophobic and charged monomers, we can further optimize the NP-IgG binding.

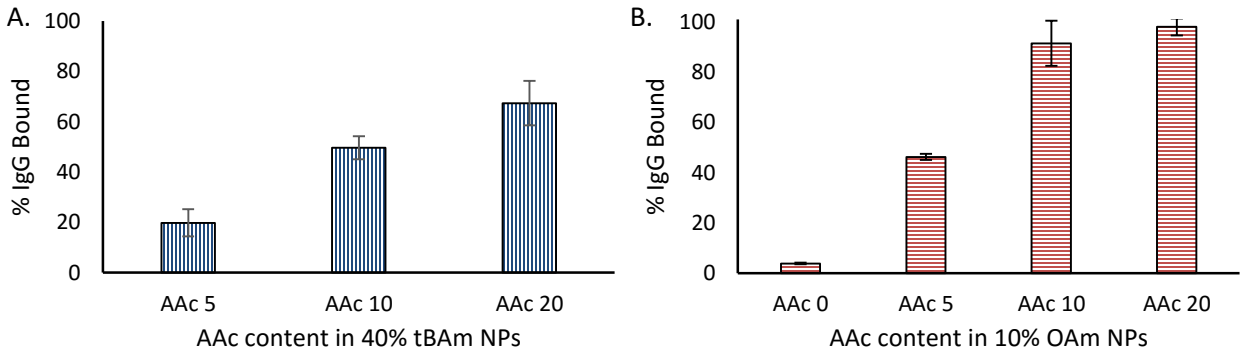

Figure 3.3. Capture of FITC-IgG (20 μg/mL) using AAc NPs (250 μg/mL) with A. 40% tBAm or B. 10% OAm in water at 37 °C after 30 min incubation.

E. Optimization of NP-IgG Binding in Sodium Phosphate Buffer.

Monomer compositions were optimized by increasing the feed ratio of carboxylate groups and decreasing the feed ratio of hydrophobic groups to maximize NP-IgG binding.

Optimized NPs were screened against polyclonal FITC-IgG (Figure 3.4). To determine the differences in NP-IgG binding among the highest binding NPs, FITC-IgG (20 μg/mL) was tested against lower concentrations of the optimized NPs (100 μg/mL) in sodium phosphate buffer (SPB, pH 5.5). These buffer conditions were chosen because Lee *et al.* reported that the NP affinity to IgG was maximal in SPB solution at pH 5.5.[14] This was likely due to the pI of IgG (6.4 – 9.0), with which a more acidic solution should increase the overall positive charge of IgG. This would allow a greater amount of electrostatic interactions between negatively charged NPs and IgG, thus maximizing NP-IgG affinity at this pH.

However, changing the binding conditions from water to SPB (35 mM, pH 5.5) did not affect the NP-IgG binding trends (Figures 3.2, 3.3, and 3.S1). Reducing the hydrophobicity of the NPs caused an increase in NP-IgG binding (Figure 3.4). The partition coefficients (log *P,* water/octanol) of tBAm, HAm, and OAm have values of 0.8, 2.5, and 3.5 respectively. The monomers with larger log P values are less water soluble and have a greater hydrophobic surface area. The NP with the most hydrophobic monomer, **OAm5AAc20** has the lowest capacity for IgG, while the NP with the least hydrophobic monomer, **tBAm5AAc20**, shows the highest capacity for IgG.

The NP-IgG binding was also evaluated to determine the effect of the charged monomer, AAc, in SPB (35 mM, pH 5.5) compared to water. Similar trends were observed when the NPs were evaluated in buffer, compared to water. Both screens showed that increasing the feed ratio of AAc from 20% to 35% leads to an increase in amount IgG bound by OAm and HAm NPs. In contrast, there was a decrease in IgG bound by tBAm NPs when increasing the feed ratio of AAc from 20% to 35% (Figure 3.4). In this case, **HAm5AAc35** shows the highest capacity for IgG, followed by **OAm5AAc35**, then **tBAm5AAc35**. This shows that NP-IgG

binding is influenced not by only the amount and type of hydrophobic monomers used or a change in feed ratio of negatively charged monomers, but rather by a balance between hydrophobicity and electrostatics.

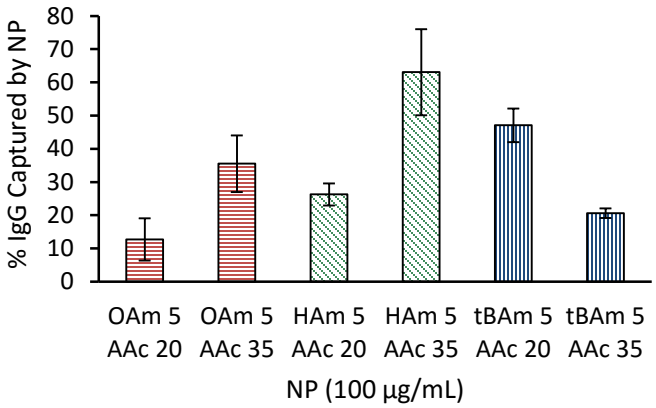

Figure 3.4. Capture of FITC-IgG (20 µg/mL) using NPs in SPB (35 mM, pH 5.5) at 37 °C after 30 min incubation.

F. The Hydrophobicity of Monomer Side Chains Affects NP Swelling and NP-IgG Binding.

Yoshimatsu *et al.* reported that NPs below their LCST are water swollen and have low affinity to some biomacromolecules, likely due to both polymer chain hydration and the separation of the functional monomers in the polymer in the water swollen state.[22] This phenomenon is similar to PEGylation, which causes loss in binding affinity of certain biomacromolecules. This is attributed to steric repulsion caused by the water swollen PEG chains.[31-33]

By analogy a hydrophilic solvent swollen NP is expected to have low biomacromolecular affinity. Acrylic acid is highly water solvated (log P = 0.3),[34] thus polyAAc, or a copolymer

with a high percentage of AAc, exists in a water swollen state. This could explain the difference in NP-IgG binding trend for the tBAm NPs when increasing the feed ratio of AAc from 20% to 35%. The NPs with the most hydrophobic monomers, OAm and HAm, swell much less through their temperature induced volume change (LCST) than NPs with the less hydrophobic monomer, tBAm. **OAm5AAc20** and **OAm5AAc35** have a temperature induced volume change of ~3 x 10^6 nm^3, while the NPs with a comparable amount of a slightly less hydrophobic monomer, **HAm5AAc20** and **HAm5AAc35**, have a larger volume change of ~20 x 10^6 nm^3. The NPs with the least hydrophobic monomer, **tBAm5AAc20** and **tBAm5AAc35**, have a dramatic temperature dependent volume change of ~500 x 10^6 nm^3 (Table 3.S1B). This shows how sensitive NP structure is to small changes in monomer hydrophobicity.

G. NMR Studies of Side Chain Solvation.

Studying the structure of these NPs can elucidate why NPs with increasingly hydrophobic monomers swell less. As the IgG affinity trends appear to be attributed in part to differences in swelling and polymer chain solvation, it is important to understand why tBAm containing NPs have a greater volume increase than OAm and HAm NPs. The reduced swelling could be due to intra and inter chain association of the more hydrophobic HAm and OAm side chains.[35] This intramolecular self-association could cause noncovalent crosslinking of the hydrophobic groups in the HAm and OAm NPs. Intrachain crosslinking by hydrophobic groups would reduce the amount of swelling with HAm and OAm NPs compared to the tBAm NPs. The extent of intramolecular chain association could be related to the accessibility of the hydrophobic groups to binding interactions with biomacromolecules (Scheme 3.1). To

determine if this is occurring, ^{1}H-NMR experiments were performed in methanol and in water with **tBAm5AAc35**, **HAm5AAc35**, and **OAm5AAc35** to determine the influence of solvent on intraparticle associations (Figure 3.5). Although these NPs are 2% crosslinked, the individual chains remain highly mobile, leading to an averaging of local dipolar interactions and relatively sharp lines in ^{1}H-NMR. Aggregation or strong intramolecular association of the polymer chains can lead to dehydration, effectively noncovalently crosslinking the polymer chains, and restricting chain movements, which leads to the disappearance of peaks from the spectrum as they broaden beyond detection.

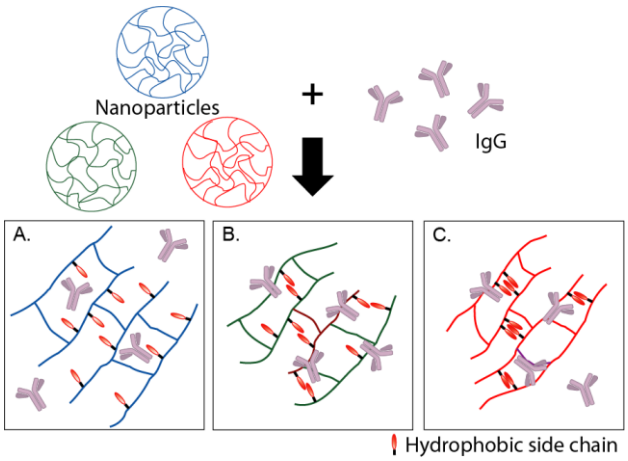

Scheme 3.1. Inter and intra molecular crosslinking of hydrophobic side chains affect IgG binding. Increasing hydrophobicity of side chain is represented by an increasingly red color, with A. representing **tBAm5AAc35**, B. **HAm5AAc35**, and C. **OAm5AAc35**.

In methanol (Figure 3.5A), the polymer chains are solvated, and the side chains show relatively sharp peaks in the ^{1}H-NMR. The peaks in methanol arising from the hydrophobic monomers are represented by peaks II or III in figure 3.5. Peak II (1.2 ppm) is assigned to the terminal methyl of the tBAm group and the methylene protons in HAm and OAm, while

peak III (0.9 ppm) arises from the terminal methyl for HAm and OAm. Peak I (3.9 ppm), is assigned to the methine peak in NiPAm. These sharp lines indicate free movement of all side chains in methanol, unhindered by aggregation or strong self-associations.

In water (Figure 3.5B), the terminal methyls of tBAm show a sharp peak at 1.2 ppm (peak II) and the methine peak in the isopropyl of NiPAm is observed as a sharp peak at 3.9 ppm (peak I) indicating that **tBAm5AAc35** is well solvated in water with little sign of self-associations or clustering of the side chains. In contrast, the peak assigned to the terminal methyl of HAm (0.9 ppm, peak III) is observed, but has significantly broadened, while the peak assigned to the terminal methyl of OAm (0.9 ppm, peak III) is broadened beyond detection. The loss of peak III indicates a degree of aggregation or self-association of the HAm and OAm side chains in water.

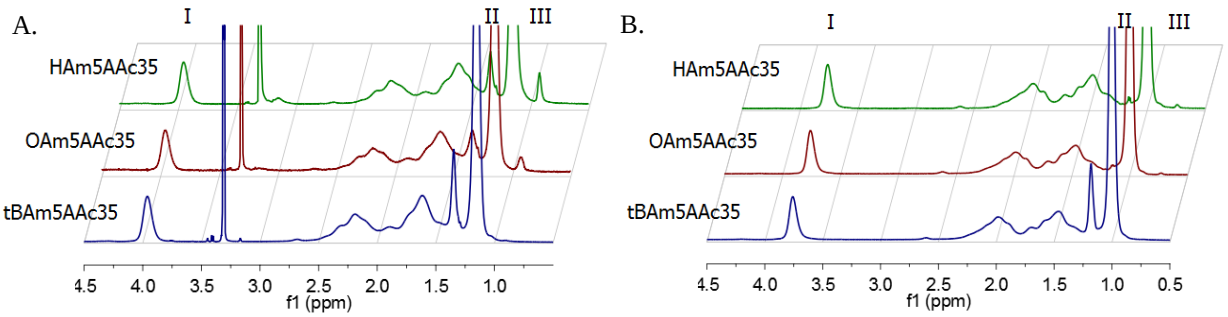

Figure 3.5. ^{1}H-NMR of **HAm5AAc35**, **OAm5AAc35**, and **tBAm5AAc35** in A. deuterated methanol and B. H_2O/D_2O (90:10) with water suppression. Peak I (3.9 ppm) represents the methine of NiPAm, peak II (1.8 ppm) represents either the methylene peaks in OAm and HAm or the terminal methyl in tBAm, and peak III (0.9 ppm), represents the terminal methyl in OAm and HAm.

Peak I of **HAm5AAc35** and **OAm5AAc35** remains sharp in water, despite the loss of peak III. These results establish that the polymer chains in HAm and OAm NPs are not fully collapsed and have not aggregated, since only the HAm and OAm monomer peaks have broadened, and the NiPAm peak remains unaffected by the solvent change. Thus, the HAm and OAm monomer side chains are likely undergoing intramolecular association in the NP in water. The reactivity ratios of all the monomers all are ~1 or lower, suggesting the monomer distribution is random in the polymer chains.[36] Some monomers, like BIS, favors reacting with itself slightly more than all other monomers, and thus would be consumed earlier.[37] With the random nature of these NPs and the low feed ratio of these monomers, the HAm and OAm are likely randomly distributed throughout the NP. Aggregation or self-association of these groups would result in noncovalent intramolecular crosslinking of the hydrophobic side chains in OAm and HAm NPs. This will result in a lower degree of swelling in water. Increased self-association would explain the smaller amount of temperature induced volume change of the OAm and HAm NPs compared to tBAm NPs. This shows that the optimization of NP-IgG binding requires a balance between the different intermolecular interactions that contribute to binding, as well as how the functional groups interact with each other intramolecularly to affect the structure of the NPs.

H. Effect of pH on NP-IgG Capacity.

Changes in pH or salt concentration have been reported to influence the strength of weak intermolecular interactions between biomacromolecules and NPs. These changes not only modulate the strength of the individual intermolecular interactions, but also alter the presentation of functional groups on each binding partner.[22] Lee *et al.* reported that NP-IgG

affinity could be modulated by increasing the pH of the solution from 5.5 to 7.3.[14] Analysis of the putative site of their NP-IgG interaction from X-ray crystallographic analysis revealed that increasing pH would result in deprotonation of a number of histidines that were involved in binding. This would diminish electrostatic interactions with negatively charged NPs, reducing NP-IgG affinity. Changes in salt concentrations and temperature have also been shown to modulate NP affinity to biomacromolecules. For example, an increase in salt concentration results in decreased NP-IgG affinity, due in part to swelling of the NPs in buffers with high salt concentrations.[14-15] NiPAm NPs are also known to swell at temperatures below their LCST, which in some cases can also result in loss of affinity to biomacromolecules.[4] With the use of one or more combinations of temperature, pH, and salt concentration, NP-IgG affinity can be modulated. These variables were evaluated to develop conditions for IgG release from the NP.

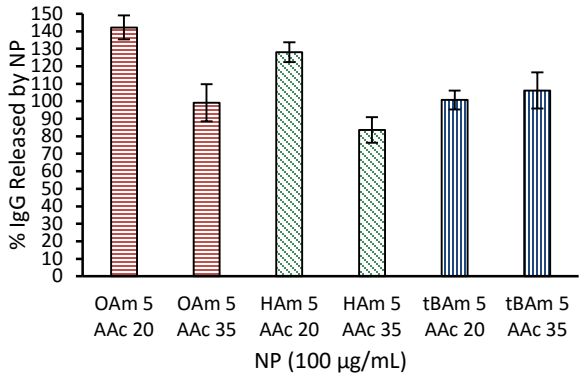

Figure 3.6. Release of the IgG from the NP-IgG complex (Figure 3.4) in PBS (35 mM, pH 7.3, 150 mM NaCl) solution at 25 °C after 30 min incubation.

The pelleted NP-IgG complexes (Figure 3.4) that were produced from IgG-NP solutions in SPB (35 mM, pH 5.5) at 37 °C were reconstituted in PBS (35 mM, pH 7.3, 150 mM NaCl) and cooled to 25 °C, a temperature below the measured LCST (27 – 32 °C), for 30 min. The NPs then were pelleted and the supernatant was analyzed for the presence of FITC-IgG (Figure 3.6). The optimized NPs tested in figure 3.4 showed almost complete IgG release from NPs. These results show that with a combination of increased pH and salt concentration and a decrease in temperature, one can modulate NP-IgG affinity, resulting in the release of bound IgG from NPs with optimized affinity for IgG.

I. Determining Structural Integrity of Bound-Released IgG Using Circular Dichroism.

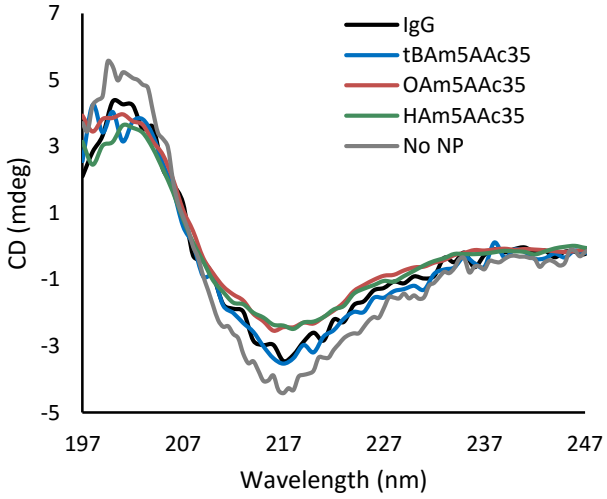

Figure 3.7. CD analysis of recovered IgG after thermal stress. A control (IgG) sample shows the CD spectrum of native IgG without heating (IgG). All other samples are of IgG heated to 60 °C for 5 min with or without NPs. The NPs were first pelleted (SPB, pH 5.5), and unbound IgG was removed. The IgG bound to NPs were then released (PBS), the NPs were pelleted, and the released IgG was analyzed.

Heat shock proteins minimize aggregation of biomacromolecules at elevated temperatures by preventing loss of function associated in part to aggregation. A successful polymer alternative would need to not only function as an affinity agent, but also sequester biomacromolecules during thermal stress and stabilize the complexed biomacromolecules by preventing denaturation and loss of function. This behavior may be confirmed by evaluation of the IgG released by the NPs following exposure to thermal stress to determine if it has maintained the secondary structure of native IgG. To evaluate this, the ellipticity of the recovered IgG was determined using circular dichroism spectroscopy (CD, Figure 3.7). The ellipticity of IgG recovered from **tBAm5AAc35**, **HAm5AAc35**, and **OAm5AAc35** were superimposable with that of native IgG. These studies reveal that the IgG recovered from all solutions had retained its native secondary structure. The ellipticity of IgG recovered from a solution without NPs also appeared superimposable with the native IgG structure. This was suspected to be due to the centrifugation step used to remove NPs from solution, which could cause aggregated IgG to pellet, causing only native IgG to be observed by CD. Though these NPs exhibit the potential to serve as artificial IgG heat protectant at 60 °C, additional analysis of the recovered IgG is needed to confirm the extent, if any, of IgG aggregation that has taken place.

J. Determining Structural Integrity of Bound-Released IgG Using SEC-HPLC.

To establish if the bound-released IgG has retained its' native structure, the recovered IgG was evaluated by size exclusion chromatography (SEC) for evidence of IgG aggregation (Figure 3.8). Under the experimental conditions, the peak at ~21 min is identified as native IgG. The peak at ~11 min is identified as an IgG aggregate. With an IgG solution without NPs,

is heated for five min at 60 °C , a large peak at ~11 min is observed, as well as the native IgG peak at ~21 min. This shows that a significant portion of IgG is aggregating after heating. The supernatant from **OAm5AAc35** and **HAm5AAc35**, NPs which showed high capacity for IgG, showed two peaks on SEC-HPLC at ~11 min and at ~21 min. This shows that although some native IgG is recovered, large quantities of IgG aggregates are being formed. In contrast, the supernatant from **tBAm5AAc35** showed a single peak on SEC-HPLC at ~21 min. The results establish that **tBAm5AAc35** was most effective in preventing IgG aggregation. The recovered IgG was present almost exclusively in its native state.

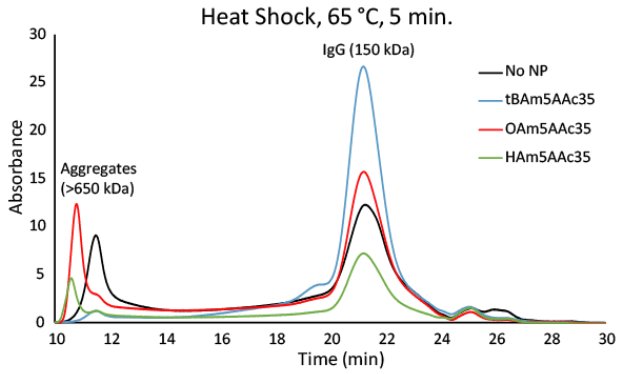

Figure 3.8. SEC-HPLC analysis of IgG after thermal stress.

OAm5AAc35 and **HAm5AAc35** bind more IgG compared to **tBAm5AAc35**. It is interesting therefore, that **tBAm5AAc35** is more effective at preventing aggregation. Many mechanisms for preventing protein aggregation using polymers have been reported. NiPAm NPs have been reported to assist in refolding of lysozyme by solubilizing aggregates[21] and/or preventing aggregation by binding denatured protein as it unfolds.[4] Other artificial chaperones help prevent aggregation by taking advantage of a cooperative effect between

two compounds to bind to denatured proteins and release refolded proteins.[5, 38] Protein refolding is a kinetically competitive process between protein refolding and aggregation. By eliminating the aggregation mechanism by binding to denatured proteins before they can aggregate, these artificial chaperone systems can encourage protein refolding over aggregation.[38] These methods suggest that these heat protectants actively assist in refolding denatured proteins.

One possible explanation for the IgG aggregation observed is that the more hydrophobic OAm and HAm NPs are assisting in the aggregation of IgG at its' T_m. Hydrophobic polymers have been reported in some cases to cause the denaturation and loss of function of proteins through strong intermolecular interactions between hydrophobic regions in proteins to the hydrophobic polymer.[39] As **HAm5AAc35** and **OAm5AAc35** have a more hydrophobic monomer than **tBAm5AAc35**, HAm and OAm might induce protein aggregation, rather than preventing it, while the less hydrophobic tBAm is able to sequester and isolate IgG without causing aggregation.

K. Size Change of the NP-IgG Complex.

Another possible explanation for how these NPs prevent loss of function of IgG lies in the consideration of the volume and IgG capacity of the three NPs under the binding conditions per IgG bound. Assuming these NPs protect IgG by sequestering and isolating IgG as it unfolds, NPs that more effectively isolate IgG would provide better protection from thermal stress. To show if there is a difference in the IgG concentration per NP volume, we evaluated the hydrodynamic size of the NPs (1 mg/mL) as a function of IgG concentration from 50 – 200 μg/mL in SPB (35 mM, pH 5.6) at 37 °C (Figure 9). No cha3.nge in size was observed

with addition of IgG to **HAm5AAc35**, suggesting that IgG binds to the interior of the NP. In contrast, addition of IgG to a solution of **OAm5AAc35** caused an initial decrease in size, followed by an increase in size upon further addition of IgG. This shows that IgG is not likely binding solely to the surface of the NP, but also being bound throughout the NP in the core. We suspect that the binding event could cause charge neutralization inside the NP, reducing electrostatic repulsion, causing the NP to shrink initially. IgG would then bind to the surface of the NP, which would cause the NP to increase in size. Finally, addition of IgG to a solution of **tBAm5AAc35** causes an increase in size. With the size increase of the **tBAm5AAc35**-IgG complex, IgG is possibly adding to the surface of the NP, rather than binding throughout. Thus, IgG is suspected to bind to the three optimized NPs in different locations (Scheme 3.2).

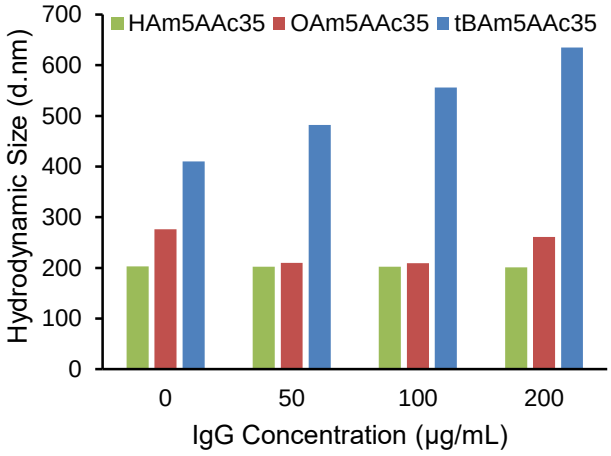

Figure 3.9. DLS analysis of NP-IgG complex (NP 1 mg/mL) at various IgG concentrations (50 – 200 µg/mL) in SPB (35 mM, pH 5.6) at 37 °C.

It appears that NPs with the ability to sequester and isolate IgG have a higher ability to reduce aggregation. This sequestration and isolation depends on the number of IgG

molecules in a given volume of space, thus the concentration of IgG per NP must be considered to be an important factor. As seen with the SEC-HPLC data, more IgG will aggregate in the presence of **HAm5AAc35** than with **OAm5AAc35**, **tBAm5AAc35**, or without NPs. From the DLS titration, IgG is 800 and 120 times more concentrated on **HAm5AAc35** and **OAm5AAc35** respectively, compared to **tBAm5AAc35**. This shows that sequestration and isolation of IgG could play an important role in preventing denaturation.

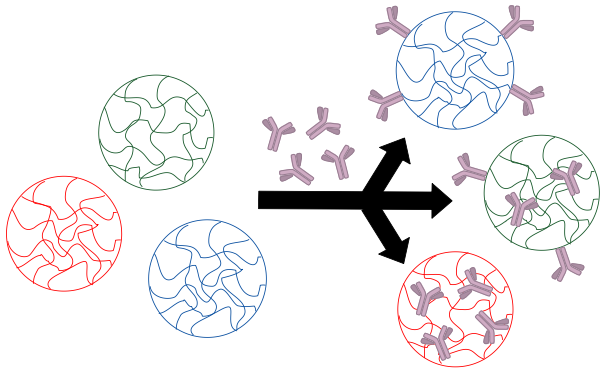

Scheme 3.2. Three different places IgG can bind to NPs.

L. Hydrophobicity of NPs Above and Below LCST.

HSP60 operates by first binding proteins in their hydrophobic binding pocket to isolate individual proteins. When assisting in refolding, ATP binds to HSP60, which causes the binding domain to go through a conformational change, changing the hydrophobic binding pocket to a more hydrophilic binding pocket.[3] This allows the bound protein a chance to refold in an isolated hydrophilic environment, preventing aggregation. In an effort to establish if the NPs are operating by a similar mechanism, pyrene fluorescence was used to probe the microenvironment of NPs above and below LCST to determine the extent of change in hydrophobicity as the NP passes through the LCST transition. NiPAm based NPs were reported to provide a hydrophilic environment, although somewhat more hydrophobic than

water,[40] and the transition through LCST is expected to give a more hydrophobic microenvironment above LCST, when the NPs are collapsed, and a more hydrophilic microenvironment below LCST, when the NPs are swollen (Scheme 3.3). I used a fluorescent probe, pyrene, to evaluate the change in hydrophobicity as the NP passes through its LCST. The ratio between the intensities of the first and third peaks (I_1/I_3, 375 and 386 nm) in the fluorescence spectrum of pyrene is sensitive to the polarity of the local environment. The I_1/I_3 value decreases with increasing hydrophobicity.[41]

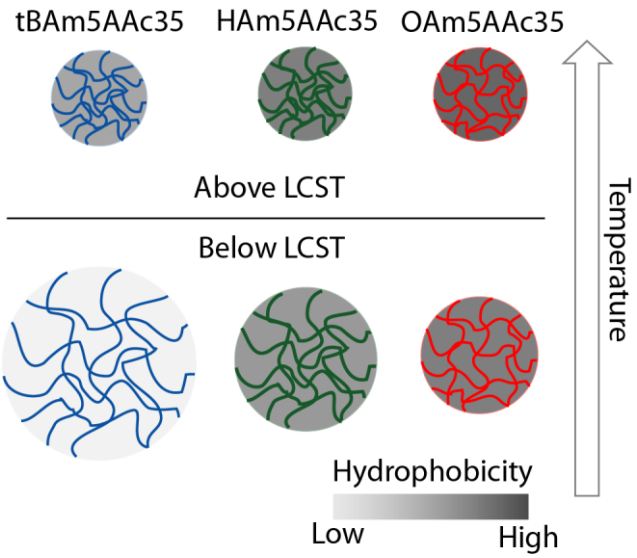

Scheme 3.3. Size and hydrophobicity of NPs above and below LCST.

Each NP solution (2 mg/mL) was treated with a solution of pyrene (0.1 mM). The solutions were excited at 335 nm, and the intensity of the emission peaks at 375 and 386 nm were compared at 15 and 40 °C to monitor changes in hydrophobicity of the NP solution (Table 3.2). The I_1/I_3 values at all temperatures increase with increasing hydrophobicity of the side chains (**OAm5AAc35** < **HAm5AAc35** < **tBAm5AAc35**). **OAm5AAc35** was shown to

have no change in polarity above and below LCST, while **HAm5AAc35** was shown to be slightly more hydrophobic above LCST than below. **tBAm5AAc35** was shown to be significantly more hydrophobic above LCST than below. This significant change shows that **tBAm5AAc35** could be operating by a similar mechanism as HSP60. The IgG binds to the hydrophobic **tBAm5AAc35** (I_1/I_3 = 1.17), to capture and isolate IgG. Upon cooling below LCST, **tBAm5AAc35** becomes more hydrophilic (I_1/I_3 = 1.37), ultimately releasing the bound IgG. During the transition, sufficient time would elapse to allow any partially unfolded portions to refold under isolation. In contrast, there was no conformational change above and below LCST for **HAm5AAc35** and **OAm5AAc35**, likely due to the intramolecular crosslinking of the HAm and OAm side chains. This shows that the mechanisms for protection against thermal stress could vary between the three NPs tested. Isolation of IgG appears to be a very important factor in thermal protection.

Table 3.2. Pyrene fluorescence in NP environment, above and below LCST.

	I_1/I_3 (15 °C)	I_1/I_3 (40 °C)
tBAm5AAc35	1.37	1.17
HAm5AAc35	1.05	1.09
OAm5AAc35	0.93	0.94

M. VP-DSC Analysis of T_m of IgG.

Polymer-biomacromolecule interactions can produce a range of responses. Thermal stabilization of biomacromolecules by NPs is known, and can arise from a variety of mechanisms. Separation and isolation as described above, is one. Another considers the effect of NP-biomacromolecule binding on its denaturation temperature (T_m). To obtain additional information on the protection of IgG by these NPs, IgG was mixed either in

solutions with one of the three NPs or in a control solution without NPs. The solutions were heated past the T_m of IgG (~60 °C) and differences in the DSC thermograms were compared. The thermogram of the control solutions of NPs in buffer with no IgG showed no peak. This is likely due to swollen nature of the NPs in buffer, which causes the thermogram to broaden beyond detection under these experimental conditions.

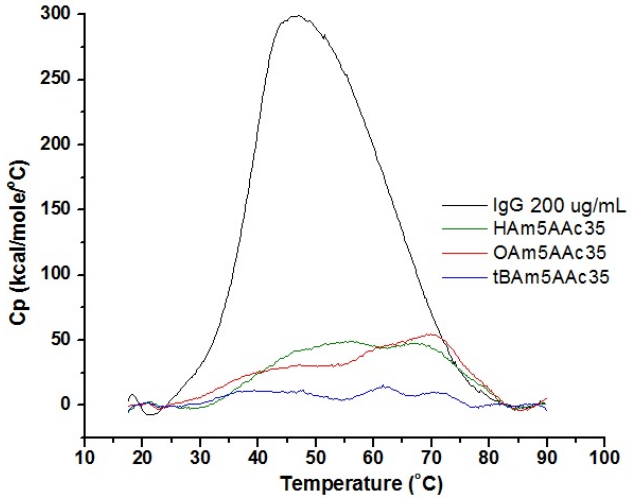

Figure 3.10. VP-DSC trace of IgG (200 μg/mL) with addition of various NPs (1 mg/mL). Solutions were heated from 15 – 90 °C at 50 °C/h under ~25 psi.

We envision several scenarios. The NPs could prevent aggregation of unfolded IgG by isolating the unfolded IgG. An alternative mechanism is that the NPs capture and stabilize whole IgG so that it does not unfold and denature. For the former mechanism, the endotherm and T_m of IgG would remain the same in the presence or absence of NPs, as IgG would still unfold at this temperature. For the latter scenario, IgG's endotherm would be suppressed or its T_m would increase with addition of NPs. The change in T_m could indicate how well the NPs suppress thermal denaturation by stabilizing the protein. However, if the NPs were

unsuccessful at protecting IgG from thermal stress, but instead assisted in denaturation, the T_m of IgG could shift to lower temperatures.

From the data (Figure 3.10), the thermogram of IgG (black) alone ranged from 20 to 70 °C with a maximum of ~45 °C (T_m). The broadness of the endotherm is a result of the polyclonal nature of the IgG being used, with evidence of unfolding of multiple IgG domains occurring over several overlapping steps that cannot be resolved.[15, 42] With addition of either **HAm5AAc35**, **OAm5AAc35**, or **tBAm5AAc35**, the endothermic IgG peaks were all smaller and broader. With **HAm5AAc35** and **OAm5AAc35**, the thermograms showed that T_m had shifted from 45 °C to 57 °C and 70 °C, respectively (Table 3.S3), while also having a much lower enthalpy transition. In the case of **tBAm5AAc35**, the endotherm had disappeared, suggesting either that denaturation of IgG did not occur under the conditions of the experiment, or the transition is obscured by factors that include the NP-protein interaction. Each of these cases suggest that IgG binding to the NPs results in an apparent increase in T_m, which in turn would inhibit IgG denaturation to some degree up to 90 °C.

The DSC results show that addition of **tBAm5AAc35** to solutions of IgG resulted in prevention of IgG denaturation from thermal stress up to 90 °C (~30 °C above IgG's T_m), while the solutions with **OAm5AAc35** and **HAm5AAc35** prevented some, but not all IgG from denaturing. This was evident by the disappearance of T_m in the thermogram, which suggests that **tBAm5AAc35** is either suppressing IgG unfolding, or binding as it begins to unfold, thus isolating IgG. As IgG does not readily refold without the help of chaperone proteins,[43] retention (or recovery) of native protein after thermal stress can be associated with assistance from NPs. By binding to IgG before or as it unfolds, the kinetically driven aggregation mechanism is prevented, assuming IgG is isolated, allowing an opportunity for

IgG to refold, if necessary, during its release from **tBAm5AAc35**. The CD and SEC-HPLC data in combination with this DSC data shows that **tBAm5AAc35** is able to prevent irreversible IgG aggregation.

In contrast, the IgG solutions with **OAm5AAc35** and **HAm5AAc35** show shifts in the thermogram, as well as a reduction in the thermogram peak area. This implies that **OAm5AAc35** and **HAm5AAc35** are also binding to IgG, but are not completely preventing denaturation. This is evident with the CD and SEC-HPLC data, where despite the high quantity of IgG bound by **OAm5AAc35** and **HAm5AAc35**, much of the recovered IgG was present as large aggregates upon heating above the T_m. The difference in thermal protection of these NPs is suspected to be due to the high density of IgG bound to **OAm5AAc35** (25 x 10^{-6} IgG/nm^3) and **HAm5AAc35** (8.6 x 10^{-6} IgG/nm^3), which implies that these NPs bind more IgG per volume than **tBAm5AAc35** (0.34 x 10^{-6} IgG/nm^3). This means that bound IgG is in closer proximity within **OAm5AAc35** and **HAm5AAc35** compared to **tBAm5AAc35**, resulting in reduced IgG isolation, and causing aggregation within the NP. This causes incomplete protection from aggregation of IgG with **OAm5AAc35** and **HAm5AAc35**, but full protection with **tBAm5AAc35**.

N. Conclusion.

IgG binding was tested against a series of NPs with varying amounts of functional monomers. The functional monomers were chosen to encourage intermolecular interactions with the Fc domain of IgG. These included three hydrophobic monomers, t-butylacrylamide (tBAm), *N*-octylacrylamide (OAm), and *N*-hexylacrylamide (HAm) to complement the hydrophobic nature of IgG, in addition to a negatively charged monomer, AAc, to encourage

electrostatic interactions with the net positive IgG. Lowering the feed ratio of hydrophobic monomer in the NPs resulted in an increase in IgG bound to the NP. Increasing the feed ratio of negatively charged AAc also caused an increase in bound IgG. Using monomers of different hydrophobicities (OAm, HAm, or tBAm) also changed the amount of IgG bound. A lower feed ratio of the more hydrophobic monomers was necessary for comparable NP-IgG binding to a NP with a less hydrophobic monomer.

A balance between increasing the feed ratio of negatively charged monomer and decreasing the feed ratio of hydrophobic monomer was important for IgG binding. The NPs with the less hydrophobic monomer, tBAm, were shown to have a larger temperature induced volume change than NPs with the more hydrophobic OAm and HAm. The origin of this effect was due to intramolecular crosslinking of the OAm and HAm side chains (NMR). Without the noncovalent crosslinking, the NPs become more water swollen with increasing AAc content. This swelling could possibly reverse the effect of the trend observed, with less NP-IgG binding after exceeding a limit of electrostatic contribution.

To protect a biomacromolecule from aggregation, the NP must at the very least not cause denaturation of the biomacromolecule upon binding. Engineering an IgG heat protectant requires making an affinity agent that will also prevent aggregation at above its T_m. To test this, IgG was heated to 60 °C for 5 min and released into solution by cooling the solutions for 2 h at 4 °C by three optimized NP-IgG binders, **HAm5AAc35**, **OAm5AAc35**, and **tBAm5AAc35**, and the structural integrity of the released IgG was evaluated by CD and SEC-HPLC. The results show that though **OAm5AAc35** and **HAm5AAc35** showed the highest NP-IgG binding, they were unable to prevent IgG aggregation at 60 °C for 5 min. In contrast, the IgG that was heated and recovered from **tBAm5AAc35** revealed little aggregation, with an

identical CD spectrum as native IgG. This shows that **tBAm5AAc35** acted as the best artificial heat protectant, despite the lower NP-IgG binding.

DLS and DSC analysis of NP-IgG binding was used to analyze the mechanism of IgG stabilization against thermal stress. IgG was found to bind to the surface of **tBAm5AAc35**, preventing the IgG aggregation due to thermal stress. In contrast, IgG appears to bind throughout the core of **HAm5AAc35** and **OAm5AAc35**, and shows reduced, but visible signs of aggregation. This possibly shows that the reason **tBAm5AAc35** was a better heat protectant for IgG was because of the differences in local concentration of IgG. **HAm5AAc35** and **OAm5AAc35** bound 50 and 15 IgG's respectively per NP, while **tBAm5AAc35** only bound 2 IgG's per NP. The lower IgG concentration per volume of NP for **tBAm5AAc35** (0.34×10^{-6} IgG/nm^3) compared to **HAm5AAc35** (8.6×10^{-6} IgG/nm^3) and **OAm5AAc35** (25×10^{-6} IgG/nm^3) would therefore better isolate and prevent aggregation of IgG.

To determine if these NPs were functioning like HSP60, pyrene fluorescence of each NP solution was analyzed above and below their LCST. **HAm5AAc35** and **OAm5AAc35** were shown to have a minimal change in their I_1/I_3 value above and below LCST, indicating a minimal change in hydrophobicity. In contrast, **tBAm5AAc35** showed a large change above (1.17) and below (1.37) LCST, which indicated that the NP created a more hydrophobic environment above LCST upon IgG binding, and a more hydrophilic environment below LCST upon IgG release, much like with HSP60. This suggests that the **tBAm5AAc35** operates by a similar mechanism as HSP60 as a thermal heat protectant. This study shows that finding an optimal NP-IgG binder requires a balance between optimizing intermolecular interactions and optimizing NP structure under different conditions. The functions and affinities of these NPs appear to be very sensitive to small changes in monomer composition.

O. Materials and Methods.

- Materials.

The following materials were obtained from commercial sources: *N*-isopropylacrylamide (NIPAm), and acrylic acid (AAc) were obtained from Aldrich; polyclonal IgG from human serum with and without FITC label were obtained from Jackson ImmunoResearch; *N,N*'-methylenebisacrylamide (BIS) was from Fluka. All other solvents and compounds were obtained from Fisher Scientific Inc. or VWR International LLC. NIPAm was crystallized from hexane before use. AAc was purified using vacuum distillation over copper wire. *N*-hexylacrylamide (HAm) and *N*-octylacrylamide (OAm) were synthesized from previously published procedures.[24] Other chemicals were used as received. Water used in polymerization and characterization was purified using a Barnstead Nanopure Diamond™ system. Labconco Freezone 2.5 was used for lyophilization.

- NP synthesis.[25]

Nanoparticles were synthesized using a modified free radical precipitation polymerization.[44-49] Briefly, stock solutions of NiPAm (A mol%), AAc (B mol%), BIS (2 mol%), and SDS (0.04 – 0.16 mg/mL) were prepared by dissolving the monomers in nanopure water. The OAm, HAm, and tBAm (C mol%) stock solutions were prepared by dissolving the monomers in a minimal amount of ethanol (Figure 3.1). Monomers were added in the desired ratios to generate a total monomer concentration of 65 mM in 25 mL of water. The solutions were degassed for 30 min with nitrogen while stirring. The initiator (APS, 0.6 mg/mL) was dissolved in minimal volume of acetone (~200 μL). The initiator was then injected into the reaction mixture after degassing, and the flask was immersed into an

oil bath at 60 °C for 3 h with stirring under a nitrogen atmosphere. The polymer solutions were purified by dialysis against deionized water (4 L for 100 mL crude NP) using a 12 – 14 kDa MWCO regenerated cellulose membrane, and changing the water twice daily for 2 d. After dialysis, 5 mL of the NP solution was lyophilized to determine weight based concentration and yield.

- NP Characterization.

Dynamic Light Scattering (DLS). The DLS measurements were performed using the Zeta-sizer Nano DLS (Malvern). NP solutions were diluted 10X from dialyzed solutions and scanned for average hydrodynamic diameter (d_h) at room temperature in nanopure water.

The temperature induced volume change (ΔV, Table 3.S1B) was calculated using r_H determined by DLS at the NPs largest and smallest size measured, assuming the NPs are spherical.

$$\Delta V = (4/3\ \pi\ r_{H(\text{above LCST})}{}^3) - (4/3\ \pi\ r_{H(\text{below LCST})}{}^3)$$

- Multiangle Light Scattering (MALS) and Refractive Index (RI).

The weight averaged molecular weight (Mw), radius of gyration (r_g), and refractive index increment (dn/dc) values for the NPs were determined using batch mode injection of NP solutions with increasing concentrations that varied for each NP from 1 – 250 μg/mL. Molecular weight measurements were determined using the DAWN-HELEOS (Wyatt Technology Corporation) instrument attached to the Optilab rEX (Wyatt Technology Corporation) system to determine MALS and dn/dc, respectively. The data collection and

analysis was performed using the Astra software (Wyatt Technology Corporation), and the data was fit using a Zimm plot.

Density measurements were determined by calculating the molecular weight of one NP, as determined by MALS, per volume of one NP, as determined by DLS.

$$\rho = (MW_{MALS} / 6.022x10^{23}) / (4/3\ \pi\ r_H^3)$$

- Nuclear Magnetic Resonance (NMR) spectroscopy.

NMRs were run using a Bruker AVANCE600 instrument with a BBO probe (600MHz) and analysis was done using the XwinNMR and MestReNova programs. NP solutions were either lyophilized, then redispersed into a solution of deuterated methanol, or used in the original water solution at 5 mg/mL and contained 10% D_2O for NMR field frequency locking, then run with solvent suppression to remove the water peak.

- Titrations.

NP samples (12 mL) were diluted to 0.1 mg/mL in nanopure water. NaOH (0.001 M) was then slowly titrated at ~1 drop/s into the NP solution with stirring, and the pH was measured using a Vernier pH meter. A Vernier drop counter was used to determine volume of NaOH added during the titration, and the results were plotted using Logger Pro 3.8.7. The AAc content was determined as mols of AAc added per g NP by calculating mols of NaOH added at the endpoint per g NP used in the titration.

- IgG Assay - Affinity.

Each NP (250 μg/mL) was mixed with FITC-IgG (20 μg/mL) in SPB (35 mM, pH 5.5) to a total volume of 500 μL and heated up to 37 °C for 30 min. The NPs were then pelleted at 15 kRPM for 45 min, and the supernatant (410 μL) was removed. The pellet was reconstituted with 410 μL of PBS (35 mM, 150 mM NaCl, pH 7.3) and the mixture incubated at RT for 30 min. The NPs were then pelleted at 14 kRPM at 16 °C for 45 min, and the supernatant was removed. Samples were analyzed at Ex 485 nm, Em 515 nm.

- IgG Assay – Thermal Protectant.

Each NP (1 mg/mL) was mixed with FITC-IgG (150 μg/mL) in SPB (35 mM, pH 5.5) to a total volume of 500 μL and heated up to 60 °C for 5 min. The NPs were then pelleted at 15 kRPM for 45 min, and the supernatant A (410 μL) was removed. The pellet was reconstituted with 410 μL of PBS (35 mM, 150 mM NaCl, pH 7.3) and the mixture incubated at 4 °C for 2 h. The NPs were then pelleted at 14 kRPM at 16 °C for 45 min, and the supernatant B was removed. The supernatant B samples were run through an HPLC SEC column (TOSOH G4000SWXL) and run in SPB (100 mM, pH 7.0) at 0.75 mL/min for 25 min with UV detection at 220 nm.

The supernatant B was further analyzed by CD. The samples were analyzed from 197 – 250 nm at 50 nm/min at RT. Each result was averaged over 10 runs. A background scan using PBS buffer was subtracted from every sample.

- VP-DSC.

Samples were analyzed using a VP-DSC calorimeter (MicroCal Inc.) with a cell volume of 0.5 mL. The solutions were prepared with 200 μg/mL of IgG in SPB (35 mM, pH 5.6), with NPs (1 mg/mL). Two types of control solutions were made, either without IgG or without NPs. The SPB buffer solution was added in its place. Each sample was degassed under vacuum (14 psi) with stirring for at least 5 min at RT immediately prior to injection. The samples were analyzed from 15 – 90 °C at an increase of 50 °C/h at a pressure of ~25 psi. A solution of SPB (35 mM, pH 5.6) buffer was used in the reference cell. Each thermogram was analyzed using Origin 7.0 software supplied the manufacturer, a blank run of buffer in buffer was first subtracted from each thermogram. The baseline was then corrected using a progress integration baseline, and then fit to a non-two state model for 3 transitions.

P. Supplementary Information.

Table 3.S1A. Summary of NP compositions and sizes, determined by DLS.

Sample	tBAm (mol%)	AAc (mol%)	NiPAm (mol%)	BIS (mol%)	DLS Size (d.nm)	DLS PDI
tBAm10	10	0	88	2	98	0.02
tBAm20	20	0	78	2	99	0.01
tBAm5AAc20	5	20	73	2	811	0.08
tBAm5AAc35	5	35	58	2	251	0.24
tBAm20AAc5	20	5	73	2	187	0.08
tBAm20AAc10	20	10	68	2	107	0.08
tBAm20AAc20	20	20	58	2	160	0.05
tBAm30AAc10	30	10	58	2	97	0.07
tBAm30AAc20	30	20	48	2	164	0.01
tBAm40AAc5	40	5	53	2	111	0.05
tBAm40AAc10	40	10	48	2	138	0.06
tBAm40AAc20	40	20	38	2	128	0.02

Sample	OAm (mol%)	AAc (mol%)	NiPAm (mol%)	BIS (mol%)	DLS Size (d.nm)	DLS PDI
OAm5	5	0	93	2	518	0.20
OAm10	10	0	88	2	633	0.21
OAm5AAc5	5	5	88	2	470	0.11
OAm5AAc10	5	10	83	2	315	0.29
OAm5AAc20	5	20	73	2	165	0.18
OAm5AAc35	5	35	58	2	236	0.09
OAm10AAc5	10	5	83	2	594	0.36
OAm10AAc10	10	10	78	2	589	0.11
OAm10AAc20	10	20	68	2	716	0.07

Sample	HAm (mol%)	AAc (mol%)	NiPAm (mol%)	BIS (mol%)	DLS Size (d.nm)	DLS PDI
HAm5AAc5	5	5	88	2	284	0.27
HAm5AAc10	5	10	83	2	232	0.26
HAm5AAc20	5	20	73	2	284	0.08
HAm5AAc35	5	35	58	2	278	0.08

Table 3.S1B. Summary of density and LCSTs of NPs.

Sample name	r_H (nm, DLS)	r_g (nm, MALS)	r_g/r_H	ρ (x10^{-2} g/mL)	ΔV (x10^6 nm^3)	LCST (°C)
tBAm5AAc20	414	248	0.60	0.01	510	27
tBAm5AAc35	126	81	0.64	0.11	550	27
OAm5AAc20	83	*177*	*2.17*	*1.6*	2	27
OAm5AAc35	118	74	0.63	0.75	4	27
HAm5AAc20	142	104	0.62	0.64	21	32
HAm5AAc35	139	100	0.67	0.87	20	DNO

DNO = Did not observe

Table 3.S2. Titrations to determine AAc content in NP.

Sample	Theoretical mmol AAc/g NP	Calculated mmol AAc/g NP	% Incorporation
tBAm5AAc20	1.9	1.9	100
tBAm5AAc35	3.6	3.6	100
OAm5AAc20	1.9	1.7	90
OAm5AAc35	3.5	3.3	94
HAm5AAc20	1.9	2.0	100
HAm5AAc35	3.5	3.6	100

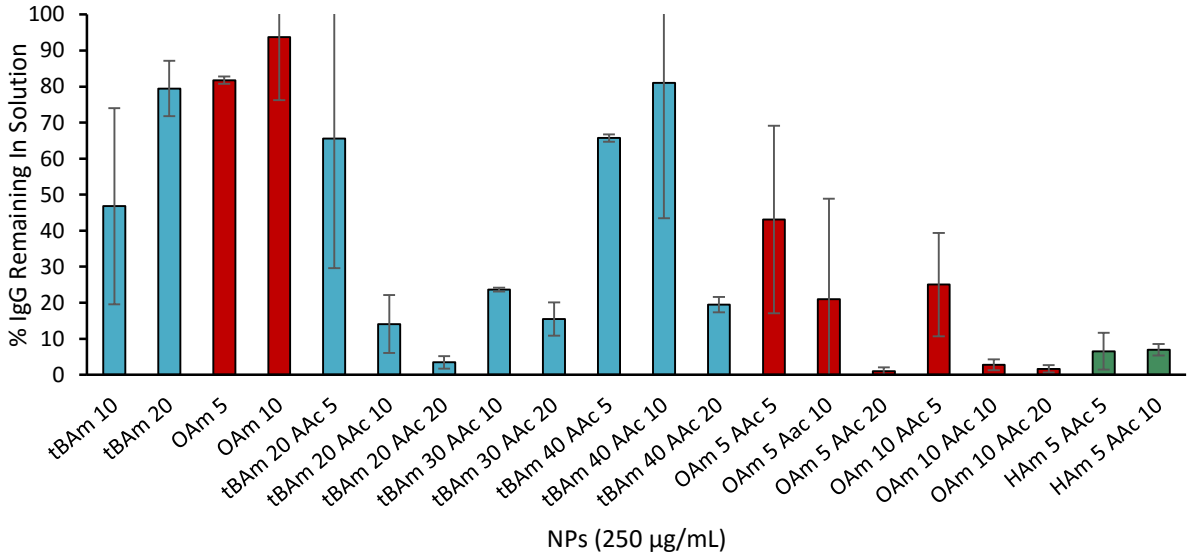

Figure 3.S1. Data shows the percent of FITC-IgG (20 µg/mL) remaining in solution after addition of NPs (250 µg/mL) in SPB (35 mM, pH 5.5) at 37 °C with 30 min incubation.

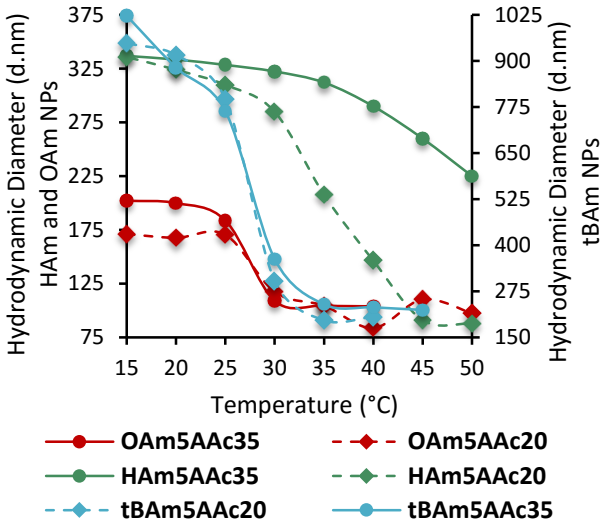

Figure 3.S2. Change in hydrodynamic radius of different NPs from 15 to 50 °C

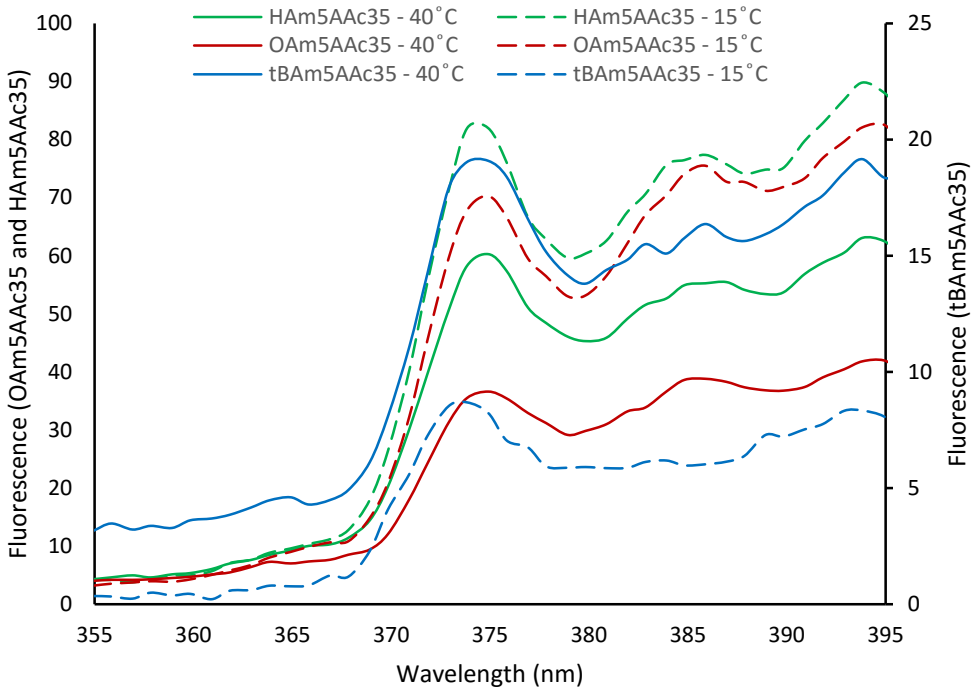

Figure 3.S3. Pyrene fluorescence in three NP solutions (2 mg/mL, water). Pyrene was dissolved in EtOH to 2 μM and added into the NP solution (0.5% volume). Each solution was incubated at either 15 or 40 °C for 10 min before measurement. The solutions were excited at 335 nm.

Table 3.S3. Denaturation temperatures and enthalpy if thermal denaturation of IgG in presence or absence of NPs from figure 3.4.

Condition	T_m (°C)	ΔH (kcal/mol)
No Polymer	45	3940
tBAm5AAc35	Not Observed	Broad
OAm5AAc35	70	Broad
HAm5AAc35	57	Broad

Q. References.

1. Feder, M. E.; Hofmann, G. E., Heat-shock proteins, molecular chaperones, and the stress response: Evolutionary and ecological physiology. *Annu Rev Physiol* **1999,** *61*, 243-282.

2. Bepperling, A.; Alte, F.; Kriehuber, T.; Braun, N.; Weinkauf, S.; Groll, M.; Haslbeck, M.; Buchner, J., Alternative bacterial two-component small heat shock protein systems. *P Natl Acad Sci USA* **2012,** *109* (50), 20407-20412.

3. Ranford, J. C.; Coates, A. R.; Henderson, B., Chaperonins are cell-signalling proteins: the unfolding biology of molecular chaperones. *Expert Rev Mol Med* **2000,** *2* (8), 1-17.

4. Beierle, J. M.; Yoshimatsu, K.; Chou, B.; Mathews, M. A. A.; Lesel, B. K.; Shea, K. J., Polymer Nanoparticle Hydrogels with Autonomous Affinity Switching for the Protection of Proteins from Thermal Stress. *Angew Chem Int Edit* **2014,** *53* (35), 9275-9279.

5. Nomura, Y.; Sasaki, Y.; Takagi, M.; Narita, T.; Aoyama, Y.; Akiyoshi, K., Thermoresponsive controlled association of protein with a dynamic nanogel of hydrophobized polysaccharide and cyclodextrin: Heat shock protein-like activity of artificial molecular chaperone. *Biomacromolecules* **2005,** *6* (1), 447-452.

6. Akiyoshi, K.; Sasaki, Y.; Sunamoto, J., Molecular chaperone-like activity of hydrogel nanoparticles of hydrophobized pullulan: Thermal stabilization with refolding of carbonic anhydrase B. *Bioconjugate Chem* **1999,** *10* (3), 321-324.

7. Hirakura, T.; Nomura, Y.; Aoyama, Y.; Akiyoshi, K., Photoresponsive nanogels formed by the self-assembly of spiropyrane-bearing pullulan that act as artificial molecular chaperones. *Biomacromolecules* **2004,** *5* (5), 1804-1809.

8. Lee, J.; Ko, J. H.; Lin, E. W.; Wallace, P.; Ruch, F.; Maynard, H. D., Trehalose hydrogels for stabilization of enzymes to heat. *Polym Chem-Uk* **2015,** *6* (18), 3443-3448.

9. Sandanaraj, B. S.; Vutukuri, D. R.; Simard, J. M.; Klaikherd, A.; Hong, R.; Rotello, V. M.; Thayumanavan, S., Noncovalent modification of chymotrypsin surface using an amphiphilic polymer scaffold: Implications in modulating protein function. *J Am Chem Soc* **2005,** *127* (30), 10693-10698.

10. Lee, J.; Lin, E. W.; Lau, U. Y.; Hedrick, J. L.; Bat, E.; Maynard, H. D., Trehalose Glycopolymers as Excipients for Protein Stabilization. *Biomacromolecules* **2014,** *15* (11), 4376-4376.

11. Sasaki, Y.; Nomura, Y.; Sawada, S.; Akiyoshi, K., Polysaccharide nanogel-cyclodextrin system as an artificial chaperone for in vitro protein synthesis of green fluorescent protein. *Polym J* **2010,** *42* (10), 823-828.

12. Chames, P.; Van Regenmortel, M.; Weiss, E.; Baty, D., Therapeutic antibodies: successes, limitations and hopes for the future. *Brit J Pharmacol* **2009,** *157* (2), 220-233.

13. Latza, P.; Gilles, P.; Schaller, T.; Schrader, T., Affinity Polymers Tailored for the Protein A Binding Site of Immunoglobulin G Proteins. *Chem-Eur J* **2014,** *20* (36), 11479-11487.

14. Lee, S. H.; Hoshino, Y.; Randall, A.; Zeng, Z. Y.; Baldi, P.; Doong, R. A.; Shea, K. J., Engineered Synthetic Polymer Nanoparticles as IgG Affinity Ligands. *J Am Chem Soc* **2012,** *134* (38), 15765-15772.

15. Martin, N.; Ma, D. W.; Herbet, A.; Boquet, D.; Winnik, F. M.; Tribet, C., Prevention of Thermally Induced Aggregation of IgG Antibodies by Noncovalent Interaction with Poly(acrylate) Derivatives. *Biomacromolecules* **2014,** *15* (8), 2952-2962.

16. Lahari, C.; Jasti, L. S.; Fadnavis, N. W.; Sontakke, K.; Ingavle, G.; Deokar, S.; Ponrathnam, S., Adsorption Induced Enzyme Denaturation: the Role of Polymer Hydrophobicity in Adsorption and Denaturation of alpha-Chymotrypsin on Allyl Glycidyl Ether (AGE)-Ethylene Glycol Dimethacrylate (EGDM) Copolymers. *Langmuir* **2010,** *26* (2), 1096-1106.

17. Pan, H.; Qin, M.; Meng, W.; Cao, Y.; Wang, W., How Do Proteins Unfold upon Adsorption on Nanoparticle Surfaces? *Langmuir* **2012,** *28* (35), 12779-12787.

18. Jasti, L. S.; Fadnavis, N. W.; Addepally, U.; Daniels, S.; Deokar, S.; Ponrathnam, S., Comparison of polymer induced and solvent induced trypsin denaturation: The role of hydrophobicity. *Colloid Surface B* **2014,** *116*, 201-205.

19. Deng, Z. J.; Liang, M. T.; Monteiro, M.; Toth, I.; Minchin, R. F., Nanoparticle-induced unfolding of fibrinogen promotes Mac-1 receptor activation and inflammation. *Nat Nanotechnol* **2011,** *6* (1), 39-44.

20. Zhang, D. M.; Neumann, O.; Wang, H.; Yuwono, V. M.; Barhoumi, A.; Perham, M.; Hartgerink, J. D.; Wittung-Stafshede, P.; Halas, N. J., Gold Nanoparticles Can Induce the Formation of Protein-based Aggregates at Physiological pH. *Nano Lett* **2009,** *9* (2), 666-671.

21. Masahiko Nakamoto; Tadashi Nonaka; Kenneth J. Shea; Yoshiko Miura; Hoshino, Y., Design of Synthetic Polymer Nanoparticles That Facilitate Resolubilization and Refolding of Aggregated Positively Charged Lysozyme. *J Am Chem Soc* **2016,** *138* (13), 4282 - 4285.

22. Yoshimatsu, K.; Lesel, B. K.; Yonamine, Y.; Beierle, J. M.; Hoshino, Y.; Shea, K. J., Temperature-Responsive "Catch and Release" of Proteins by using Multifunctional Polymer-Based Nanoparticles. *Angew Chem Int Edit* **2012,** *51* (10), 2405-2408.

23. Buis, B.; Wever, P. C.; Koomen, G. C. M.; vanAcker, B. A. C.; Groothoff, J. W.; Krediet, R. T.; Arisz, L., Clearance ratios of amylase isoenzymes and IgG subclasses: Do they reflect glomerular charge selectivity? *Nephron* **1997,** *75* (4), 444-450.

24. Chou, B.; Mirau, P.; Jiang, T.; Wang, S. W.; Shea, K. J., Tuning Hydrophobicity in Abiotic Affinity Reagents: Polymer Hydrogel Affinity Reagents for Molecules with Lipid-like Domains. *Biomacromolecules* **2016,** *17* (5), 1860-8.

25. Yoshimatsu, K.; Koide, H.; Hoshino, Y.; Shea, K. J., Preparation of abiotic polymer nanoparticles for sequestration and neutralization of a target peptide toxin. *Nat Protoc* **2015,** *10* (4), 595-604.

26. Arleth, L.; Xia, X. H.; Hjelm, R. P.; Wu, J. Z.; Hu, Z. B., Volume transition and internal structures of small poly(N-isopropylacrylamide) microgels. *J Polym Sci Pol Phys* **2005,** *43* (7), 849-860.

27. Brewer, A. K.; Striegel, A. M., Characterizing the size, shape, and compactness of a polydisperse prolate ellipsoidal particle via quadruple-detector hydrodynamic chromatography. *Analyst* **2011,** *136* (3), 515-519.

28. Tande, B. M.; Wagner, N. J.; Mackay, M. E.; Hawker, C. J.; Jeong, M., Viscosimetric, hydrodynamic, and conformational properties of dendrimers and dendrons. *Macromolecules* **2001,** *34* (24), 8580-8585.

29. Smith, M. H.; Lyon, L. A., Tunable Encapsulation of Proteins within Charged Microgels. *Macromolecules* **2011,** *44* (20), 8154-8160.

30. Smith, M. H.; Herman, E. S.; Lyon, L. A., Network Deconstruction Reveals Network Structure in Responsive Microgels. *J Phys Chem B* **2011,** *115* (14), 3761-3764.

31. Fishburn, C. S., The pharmacology of PEGylation: Balancing PD with PK to generate novel therapeutics. *J Pharm Sci-Us* **2008,** *97* (10), 4167-4183.

32. Veronese, F. M., Peptide and protein PEGylation: a review of problems and solutions. *Biomaterials* **2001,** *22* (5), 405-417.

33. Schottler, S.; Becker, G.; Winzen, S.; Steinbach, T.; Mohr, K.; Landfester, K.; Mailander, V.; Wurm, F. R., Protein adsorption is required for stealth effect of poly(ethylene glycol)- and poly(phosphoester)-coated nanocarriers. *Nat Nanotechnol* **2016,** *11* (4), 372-377.

34. Hunt, E. K., *Health Effect Assessments of the Basic Acrylates*. CRC Press, Inc.: Florida, USA, 1993; p 144.

35. Chou, B.; Mirau, P.; Jiang, T.; Wang, S.-W.; Shea, K. J., Tuning Hydrophobicity in Abiotic Affinity Reagents: Polymer Hydrogel Affinity Reagents for Molecules with Lipid-like Domains. *Biomacromolecules* **2016,** *17* (5), 1860 - 1868.

36. Brandrup, J.; Immergut, E. H., *Polymer Handbook, Third Edition*. John Wiley & Sons, Inc.: Canada, 1989.

37. Baselga, J.; Llorente, M. A.; Nieto, J. L.; Hernandezfuentes, I.; Pierola, I. F., Polyacrylamide Networks - Sequence Distribution of Crosslinker. *Eur Polym J* **1988,** *24* (2), 161-165.

38. Dong, X. Y.; Wang, Y.; Shi, J. H.; Sun, Y., Size exclusion chromatography with an artificial chaperone system enhanced lysozyme renaturation. *Enzyme Microb Tech* **2002,** *30* (6), 792-797.

39. Gray, J. J., The interaction of proteins with solid surfaces. *Curr Opin Struc Biol* **2004,** *14* (1), 110-115.

40. Cabaleiro-Lago, C.; Quinlan-Pluck, F.; Lynch, I.; Lindman, S.; Minogue, A. M.; Thulin, E.; Walsh, D. M.; Dawson, K. A.; Linse, S., Inhibition of Amyloid beta Protein Fibrillation by Polymeric Nanoparticles. *J Am Chem Soc* **2008,** *130* (46), 15437-15443.

41. Dong, D. C.; Winnik, M. A., The Py scale of solvent polarities. Solvent effects on the vibronic fine structure of pyrene fluorescence and empirical correlations with E_T and Y values. *Photochemistry and Photobiology* **1982,** *35*, 17 - 21.

42. Vermeer, A. W. P.; Norde, W.; van Amerongen, A., The unfolding/denaturation of immunogammaglobulin of isotype 2b and its F-ab and F-c fragments. *Biophys J* **2000,** *79* (4), 2150-2154.

43. Maeda, Y.; Ueda, T.; Imoto, T., Effective renaturation of denatured and reduced immunoglobulin G in vitro without assistance of chaperone. *Protein Eng* **1996,** *9* (1), 95-100.

44. Hoshino, Y.; Urakami, T.; Kodama, T.; Koide, H.; Oku, N.; Okahata, Y.; Shea, K. J., Design of Synthetic Polymer Nanoparticles that Capture and Neutralize a Toxic Peptide. *Small* **2009,** *5* (13), 1562-1568.

45. Hoshino, Y.; Haberaecker, W. W.; Kodama, T.; Zeng, Z. Y.; Okahata, Y.; Shea, K. J., Affinity Purification of Multifunctional Polymer Nanoparticles. *J Am Chem Soc* **2010,** *132* (39), 13648-13650.

46. Zeng, Z. Y.; Hoshino, Y.; Rodriguez, A.; Yoo, H. S.; Shea, K. J., Synthetic Polymer Nanoparticles with Antibody-like Affinity for a Hydrophilic Peptide. *Acs Nano* **2010,** *4* (1), 199-204.

47. Hoshino, Y.; Koide, H.; Oyama, D.; Yonamine, Y.; Lee, S. H.; Oku, N.; Shea, K. J., Design of polymer nanoparticles that are capable of neutralizing toxicity of fetal proteins. *Abstr Pap Am Chem S* **2011,** *241*.

48. Hoshino, Y.; Koide, H.; Furuya, K.; Haberaecker, W. W.; Lee, S. H.; Kodama, T.; Kanazawa, H.; Oku, N.; Shea, K. J., The rational design of a synthetic polymer nanoparticle that neutralizes a toxic peptide in vivo. *P Natl Acad Sci USA* **2012,** *109* (1), 33-38.

49. Mcphee, W.; Tam, K. C.; Pelton, R., Poly(N-Isopropylacrylamide) Latices Prepared with Sodium Dodecyl-Sulfate. *J Colloid Interf Sci* **1993,** *156* (1), 24-30.

Chapter 4

A Novel Cysteine Active End-Cap for Self Immolative Polymers

A. Introduction

Self-immolative (SI) polymers are kinetically stable materials that degrade into individual monomer components upon the activation and release of a trigger molecule (Figure 4.1). Their unique ability to amplify a signal by releasing multiple reporters per activation event has stimulated interest in their use.[1-4] Since SI polymers only require a small amount of stimulus to initiate degradation, their use would require less invasive methods for removal. Many studies of SI polymers have been conducted to identify end-caps that respond to unique stimuli, increasing potential applications. Removal of the end-cap unmasks reactive end groups that initiate depolymerization.[1-6] The combination of selective responsiveness, signal amplification, and diverse possibilities of signal output has drawn much attention to the use of SIPs for different applications.

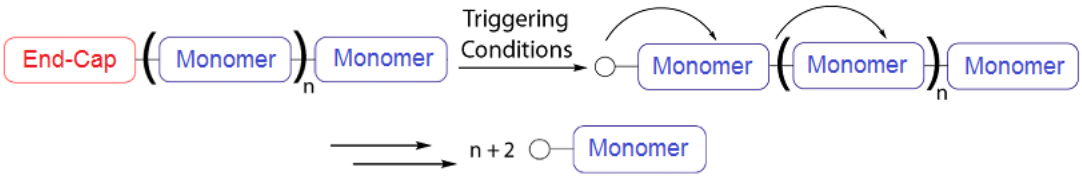

Figure 4.1. Summary of SI polymer function.

Much research has been done expanding the uses of SI polymers. Many groups have worked on optimizing monomer compositions,[7-8] studying effects of chain length on polymer

degradation,[5] or monitoring effects of solvent conditions to affect the rate of degradation.[9-10] By using different types of polymers and altering the rates of degradation, SI polymers can be used for purposes ranging from adhesives,[11] controlled drug release,[12] diagnostics,[13] and more.[14]

Despite the growth of SI polymer applications, their full potential has not been tapped. Many fields could benefit from using polymers that remain stable prior to addition of a selective stimuli. The potential of SI polymers for use in the cosmetics industry is one such field that could benefit. As gel nail polishes have become more popular, it becomes apparent that new methods to improve polish removal are needed. Current methods for gel polish removal requires a 10 – 15 min soak in acetone to soften the polish, after which the polish is scrapped off. This can often lead to nail damage. Using SI polymers as a base coat can have a huge impact on the cosmetics industry. For this to work, new SI end-caps with nontoxic triggers need to be developed.

Many different end-caps for SI polymers have been reported, which respond to many different stimuli, including enzymes, nucleophiles, and acids and bases. Most studies focus on repurposing known systems, with little focus on making new, selective end-caps with innocuous triggers.[1, 3, 15-16] The synthesis of novel triggers with unique and selective stimuli that are safe to use, can expand the possible applications of SI polymers. With the wide potential range of applications for SI polymers, both biological and nonbiological, designing end-caps with non-toxic triggers can have a significant impact for SI polymers. To this end, we report a novel cysteine activated end-cap for SI polymers. An aqueous solution of cysteine may provide an innocuous and useful alternative to current end-caps, expanding the potential uses for SI polymers.

B. End-cap Design

The novel end-cap was inspired by a cysteine active fluorescein-based chemodosimeter.[17] The acrylate end group was found to be selective for cysteine over homocysteine and glutathione. The addition of cysteine to the non-fluorescent chemodosimeter was expected to cause an electron cascade, releasing a fluorescent molecule. I took advantage of this electron cascade to initiate depolymerization of a SI polymer.

A well-studied model polymer backbone, using a 4-aminobenzyl alcohol spacer, was chosen for this study to test the efficacy of my novel end-cap. Selective removal of the novel end-cap would reveal an electron rich amine, which would proceed through a cascade of repetitive 1,6-eliminations and decarboxylations until the polymer depolymerizes into the starting monomers and CO_2. This monomer was chosen because it was cheap, commercially available, had a simple and well-studied synthesis, and its depolymerization has been studied with various end-caps and under different conditions.[6-7, 9, 11]

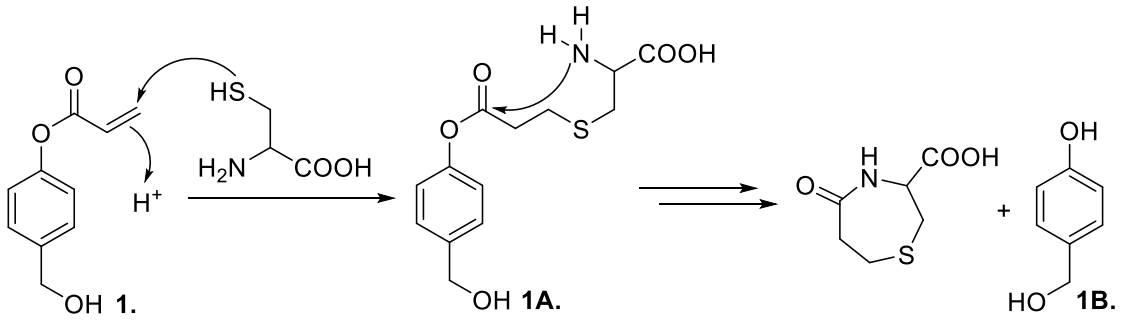

Scheme 4.1. Novel end-cap and scheme of the suspected mechanism for removal.[17]

C. HPLC Analysis of Trigger Breakdown.

To test if the novel end-cap would be selectively triggered with addition of a cysteine solution, the novel end-cap was attached to a 4-methoxyphenol monomer and tested with cysteine for its breakdown. The deprotection of **1** upon addition of cysteine is suspected to occur with a Michael addition of the thiol on cysteine to the alkene to form the Michael adduct, **1B**.[17] A 7-exo-trig cyclization then proceeds, resulting in the elimination of a 7 membered heterocyclic lactam ring.[17] The subsequent fragmentation then proceeds through a 1,6-elimination to reform the monomer, 4-methyoxyphenol (**1B**) (Scheme 4.1).

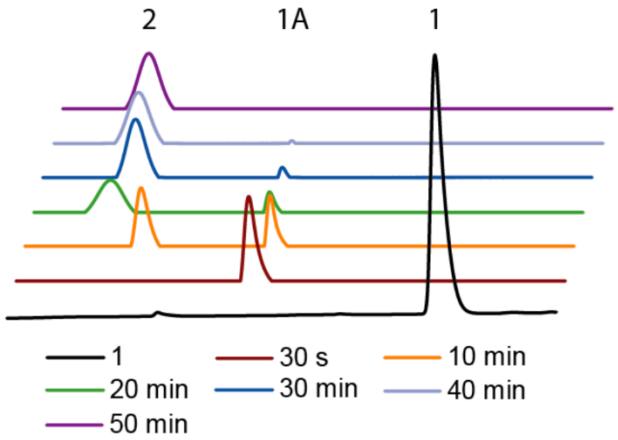

Figure 4.2. HPLC data based on scheme 4.1. HPLC scans had 5 µL injections of the mixture at 0 – 70% ACN in water over 7 min. Molecule **1** (25 µg/mL) was mixed with L-cysteine (5 mg/mL) in HEPES buffer (20 mM, CTAB 1 mM, pH 7.4). Each data point is associated with the time of the HPLC injection with 30 s being the time of L-cysteine addition to molecule **1**.

The suspected end-cap removal was tested using reverse phase HPLC by monitoring the disappearance of **1** and the appearance of **1B**. First, the purified trigger was dissolved in HEPES buffer (20 mM, CTAB 1 mM, pH 7.4) at 25 µg/mL. Next, L-cysteine (5 mg/mL) was

added, and the mixture was immediately injected into the HPLC for analysis. Each experiment was run at a gradient of 0 – 70% acetonitrile (ACN) in water over 7 min, ending in a pure ACN, then pure water wash for a total of 10 min for one run. Each run is labeled for the time since mixture of **1** with L-cysteine. As seen in figure 4.2, after 30 s, **1** has completely reacted with L-cysteine to form intermediate, **1A**, which over time forms the monomer, **1B**. This result demonstrates that the end cap reacts with L-cysteine and fragments to form the electron rich monomer in a relatively short time at room temperature in cysteine (5 mg/mL).

These results show that the initial Michael addition of cysteine to **1** occurs rapidly, with complete reaction within 30 s. The presence of the Michael product suggests that the 7-exo-trig cyclization is the rate limiting step in the degradation. The cyclization and elimination steps then proceed over 40 min until complete conversion to **1B** and the heterocyclic lactam ring is observed. Control runs of the end capped monomer, **1**, show that the end cap is relatively stable in buffer, and will not suffer from spontaneous hydrolysis without the presence of cysteine.

D. HPLC Analysis of Tetramer Breakdown

The end-cap was then attached to a short oligomer to test if the end cap was effective at stabilizing a larger molecule, and if it would lead to a rapid depolymerization upon addition of the aqueous cysteine solution. The oligomer was synthesized stepwise. Efforts towards a convergent synthesis of the oligomers were unsuccessful because dimers that were not end-capped proved to be too unstable and reactive and would degrade prior to any further reaction. The stepwise synthesis yielded the tetramer in moderate yield, but with good

purity. Every intermediate was purified and isolated using column chromatography in hexanes and ethyl acetate (full details in SI), yielding a pure tetramer for testing.

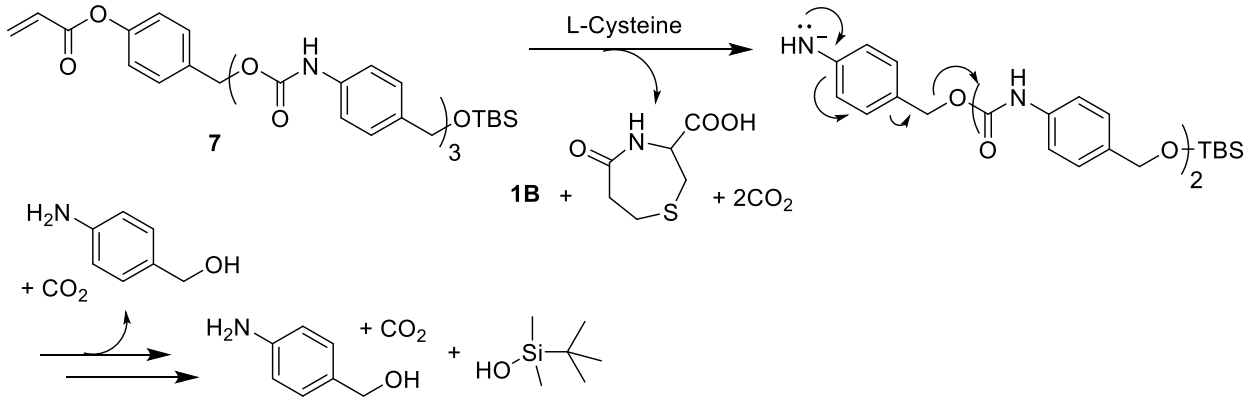

Scheme 4.2. Degradation scheme of end-capped tetramer **7**. Removal of end-cap by L-cysteine proceeds as shown in scheme 4.1. The degradation then proceeds through decarboxylation to reveal the electron-rich amine, which then proceeds through a series of 1,6-eliminations and decarboxylations until the tetramer has completely degraded.

Depolymerization of the end-capped tetramer was evaluated using reverse phase HPLC to monitor the disappearance of compound **7** (labeled **I** in Figure 4.3) and the appearance of peak **II**, the decomposition product. Tetramer **7** was dissolved in minimal ethanol, as it was insoluble in water, and then diluted with HEPES buffer (20 mM, CTAB 1 mM, pH 7.4) at 0.5 mg/mL. L-cysteine (4 mg/mL) was added, and the mixture was immediately injected into the HPLC for analysis. Detection at 254 nm was used to reveal the presence of aromatic groups, and detection at 220 nm to show the presence of amide bonds. Each experiment was run at a gradient of 0 – 75% ACN in water over 10 min, and ended in a pure ACN, then pure water wash for a total of 15 min for each run. Each run is labeled for the time of injection

4.3A. **4.3B.**

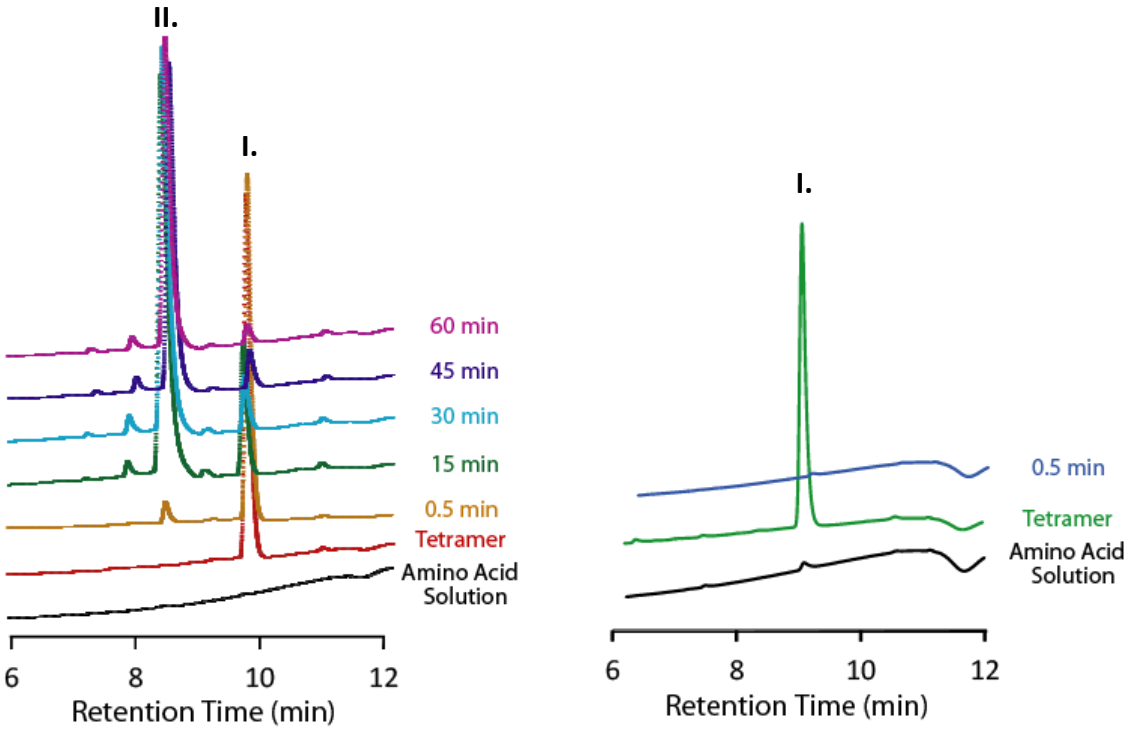

Figure 4.3. HPLC run data. A sample of tetramer **7** (0.5 mg/mL) in HEPES buffer (20 mM, CTAB 1 mM, pH 7.4) with addition of L-cysteine with **A.** detection at 254 nm, **B.** detection at 220 nm.

since addition of L-cysteine into the tetramer **7** solution. As seen in figure 4.3A, after 60 min, the tetramer, represented by peak **I**, had completely reacted with L-cysteine to form **II**. In figure 4.3B though, peak **I.**, which represents compound **7**, has completely disappeared within 30 s. This shows that all the carbamate linkages in compound **7** have been cleaved within 30 s at RT (Scheme 4.2). This experiment shows that the acrylate trigger is still active when joined to a tetramer, and the removal of the trigger upon addition of L-cysteine, leads to the complete depolymerization of the tetramer. Control runs of the tetramer **7** alone in buffer showed no spontaneous decomposition.

These results establish that despite increasing the chain length on the end-capped monomer, the end-cap still reacts rapidly with L-cysteine in water. The rapid rate of depolymerization upon addition of an aqueous solution of L-cysteine makes this end cap effective as a removable coating, as degradation occurs after a reasonable incubation time.

E. Visual Decomposition of Tetramer Film

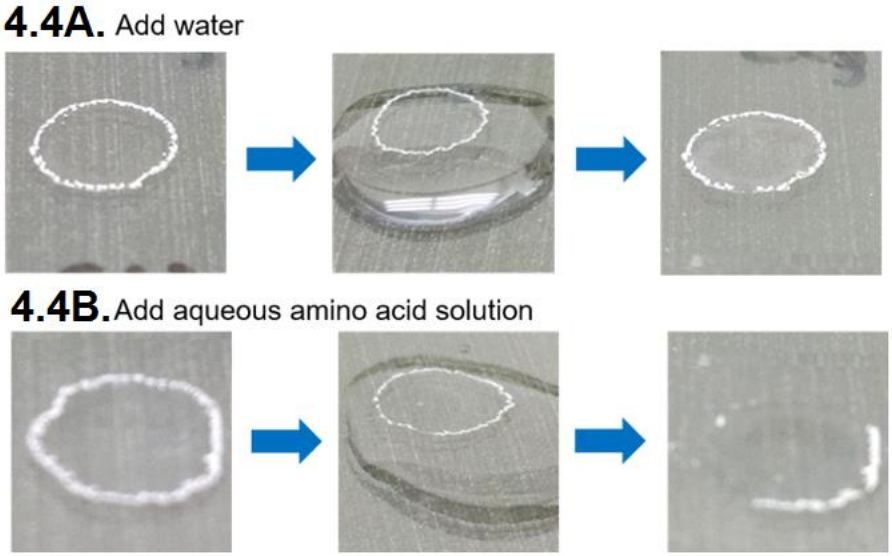

Figure 4.4. Visual observation of film decomposition. Films were made from a concentrated EtOAc solution of the tetramer **9**. The films were incubated in **A.** DI water and **B.** in a HEPES buffer solution (20 mM, CTAB 1 mM, pH 7.4) containing L-cysteine. In both cases, the first panel shows the film, the second panel shows the films incubating in the respective solutions, and the third panel shows each film after a 5 min incubation, with the aqueous solutions lightly rinsed off with DI water.

The end-capped tetramer was then tested as a film, to establish if it had similar reactivity as in the solution experiments. Tetramer **7** was dissolved in ethyl acetate to form a white

film on a clean glass slide (Figure 4.4). The films were then incubated in either DI water, or in a HEPES buffer solution (20 mM, CTAB 1 mM, pH 7.4) with L-cysteine. Each solution was then incubated for 5 min at RT. The solutions were then washed using DI water. The results show that the film that was incubated in water (Figure 4.4A) remains unaffected, while the film incubated in a L-cysteine solution (Figure 4.4B) had already begun to flake off of the glass slide. This result agrees with the HPLC data, which shows the end-cap is selectively activated by the L-cysteine solution, and proceeds towards complete degradation after incubating for 5 min in an aqueous solution.

F. Conclusion

A novel end-cap was developed for SI systems that could respond to an aqueous solution of L-cysteine. The end-cap was appended to a 4-hydroxybenzyl alcohol monomer to form the end capped monomer, **1**, which was tested for the L-cysteine stimulated degradation. The results show that end cap will react with L-cysteine, leading to reformation of the monomer**.** The end capped monomer, **1**, was also shown to resist spontaneous hydrolysis in the absence of cysteine. The novel end cap attached to a tetramer backbone (**7**). This tetramer was tested for degradation in the presence of an aqueous solution of L-cysteine and found to react and depolymerize in as little as 30 s. Visual analysis of the decomposition of a film made of tetramer **7** showed that the end-cap could stabilize a tetramer film under atmospheric conditions at RT, and would decompose upon exposure to an aqueous solution of L-cysteine in as little as 5 min. The incorporation of this novel L-cysteine active end-cap into SI polymer systems could find many applications, particularly in the cosmetics industry, where new methods for easy, non-toxic methods to remove of gel polishes would be most welcome.

Further study of this end-cap with longer chain polymers or with a different backbone are necessary to improve solubility in water, and can expand the potential uses of this SI end-cap.

G. Supplementary Information

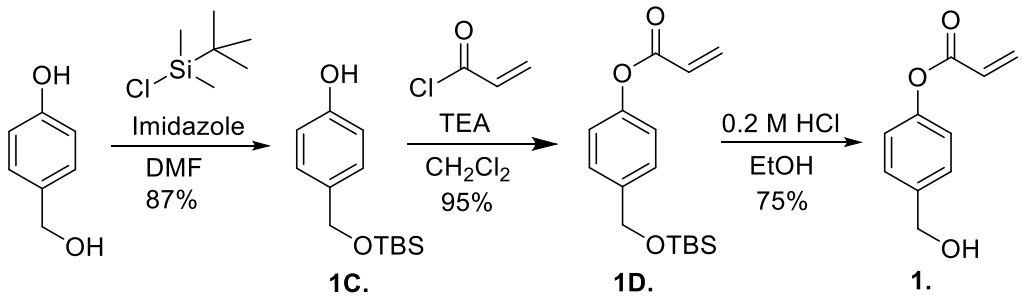

Scheme 4.S1. Synthesis of trigger.

- Synthesis of the end-capped monomer (**1**).

The end-capped monomer was prepared using a modified literature procedure (**Scheme 4.S1**).[18-19] In short, 4-hydroxybenzyl alcohol (1 eq) was mixed with tert-butyl dimethylsilyl chloride (2 eq) and imidazole (2 eq) at room temperature in dry DMF at 0 °C under N_2. After 30 min, the reaction was washed with $NaHCO_3$ and brine and product was purified using column chromatography (Hex:EtOAc, 80:20) to yield a white crystalline product, **1C**. Next, to a solution of **1C** (1 eq) and TEA (3 eq) in dry dichloromethane, acryloyl chloride was added dropwise at 0 °C under nitrogen. The reaction proceeded for 30 min, and then was washed with $NaHCO_3$ and brine, and the solvent was removed. The product was then purified using column chromatography (Hex:EtOAc 80:20) to yield an oil product, **1D**. Finally, product **1D** was mixed with 0.2 M HCl in EtOH for 5 min. The reaction

mixture was then diluted with excess EtOAc and washed with $NaHCO_3$ and brine to yield the end capped monomer, **1**. The monomer was then purified using column chromatography (Hex:EtOAc 90:10) to form a clear oil product.

1D. ^{1}H-NMR (500 MHz, $CDCl_3$) δ 7.40 (d, *J*=8.7 Hz, 2H), 7.15 (d, *J*=8.7 Hz, 2H), 6.67 (d, *J*=17.3, 1H), 6.39 (dd, *J*=17.3, 10.4 Hz, 1H), 6.07 (d, *J*=10.5 Hz, 1H), 4.80 (s, 2H), 1.07 (s, 9H), 0.17 (s, 6H)

1. ^{1}H NMR (500 MHz, $CDCl_3$) δ 7.41 (d, *J*=8.7 Hz, 2H), 7.14 (d, *J*=8.7 Hz, 2H), 6.66 (d, *J* = 17.3, 1H), 6.38 (dd, *J* = 17.3, 10.5 Hz, 1H), 6.07 (dd, *J* = 10.5, 1H), 4.74 (s, 2H).

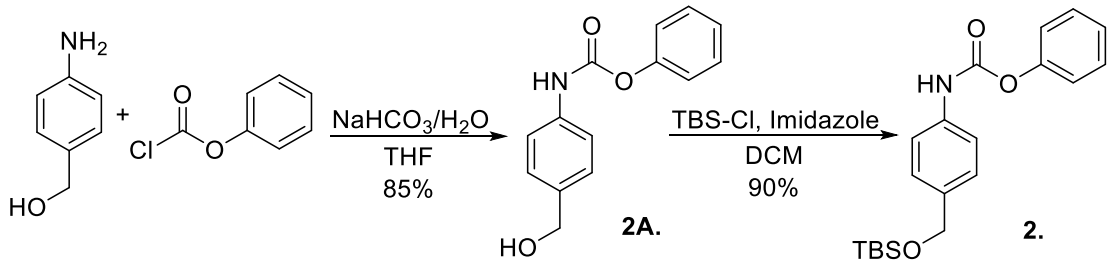

Scheme 4.S2. Activation of 4-nitrobenzyl alcohol with phenylchloroformate.

The activated monomer was synthesized according to literature procedures.[12] In short, phenylchloroformate (1.1 eq) was dissolved in THF and added dropwise to a solution of 4-aminobenzyl alcohol (1 eq) in $NaHCO_3$ (sat.) and water (**Scheme 4.S2**). The reaction proceeded at room temperature overnight, and then diluted in ethyl acetate and washed with ammonium chloride. The solvent was then evaporated and purified using column chromatography (Hex:EtOAc 70:30) to yield a tan colored solid product (**2A**). Next,

compound **2A** (1 eq) was mixed with tert-butyldimethylsilyl chloride (2 eq) and imidazole (2 eq) in dry dichloromethane at 0 °C for 1 h. The solution was then washed with $NaHCO_3$ and brine, and the solvent was removed. The product was purified using column chromatography (Hex:EtOAc 90:10) to yield a white crystalline product, **2**.

- End-capped tetramer synthesis

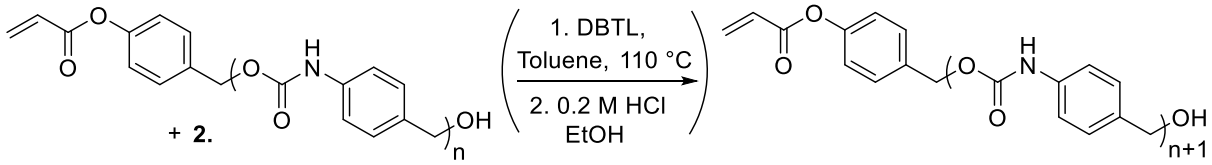

Scheme 4.S3. Tetramer synthesis.

Table 4.S1. Summary of coupling reaction components.

Starting Material	Product
1.	**3.**
4.	**5.**
6.	**7.**

The activated monomer, **2**, was used to synthesize the oligomers. For the first step, one of the deprotected oligomers, **1**, **4**, **6** (1.1 eq), was mixed with **2** (1 eq) in dry toluene at 110 °C (**Scheme 4.S3, Table 4.S1**). DBTL (0.2 eq) was then added dropwise into the reaction mixture, and the reaction proceeded for 2 h. The reaction was then cooled to room temperature and the solvent was removed under reduced pressure. The dark reddish orange oil was then purified using column chromatography (Hex:EtOAc 70:30) to yield a white or off-white solid products, **3**, **5**, and **7**. Next, the protected oligomers, **3** and **5**, were mixed in a 0.2 M HCl solution in EtOH for 5 min to yield the white solids, **4** and **6**, respectively. These products were purified using column chromatography in (Hex:EtOAc 50:50) to form white solid products.

3. 88%, HRMS *m/z* calcd for $C_{24}H_{31}O_5NSi$ $(M + Na)^+$ 464.1869, found 464.1851, ^1H NMR (500 MHz, $CDCl_3$) δ 7.49 (d, *J* = 8.4 Hz, 2H), 7.40 (d, *J* = 8.0 Hz, 2H), 7.28 (d, *J*=9.7 Hz, 2H), 7.15 (d, *J*=8.2 Hz, 2H), 6.72 (s, 1H), 6.67 (d, *J* = 17.3 Hz, 1H), 6.38 (dd, *J* = 17.3, 10.5 Hz, 1H), 6.08 (d, *J* = 10.5 Hz, 1H), 5.25 (s, 2H), 4.75 (s, 2H), 0.96 (s, 9H), 0.12 (s, 6H). ^{13}C NMR (500 MHz, $CDCl_3$) δ 206.20, 164.92, 151.57, 135.60, 133.21, 130.24, 128.84, 127.72, 122.72, 119.20, 66.31, 65.37, 34.31, 32.73, 26.43, 25.78, 23.36, 18.91, 14.46, 0.09.

4. 94%, HRMS *m/z* calcd for $C_{18}H17O_5N$ $(M + Na)^+$ 350.1004, found 350.0994, ^1H NMR (500 MHz, $CDCl_3$) δ 7.47 (d, *J* = 8.5 Hz, 2H), 7.41 (d, *J* = 7.7 Hz, 2H), 7.33 (d, *J* = 9.7 Hz, 2H), 7.19 (d, *J* = 8.5 Hz, 2H), 6.98 (s, 1H), 6.67 (d, *J* = 17.4 Hz, 1H), 6.38 (dd, *J* = 17.3, 10.5 Hz, 1H), 6.08 (d, *J* = 10.5 Hz, 1H), 5.23 (s, 2H), 4.67 (s, 2H). ^{13}C NMR (500 MHz, $CDCl_3$) δ 164.57, 150.54, 133.77, 132.91, 129.66, 127.97, 127.78, 121.80, 66.39, 64.95.

5. 54%, HRMS *m/z* calcd for $C_{32}H_{38}O_7N_2Si$ $(M + Na)^+$ 613.2346, found 613.2323, ^1H NMR (500 MHz, $CDCl_3$) δ 7.56 – 7.17 (m, 12H), 6.82 (s, 1H), 6.73 (s, 1H), 6.67 (d, *J* = 17.3, 1H), 6.38 (dd, *J* = 17.3, 10.5 Hz, 1H), 6.09 (d, *J* = 10.5 Hz, 1H), 5.25 (s, 2H), 5.19 (s, 2H), 4.74 (s, 2H), 0.98 (s, 9H), 0.14 (s, 6H). ^{13}C NMR (500 MHz, $CDCl_3$) δ 164.61, 162.03, 150.42, 133.68, 132.94, 129.69, 129.49, 127.85, 126.98, 126.26, 121.76, 115.63, 64.67, 60.51, 30.78, 26.06, 21.13, 18.43, 14.27, -5.17.

6. 98%, HRMS *m/z* calcd for $C_{26}H_{24}O_7N_2$ $(M + Na)^+$ 499.1481, found 499.1483, ^1H NMR (500 MHz, $CDCl_3$) δ 7.48 (d, *J* = 8.4 Hz, 2H), 7.41 (t, *J* = 11.5 Hz, 6H), 7.37 – 7.30 (m, 2H), 7.20 (d, *J* = 8.4 Hz, 2H), 6.89 (s, 1H), 6.86 (s, 1H), 6.68 (d, *J* = 17.3 Hz, 1H), 6.39 (dd, *J* = 17.4, 10.5 Hz, 1H), 6.09 (d, *J* = 10.6 Hz, 1H), 5.24 (s, 1H), 5.19 (s, 1H), 4.70 (s, 1H). ^{13}C NMR (500 MHz, DMSO) δ 164.60, 153.90, 150.45, 139.42, 138.15, 136.97, 134.70, 134.25, 130.90, 129.99, 129.63, 128.00, 127.65, 122.28, 118.40, 66.02, 63.06, 0.66.

7. 86%, HRMS *m/z* calcd for $C_{40}H_{45}O_9N_3Si$ $(M + Na)^+$ 762.2823, found 762.2820, ^1H NMR (500 MHz, $CDCl_3$) δ 7.47 (d, *J* = 8.4 Hz, 2H), 7.43 (m, 4H), 7.38 (dd, *J* = 8.3, 3.6 Hz, 6H), 7.34 – 7.28 (m, 2H), 7.19 (d, *J* = 8.5 Hz, 2H), 6.97 – 6.87 (m, $2H^{20}$), 6.83 (d, *J* = 6.1 Hz, 1H), 6.67 (d, *J* = 17.3 Hz, 1H), 6.38 (dd, *J* = 17.3, 10.5 Hz, 1H), 6.08 (d, *J* = 10.4 Hz, 1H), 5.24 (s, 2H), 5.18 (s, 4H), 4.74 (s, 2H), 1.32 (s, 9H), 0.98 (s, 6H). ^{13}C NMR (500 MHz, DMSO) δ 134.79, 134.18, 129.98, 129.72, 128.06, 127.24, 122.32, 118.39, 115.81, 64.78, 26.32, 18.46, 0.60, -4.72.

- Bulk polymer synthesis.

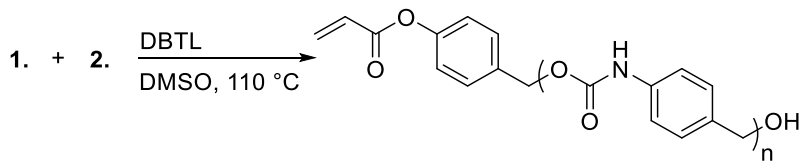

Scheme 4.S4. Bulk polymer synthesis.

Once the tetramer showed selective degradation under aqueous cysteine solution, the novel end-cap was appended to a polymer backbone to test the selectivity of the end-cap in a bulk polymer, and kinetics of degradation of the bulk polymer. To synthesize the end-capped polymer, the activated monomer, **2** (1 eq), was dissolved in dry DMSO and heated to 110 °C with DBTL (0.2 eq) for 10 min under nitrogen. Next, an excess of the end capped monomer, **1** (1 eq), was dissolved in dry DMSO and added into the reaction mixture. (**Scheme 4.S4**), and the reaction proceeded for an additional 30 min. The reaction was then cooled to room temperature, and the polymer was precipitated in methanol to form an off white solid. The polymer was then analyzed with ^{1}H-NMR and GPC to determine the size of the polymer. ^{1}H-NMR analysis showed a monomer to end-cap ratio of ~20:1, with GPC showing a polymer of M_n of 24,000 g/mol and a PDI of 1.87.

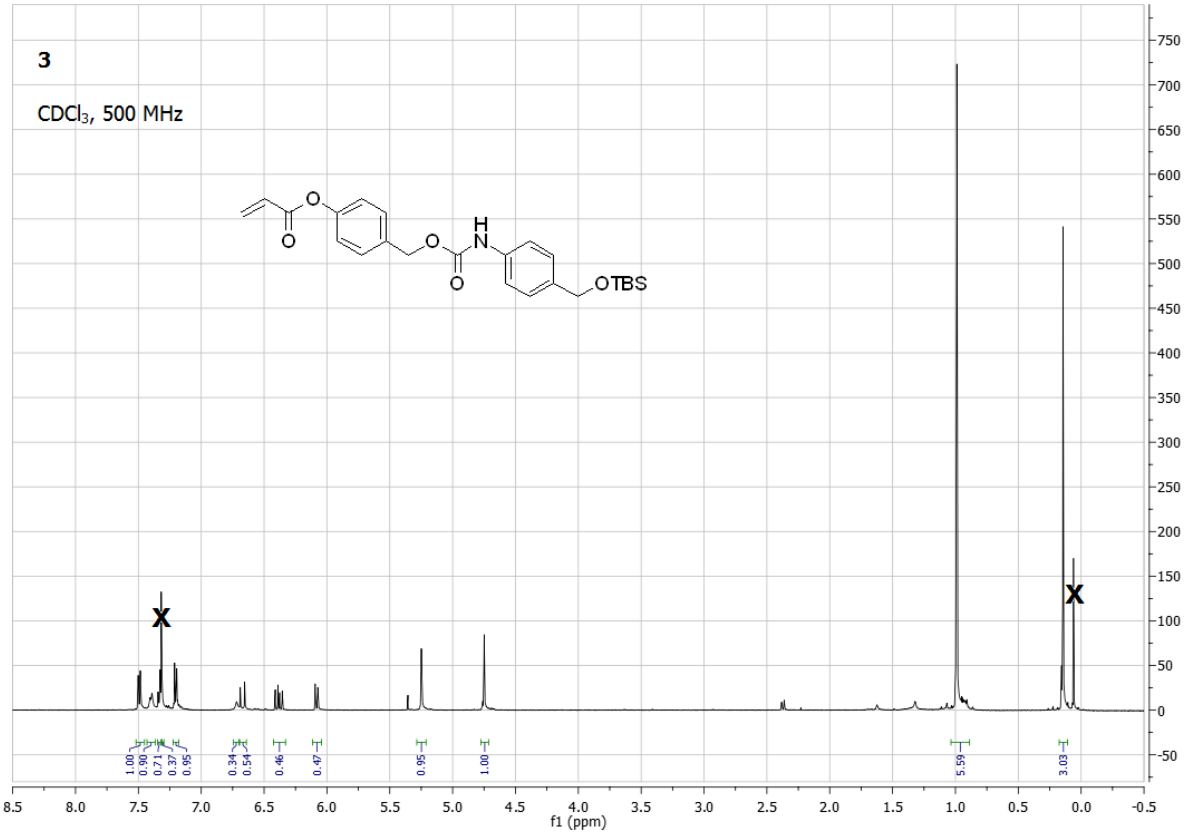
3
CDCl3, 500 MHz
OTBS
X
X
f1 (ppm)

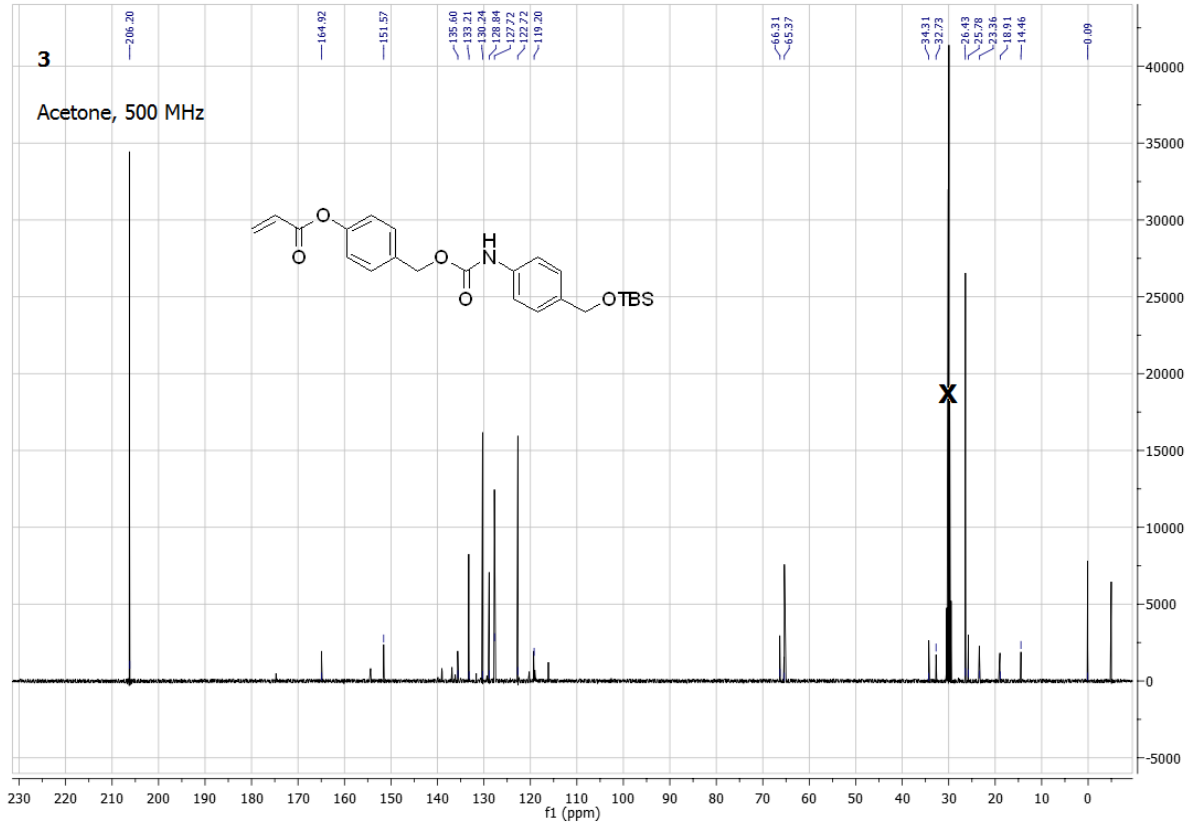
3
Acetone, 500 MHz
OTBS
X
f1 (ppm)

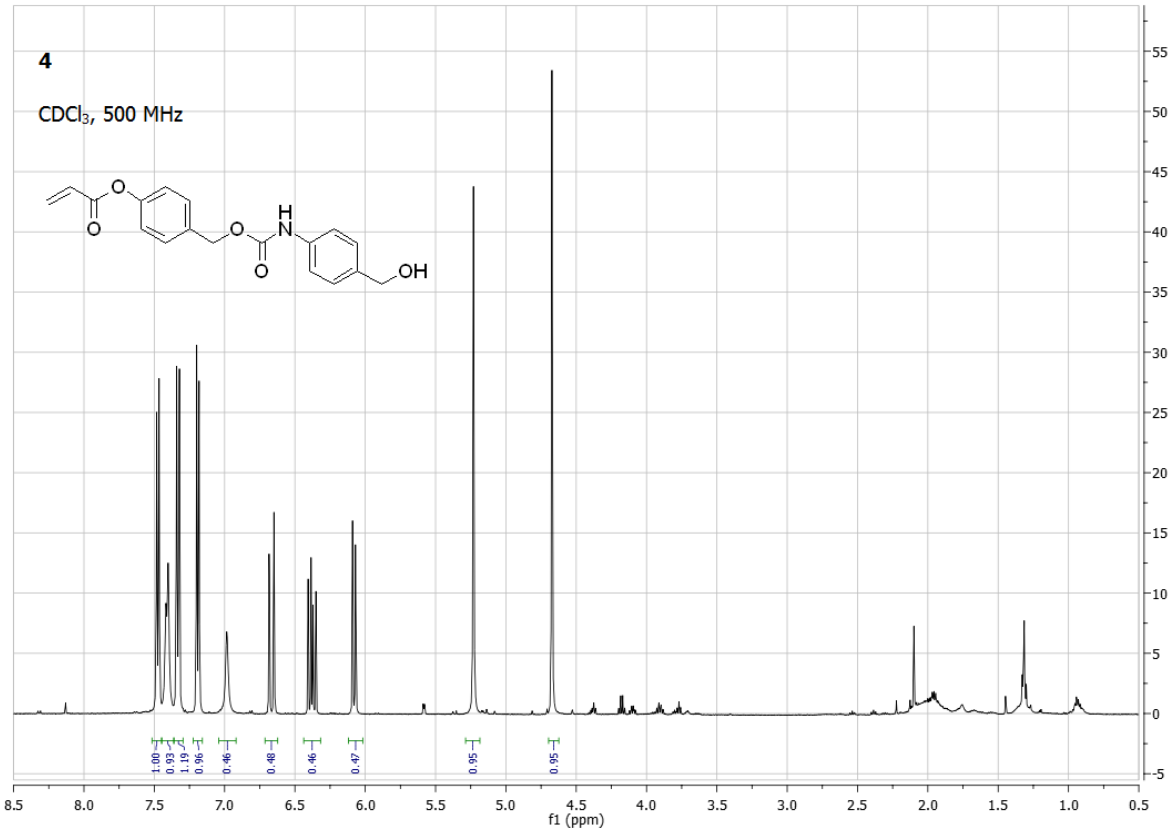
4
CDCl3, 500 MHz
OH
f1 (ppm)

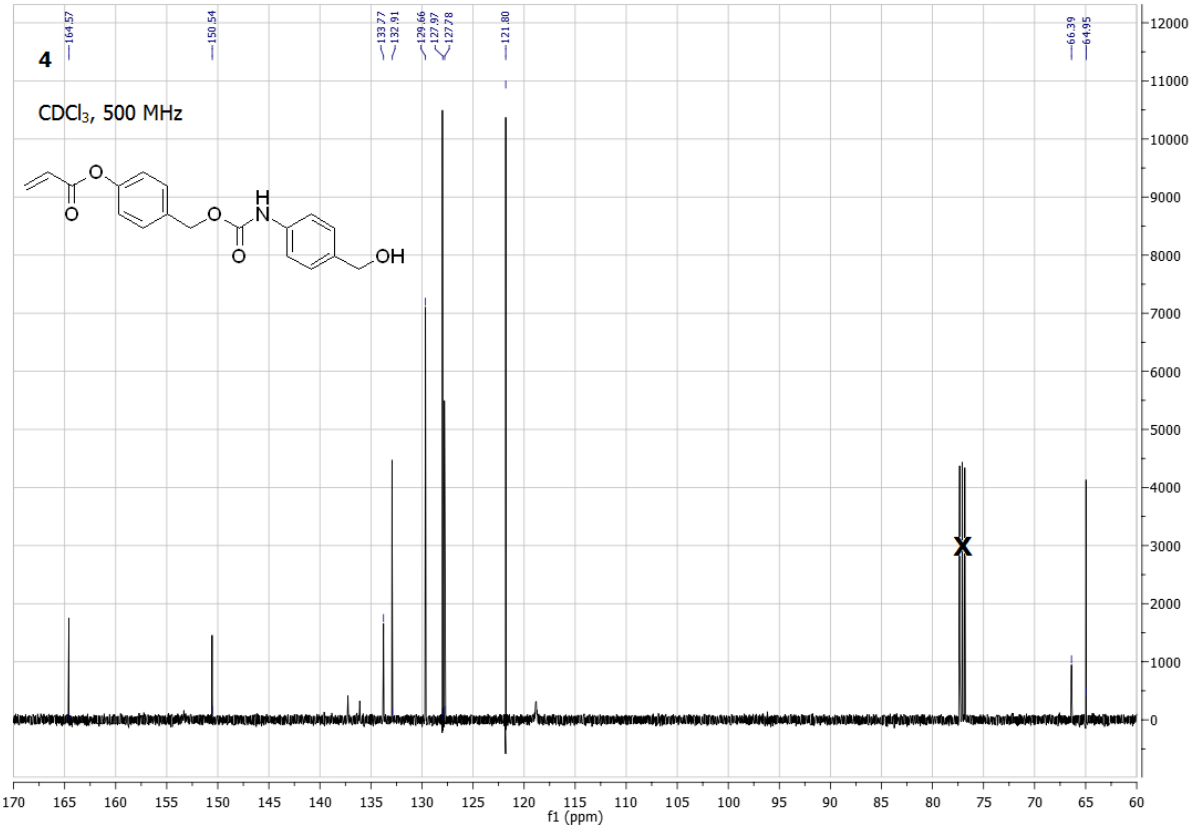
4
CDCl3, 500 MHz
OH
X
f1 (ppm)

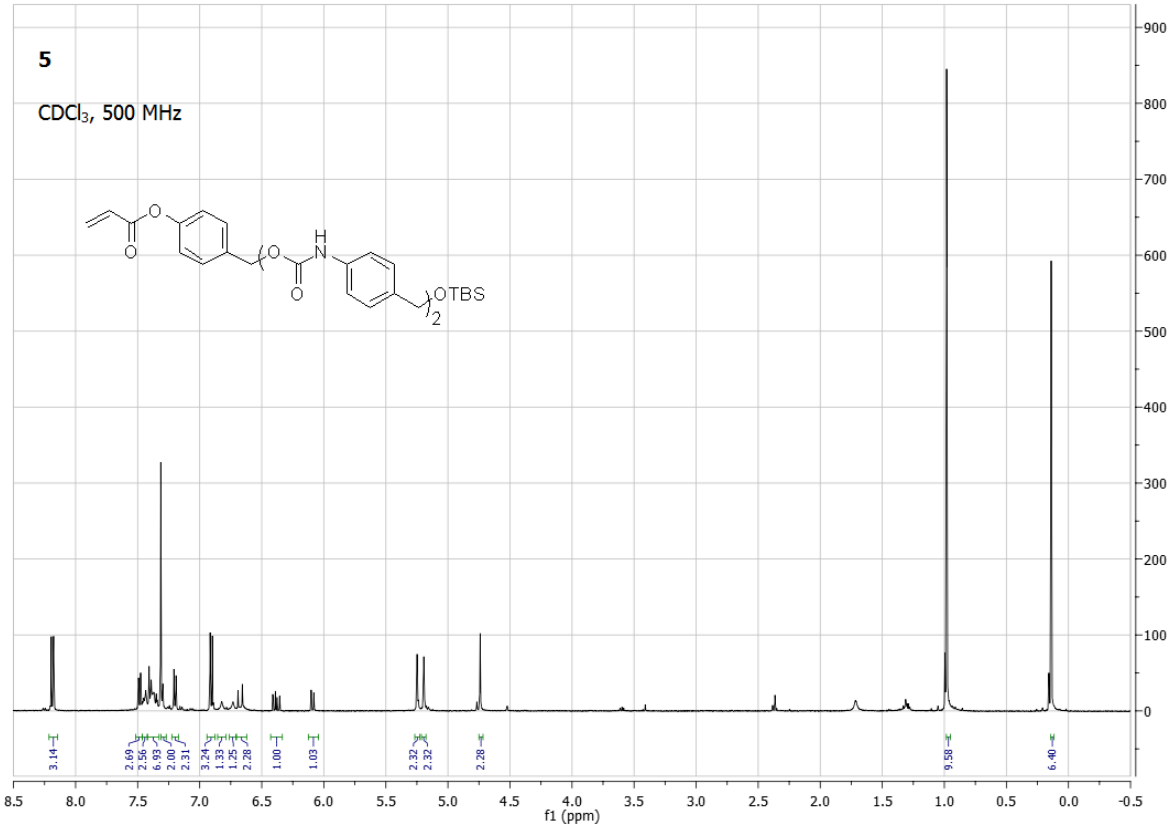
5
CDCl3, 500 MHz
OTBS
f1 (ppm)

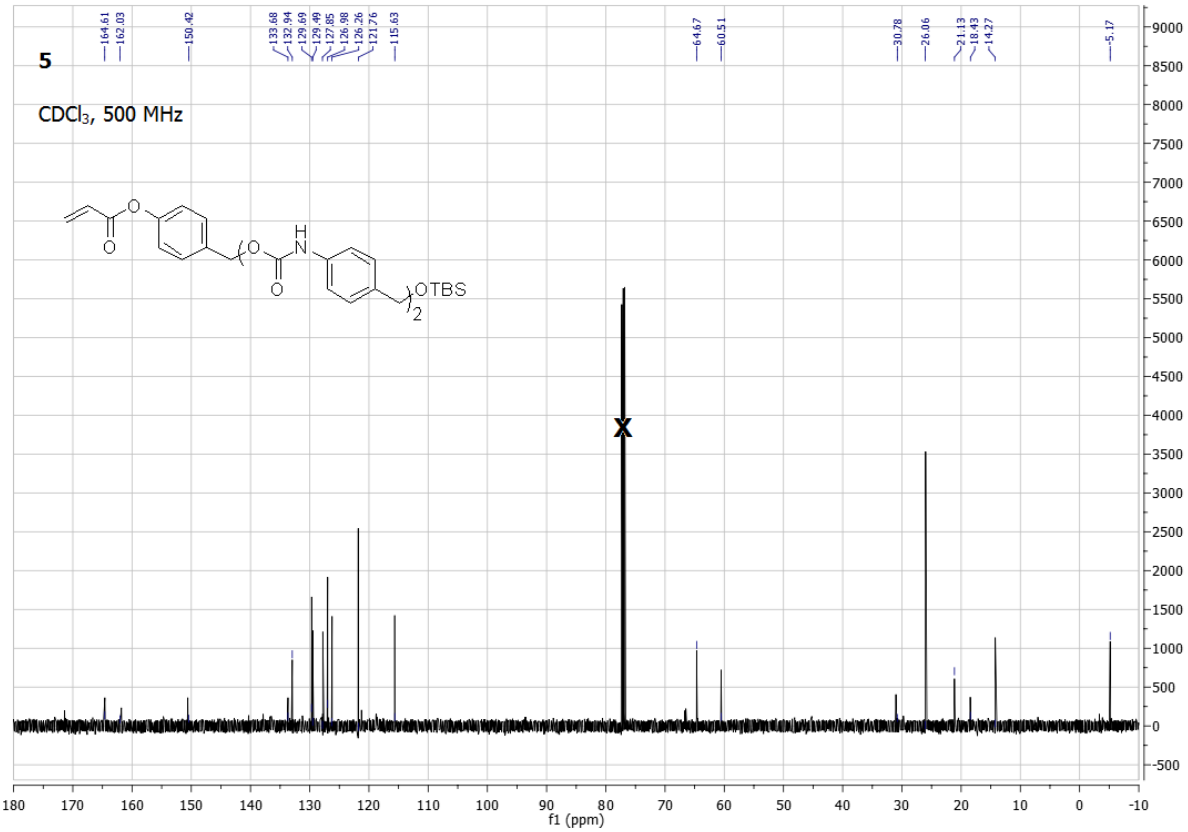
5
CDCl3, 500 MHz
OTBS
X
f1 (ppm)

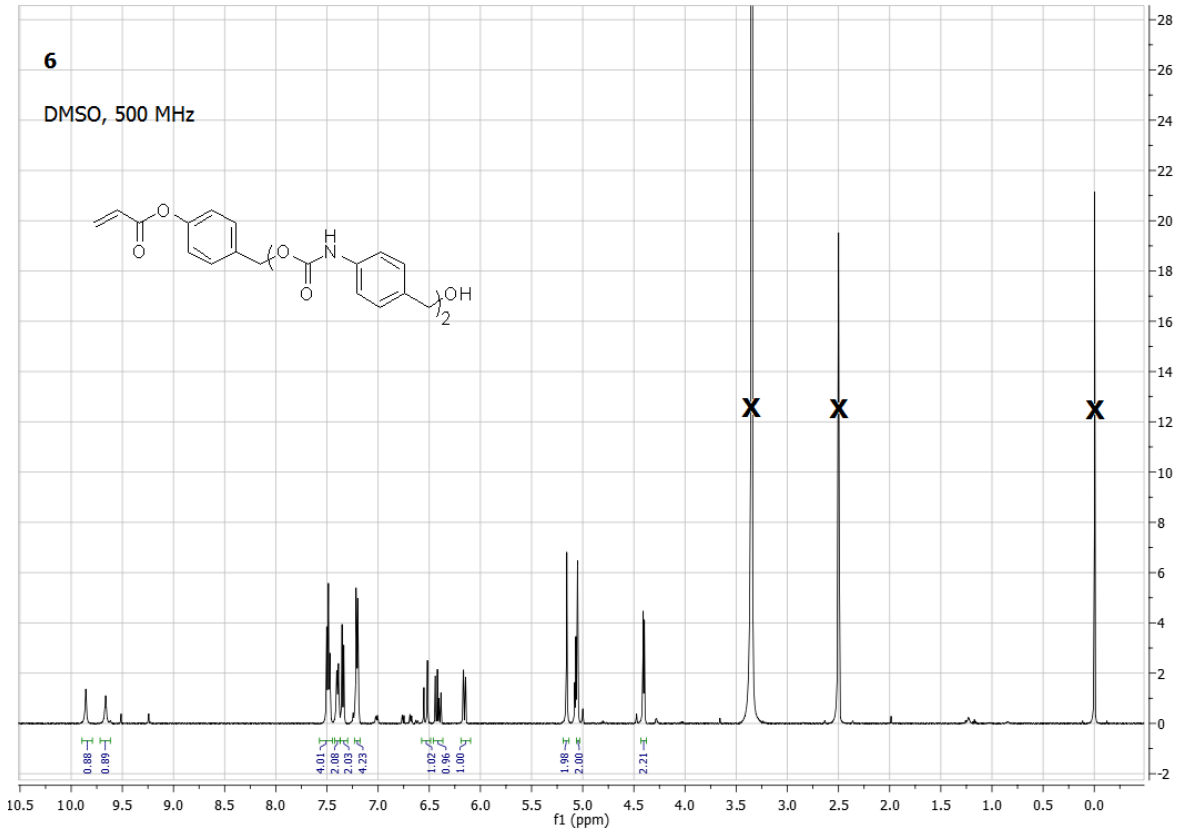
6
DMSO, 500 MHz
f1 (ppm)

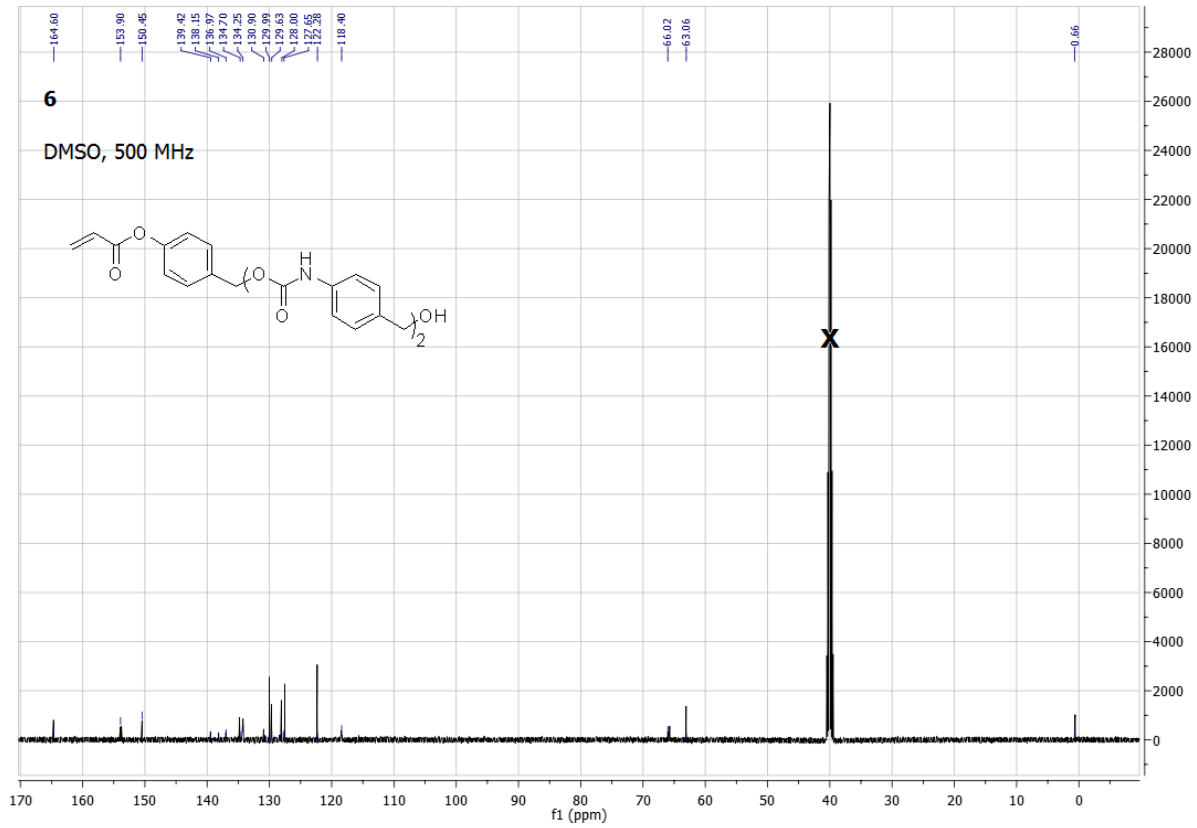
6
DMSO, 500 MHz
f1 (ppm)

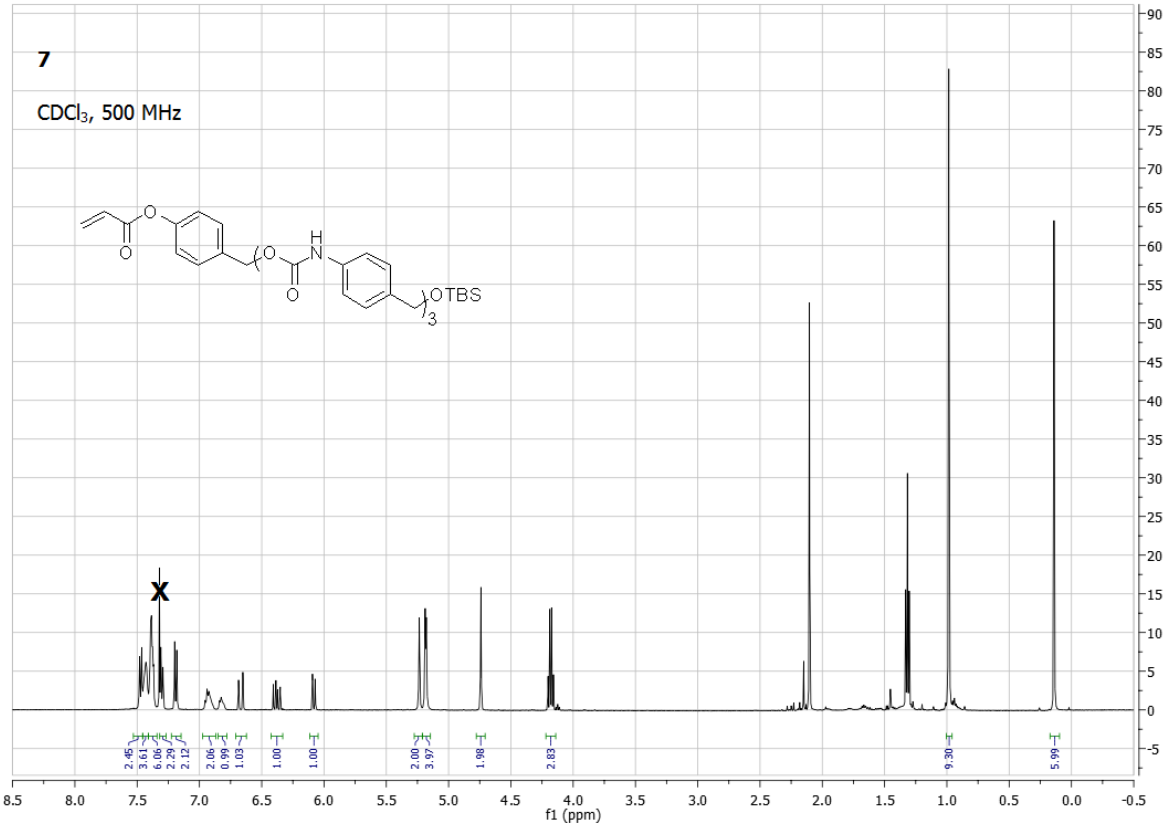
7
CDCl3, 500 MHz
OTBS
3
f1 (ppm)

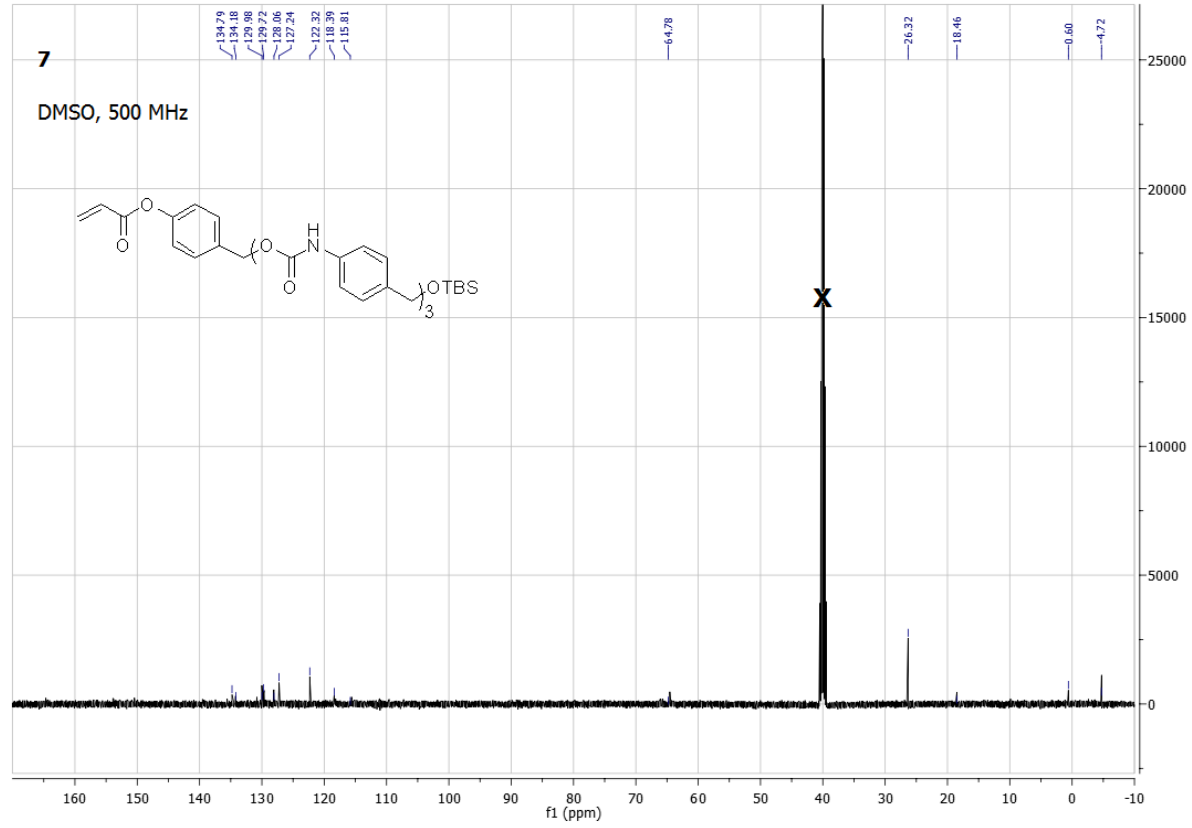
7
DMSO, 500 MHz
OTBS
3
f1 (ppm)

H. References

1. Avital-Shmilovici, M.; Shabat, D., Self-immolative dendrimers: A distinctive approach to molecular amplification. *Soft Matter* **2010,** *6*, 1073 - 1080.

2. Blencowe, C. A.; Russell, A. T.; Greco, F.; Hayes, W.; Thornthwaite, D. W., Self-immolative linkers in polymeric delivery systems. *Polym. Chem.* **2011,** *2*, 773 - 790.

3. Esser-Kahn, A. P.; Odom, S. A.; Sottos, N. R.; White, S. R.; Moore, J. S., Triggered Release from Polymer Capsules. *Macromolecules* **2011,** *44*, 5539 - 5553.

4. Peterson, G. I.; Larsen, M. B.; Boydston, A. J., Controlled Depolymerization: Stimuli-Responsive Self-Immolative Polymers. *Macromolecules* **2012,** *45*, 7317 - 7328.

5. McBride, R. A.; Gillies, E. R., Kinetics of Self-Immolative Degradation in a Linear Polymeric System: Demonstrating the Effect of Chain Length. *Macromolecules* **2013,** *46* (13), 5157-5166.

6. Peterson, G. I.; Larsen, M. B.; Boydston, A. J., Controlled Depolymerization: Stimuli-Responsive Self-Immolative Polymers. *Macromolecules* **2012,** *45* (18), 7317-7328.

7. Schmid, K. M.; Phillips, S. T., Effect of aromaticity on the rate of azaquinone methide-mediated release of benzylic phenols. *J Phys Org Chem* **2013,** *26* (7), 608-610.

8. Wong, A. D.; DeWit, M. A.; Gillies, E. R., Amplified release through the stimulus triggered degradation of self-immolative oligomers, dendrimers, and linear polymers. *Adv Drug Deliver Rev* **2012,** *64* (11), 1031-1045.

9. Robbins, J. S.; Schmid, K. M.; Phillips, S. T., Effects of Electronics, Aromaticity, and Solvent Polarity on the Rate of Azaquinone-Methide--Mediated Depolymerization of Aromatic Carbamate Oligomers. *J Org Chem* **2013,** *78* (7), 3159-3169.

10. Schmid, K. M.; Jensen, L.; Phillips, S. T., A Self-Immolative Spacer That Enables Tunable Controlled Release of Phenols under Neutral Conditions. *J Org Chem* **2012,** *77* (9), 4363-4374.

11. Kim, H.; Mohapatra, H.; Phillips, S. T., Rapid, On-Command Debonding of Stimuli-Responsive Cross-Linked Adhesives by Continuous, Sequential Quinone Methide Elimination Reactions. *Angew Chem Int Edit* **2015,** *53* (44), 13063-13067.

12. Esser-Kahn, A. P.; Sottos, N. R.; White, S. R.; Moore, J. S., Programmable Microcapsules from Self-Immolative Polymers. *J Am Chem Soc* **2010,** *132* (30), 10266-10268.

13. Baker, M. S.; Phillips, S. T., A small molecule sensor for fluoride based on an autoinductive, colorimetric signal amplification reaction. *Org Biomol Chem* **2012,** *10* (18), 3595-3599.

14. Phillips, S. T.; Robbins, J. S.; DiLauro, A. M.; Olah, M. G., Amplified Responses in Materials Using Linear Polymers that Depolymerize from End-to-End When Exposed to Specific Stimuli. *J Appl Polym Sci* **2014,** *131* (19).

15. Robbins, J. S.; Schmid, K. M.; Phillips, S. T., Effects of Electronics, Aromaticity, and Solvent Polarity on the Rate of Azaquinone-Methide-Mediated Depolymerization of Aromatic Carbamate Oligomers. *J. Org. Chem* **2013,** *78* (7), 3159 - 3169.

16. Esser-Kahn, A. P.; Sottos, N. R.; White, S. R.; Moore, J. S., Programmable Microcapsules from Self-Immolative Polymers. *J. Am. Chem. Soc.* **2010,** *132* (30), 10266-10268.

17. Yang, X. F.; Guo, Y. X.; Strongin, R. M., A seminaphthofluorescein-based fluorescent chemodosimeter for the highly selective detection of cysteine. *Org Biomol Chem* **2012,** *10* (14), 2739-2741.

18. Bosco, J. W. J.; Raju, B. R.; Saikia, A. K., Potassium Fluoride Assisted Selective Acetylation of Alcohols with Acetic Acid. *Synth. Commun.* **2004,** *34* (15), 2849 - 2855.

19. Bosco, J. W. J.; Agrahari, A.; Saikia, A. K., Molecular iodine catalyzed selective acetylation of alcohols with vinyl acetate. *Tetrahedron* **2006,** *47* (24), 4065 - 4068.

20. Polymer Handbook. *Rubber Age* **1966,** *98* (6), 147-&.